

Doctoral Theses at NTNU, 2005:119

Øystein Brandal

# Interfacial (o/w) Properties of Naphthenic Acids and Metal Naphthenates, Naphthenic Acid Characterization and Metal Naphthenate Inhibition

**NTNU**  
Norwegian University of  
Science and Technology  
Doctoral thesis  
for the degree of doktor ingeniør  
Faculty of Natural Science and Technology  
Department of Chemical Engineering

---

## **Preface**

This thesis, submitted in partial fulfilment of the requirements for the degree of dr.ing at the Norwegian University of Science and Technology, consists of five papers which are all based on experimental work carried out at Ugelstad Laboratory from July 2002 to February 2005. In addition, the thesis also includes some unpublished results which are presented in the introductory part.

I was introduced to the world of surface and colloid chemistry by Johan Sjöblom as an undergraduate student at the Norwegian University of Science and Technology, Department of Chemical Engineering, in 2001. In the spring of 2002, I received my sivilingeniør degree with a main project in the field of characterization of water-in-crude oil emulsions by means of video enhanced microscopy. About one month later, I was accepted for a PhD grant in the subject of naphthenic acids through the VISTA program, financially supported by Statoil and The Norwegian Academy of Science and Letters, and under the guidance of Johan Sjöblom.

During the three years of work, I have also been involved in a joint industrial program financed by petroleum companies (Statoil, Total, ChevronTexaco) and chemical vendors (ChampionTechnologies, AkzoNobel, BakerPetrolite). Results from this work have been followed up and presented on meetings twice a year, both domestic and abroad.

---

## **Acknowledgements**

First, I would like to express my gratitude to my supervisor, Professor Johan Sjöblom, for giving me the opportunity to join his group of surface and colloid chemistry in July 2001. His scientific skills and excellent supervision combined with regular social events have been crucial for the motivation for the last three years of work.

I would also like to thank my other colleagues at the Ugelstad Laboratory for the good working environment. Special thanks go to Ann-Mari Hanneseth for her assistance with the laboratory work, to Dr. Wilhelm Glomm for proofreading this thesis, and to my office mate, Magne Knag, for good fellowship and a lot of interesting discussions related as well as not related to the topics of chemistry.

Statoil ASA and The Norwegian Academy of Science and Letters are acknowledged for the financial support through the VISTA program. Acknowledgements are also extended to the JIP consortium consisting of oil industry (ChevronTexaco, Statoil, Total) and chemical vendors (AkzoNobel, ChampionTechnologies, BakerPetrolite). I would also like to thank Heidi Mediaas for including me into the naphthenate group at Statoil R&D Centre.

Finally, I would like to thank Nina and my family for their love and support and for always believing in me.

---

## Abstract

Deposition of metal naphthenates in process facilities is becoming a huge problem for petroleum companies producing highly acidic crudes. In this thesis, the main focus has been towards the oil-water (o/w) interfacial properties of naphthenic acids and their ability to react with different divalent cations across the interface to form metal naphthenates.

The pendant drop technique was utilized to determine dynamic interfacial tensions (IFT) between model oil containing naphthenic acid, synthetic as well as indigenous acid mixtures, and pH adjusted water upon addition of different divalent cations. Changes in IFT caused by the divalent cations were correlated to reaction mechanisms by considering two reaction steps with subsequent binding of acid monomers to the divalent cation. The results were discussed in light of degree of cation hydration and naphthenic acid conformation, which affect the interfacial conditions and thus the rate of formation of 2:1 complexes of acid and cations. Moreover, addition of non-ionic oil-soluble surfactants used as basis compounds in naphthenate inhibitors was found to hinder a completion of the reaction through interfacial dilution of the acid monomers.

Formation and stability of metal naphthenate films at o/w interfaces were studied by means of Langmuir technique with a trough designed for liquid-liquid systems. The effects of different naphthenic acids, divalent cations, and pH of the subphase were investigated. The results were correlated to acid structure, cation hydration, and degree of dissociation, which all affect the film stability against compression.

Naphthenic acids acquired from a metal naphthenate deposit were characterized by different spectroscopic techniques. The sample was found to consist of a narrow family of 4-protic naphthenic acids with molecular weights around 1230 g/mol. These acids were found to be very o/w interfacially active compared to normal crude acids, and to form Langmuir monolayers with stability depending on the aqueous pH. At high pH, addition of  $\text{Ca}^{2+}$  increased the film stability due to formation of calcium naphthenate at the surface.

A new experimental setup based on near infrared spectroscopy was used to monitor the formation, growth, and inhibition of calcium naphthenate particles in o/w systems. This method was found to be suitable for studies of particle formation rate and growth qualitatively under different experimental conditions.

---

## List of Publications

- I. Brandal, Ø., Sjöblom, J., and Øye, G.: *Interfacial Behaviour of Naphthenic Acids and Multivalent Cations in Systems with Oil and Water. I. A Pendant Drop Study of Interactions between n-Dodecyl Benzoic Acid and Divalent Cations*, J Dispersion Sci Technol, (2004), 25(3), 367-374.
- II. Brandal, Ø., and Sjöblom, J.: *Interfacial Behaviour of Naphthenic Acids and Multivalent Cations in Systems with Oil and Water. II. Formation and Stability of Metal Naphthenate Films at Water-Oil Interfaces*, J Dispersion Sci Technol, (2005), 26(1), 53-58.
- III. Brandal, Ø., Hanneseth, A-M., and Sjöblom, J.: *Interactions Between Synthetic and Indigenous Naphthenic Acids and Divalent Cations across Oil-Water Interfaces. Effects of Addition of Oil-Soluble Non-Ionic Surfactants*, Colloid Polym Sci, Accepted, 2005.
- IV. Brandal, Ø., Hanneseth, A-M., Hemmingsen, P.V., Sjöblom, J. Kim, S., Rodgers, R.P., and Marshall, A.G: *Isolation and Characterization of Naphthenic Acids from Metal Naphthenate Deposit. Molecular Properties at Oil-Water and Air-Water Interfaces*, J Dispersion Sci Technol, Accepted, 2005.
- V. Hanneseth, A-M., Brandal, Ø., and Sjöblom, J.: *Formation, Growth, and Inhibition of Calcium Naphthenate Particles in Oil-Water Systems as Monitored by means of Near Infrared Spectroscopy*, J Dispersion Sci Technol, Accepted, 2005.

---

## Complementary Work

- VI. Sjöblom, J., Aske, N., Auflem, I.H., Brandal, Ø., Havre, T.E., Sæther, Ø., Westvik, A., Johnsen, E.E., and Kallevik, H.: *Our Current Understanding of Water-in-Crude Oil Emulsions. Recent Characterization Techniques and High Pressure Performance*, Adv Colloid Interface Sci, (2003), 100-102, 399-473.
- VII. Sjöblom, J., Øye, G., Glomm, W.R., Hannisdal, A., Knag, M., Brandal, Ø., Ese, M-H., Hemmingsen, P.V., Havre, T.E., Oschmann, H-J., and Kallevik, H.: *Modern Characterization Techniques for Crude Oils and Their Emulsions*. In *Emulsions and Emulsion Stability*, Sjöblom, J. (ed), 2nd Edition, Taylor and Francis, New York (In Press), 2005.
- VIII. Brandal, Ø., and Sjöblom, J.: *Interfacial Behaviour of Naphthenic Acids and Divalent Cations in Systems with Oil and Water*, Poster presentation at: "The 4th International Conference on Petroleum Phase Behaviour and Fouling", Trondheim June 23-26, 2003.

---

## Contents

Preface .....	I
Acknowledgements.....	II
Abstract.....	III
List of Publications.....	IV
1 Introduction .....	1
2 Naphthenic Acid Chemistry.....	2
2.1 Occurrence and Structure .....	2
2.2 Naphthenic Acids in Oil-Water Bulk Systems .....	4
2.2.1 <i>Oil-Water Partitioning</i> .....	4
2.2.2 <i>Self-Association in Oil</i> .....	5
2.2.3 <i>Self-Association in Water</i> .....	7
2.2.4 <i>Interactions with other Fractions</i> .....	10
2.3 Interfacial Behaviour of Naphthenic Acids .....	11
3 Formation and Inhibition of Metal Naphthenates.....	14
3.1 Background .....	14
3.2 Reaction Mechanisms.....	15
3.3 Naphthenate Inhibition.....	18
3.4 Naphthenate Composition - Recent Discoveries.....	19
4 Experimental Techniques .....	21
4.1 Pendant Drop Technique.....	21
4.2 Langmuir Technique .....	24
4.3 Near Infrared Spectroscopy .....	28
4.4 Analytical Characterization Tools.....	30
4.4.1 <i>FT-IR Spectroscopy</i> .....	30
4.4.2 <i>NMR Spectroscopy</i> .....	31
4.4.3 <i>ESI FT-ICR Mass Spectroscopy</i> .....	32
5 Main Results .....	34
Paper I .....	35
Paper II .....	37
Paper III .....	40
Paper IV .....	44
Paper V .....	51
6 Summary and Conclusions .....	56
7 References.....	58

Papers I-V

---

## 1 Introduction

The production of acidic crudes with high total acid number (TAN) is steadily increasing as more of the recently discovered fields involve heavy crudes [1]. The acidity is predominantly caused by indigenous organic acids, which in the petroleum industry generally are termed naphthenic acids.

The naphthenic acids are causing several problems. Their detrimental effect in the environment has been known for a long time, and low molecular weight compounds present in the waste water have shown to be toxic to a variety of aquatic organisms [2-4]. From an operational point of view, producing and processing highly acidic crudes involve a number of challenges. Naphthenic acid corrosion, especially in the high temperature parts of the distillation units, is a major concern to the refining industry [5-7]. During production, the amphiphilic naphthenic acids may also accumulate at interfaces and stabilize water-in-oil emulsions [8-11], causing enhanced separation problems. Pressure drop during fluid transportation from the reservoir to the topside leads to release of carbon dioxide and to a subsequent increase in the pH of the co-produced water, which brings about a higher degree of dissociation of naphthenic acids at the o/w interface. The dissociated moieties may thus react with metal cations in the water to form metal naphthenates. Due to low interfacial affinity and low solubility in water, especially when multivalent cations are involved, the naphthenates will precipitate and start to agglomerate in the oil phase. As the density of the precipitate lies between that of oil and water, it will gradually settle and accumulate at the o/w interface and further adhere to process unit surfaces. Deposition of metal naphthenates is a problem predominantly in topside facilities like o/w separators and de-salters, and may lead to worst-case scenarios in cleaning processes and regular, costly production shutdowns.

With this background, it is clear that an improved understanding of how the naphthenic acids behave physico-chemically in o/w systems is crucial for future elimination of related problems. Although naphthenate deposition today is one of the most challenging separation issues, rather little attention has so far been directed towards a complete understanding of how the naphthenic acids and the cations react to form naphthenates. In this thesis, the main focus has been towards interfacial reactions between naphthenic acids and divalent cations for systems involving synthetic acids as well as indigenous acid mixtures.



## 2 Naphthenic Acid Chemistry

### 2.1 Occurrence and Structure

Naphthenic acids are mixtures of alkyl-substituted acyclic and cyclic structures with the general chemical formula  $C_nH_{2m+Z}O_2$ , where  $m$  indicates the carbon number and  $Z$  is zero, in the case of fatty acids, or negative, depending on the number of condensed and/or aromatic rings. Although the term "naphthenic" traditionally was used to classify only acids with cycloaliphatic derivatives, in the petroleum industry it refers normally to all the organic acids present in crude oil [12, 13]. Figure 2.1 displays some examples of possible monoprotic naphthenic acid structures for different  $Z$  values.

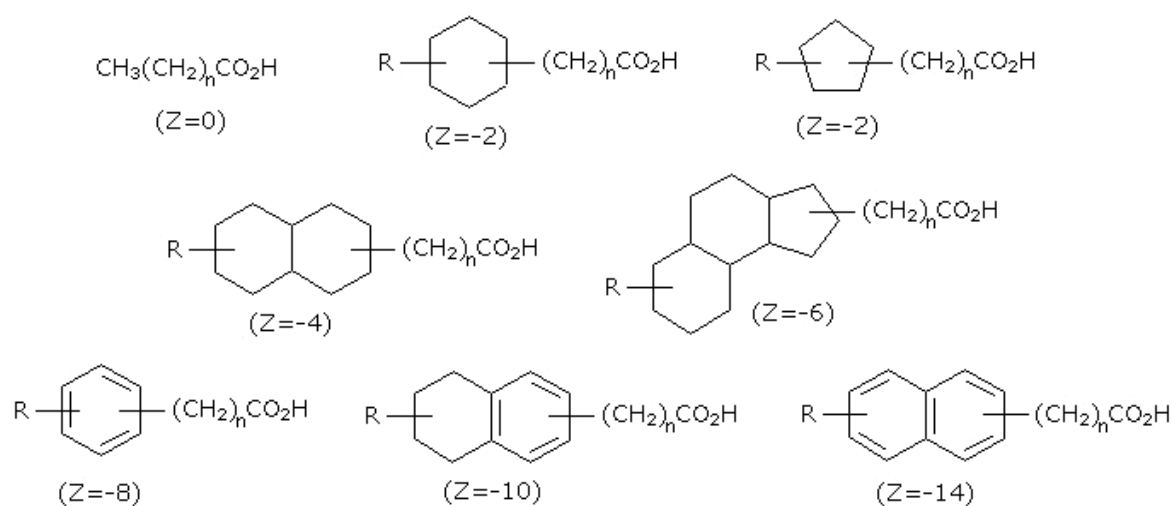


Figure 2.1: Naphthenic acid structures where  $Z$  describes the hydrogen deficiency,  $R$  is an alkyl chain, and  $n$  the number of  $CH_2$  units.

Naphthenic acids are normal constituents in nearly all crude oils, typically ranging from 0-4 %wt. The acids are predominantly found in immature heavy crudes, whereas paraffinic crudes normally have low acid contents [12, 13]. Methods based on potentiometric titration are frequently used in order to measure total acid number (TAN) [14, 15]. The naphthenic acids are assumed to generate from in-reservoir biodegradation of petroleum hydrocarbons [16-18]. This suggestion has been supported by discovery of naphthenic acids in deposits in naturally biodegraded crude oils [18, 19], and in crude

oils that have been biodegraded under laboratory conditions [20, 21]. Hence, they can be considered as biological markers and provide information on past reservoir history [19].

The naphthenic acids are complex mixtures, showing variations in structure and molecular weight. Several analytical techniques have been utilized to characterize the acids qualitatively. This includes various mass spectrometry (MS) methods [22-26], gas chromatography-mass spectrometry (GC-MS) methods [27-29], and these methods in combination with Fourier transform infrared (FT-IR) and/or nuclear magnetic resonance (NMR) spectrometry [30-32]. In addition, negative-ion electrospray ionization (ESI) coupled to high-field Fourier transform ion cyclotron resonance mass spectrometry (FT-ICR MS) has recently shown to be a powerful tool to determine detailed elemental composition of acidic crude oil compounds [33, 34]. Figure 2.2 shows an ESI FT-ICR MS spectrum of a crude oil from a field located on the Norwegian continental shelf. Around 85% of the peaks represent carboxylic groups. The spectrum illustrates very well the broad distribution of different naphthenic acid structures.

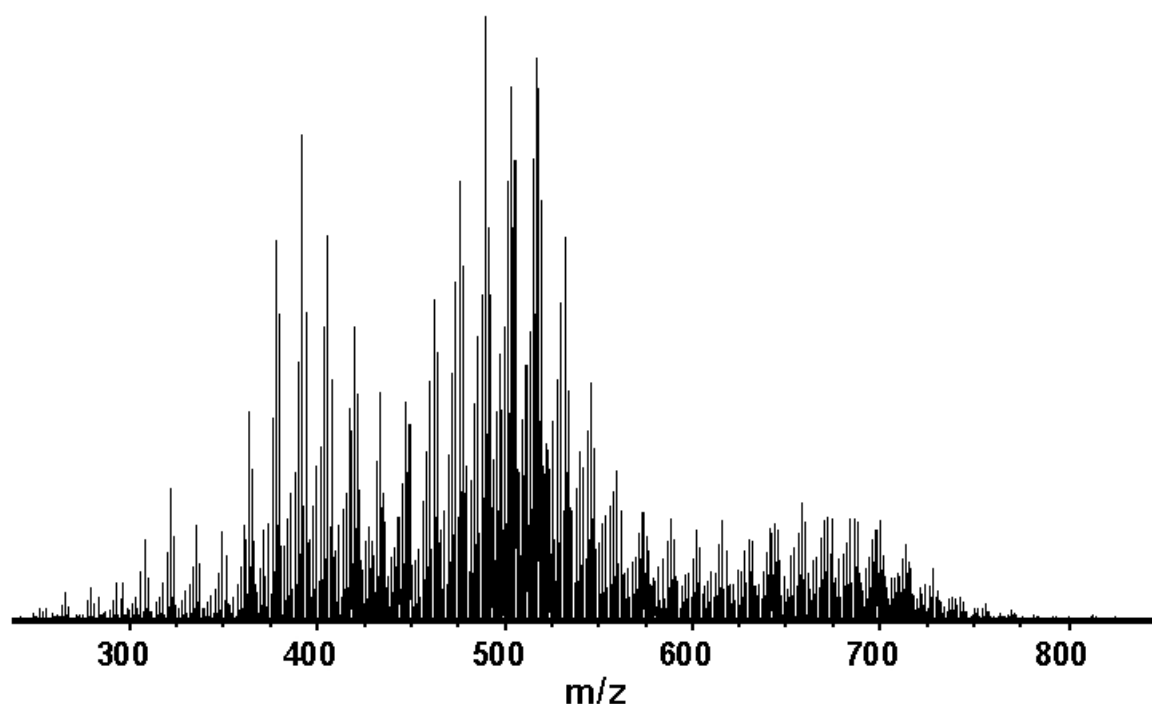


Figure 2.2: ESI FT-ICR MS spectrum of a North Sea crude oil.

## 2.2 Naphthenic Acids in Oil-Water Bulk Systems

When naphthenic acids are introduced to systems containing oil and water, several equilibria will be involved. The following parts summarize some of the fundamental processes taking place in bulk solution.

### 2.2.1 Oil-Water Partitioning

Naphthenic acids are amphiphilic molecules where the carboxylic group represents the polar part and the hydrocarbon skeleton the oil-soluble hydrophobic part. In oil-water systems, the acids may thus be distributed between the different phases. The distribution will depend strongly upon conditions like the pH and the salinity of the aqueous phase. Partitioning of naphthenic acid monomers between oil (*o*) and water (*w*) may be described by the equilibrium in equation 2.1:



where the corresponding partitioning coefficient  $K_{w/o}$  is given by

$$K_{w/o} = \frac{[RCOOH]_w}{[RCOOH]_o} \quad (2.2)$$

The degree of partitioning will accordingly depend on the solubility of the molecules in the two phases. Hence, naphthenic acids with a large hydrocarbon moiety will exhibit lower partition coefficients than compounds with smaller hydrophobic parts. The distribution of acid between the phases will also be affected by the pH: by increasing the pH, the monomers dissociate and become more water-soluble. Reinsel and co-workers [35] investigated the effects of pH, temperature, and organic acid concentration on the partition coefficients for short-chain organic acids in a crude oil-water system. At pH 5-7, more than 85% of the acids were dissolved in the aqueous phase. Moreover, they found an approximately linear descending relation between the partition coefficient and the number of carbon atoms in the hydrocarbon moiety. A similar relation was also reported by Havre and co-workers [36] from a partitioning study of a series of synthetic naphthenic acids in oil-water systems under different experimental conditions. Kocherginsky and Grishchenko [37] measured the transfer rate of long chain fatty acids

---

from octane into aqueous solution through a flat porous membrane. At pH 4, they found that the transfer rate was proportional to  $K_{w/o}$ . By increasing the pH to 12, a 20-fold increase of the rate was observed in the case of octanoic acid, and a 1000 fold in the case of oleic acid.

### 2.2.2 Self-Association in Oil

The naphthenic acids will, like other surfactants, tend to self-associate in bulk solution at certain concentrations. Carboxylic acids are known to form dimers in the oil phase through hydrogen bonding, as illustrated in figure 2.3.

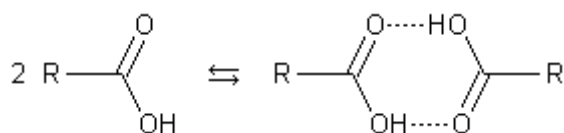


Figure 2.3: Carboxylic acid dimerization.

Dimerization of carboxylic acids in oil has been a subject of large amounts of studies. Generally, it is found to be highly dependent on concentration, solvent polarity, and the length of the carbon chain as well as the carboxylic acid conformation. Pohl and co-workers [38] measured differences in dielectric constants between non-polar solvents and dilute solutions of benzoic acid and various short-chain carboxylic acids. Generally, they found that the molar polarization of the solute decreased exponentially with increasing concentration. This effect was assumed to be a result of formation of less polar dimers. However, due to errors caused by inaccurate measurements of the most dilute solutions, the dimerization constants in n-heptane were only estimated. Later, Goodman [39] achieved more precise results by using  $^{14}\text{C}$ -labelled acids. He found that fatty acids of chain length  $\text{C}_{14}$  and below had monomer-dimer equilibrium in n-heptane, where the dimerization constant increased with increasing chain length. Takeda and co-workers [40] investigated the dimerization of benzoic acid and several short-chain carboxylic acids in solvents of different polarity by means of standard potential strength measurements. Benzoic acid was found to almost exclusively exist as dimers in n-hexane at concentrations higher than 15 mM. Moreover, the degree of self-association was found to decrease with decreasing concentration of acid. Similar observations have also been

reported by Fujii and co-workers [41], who measured the dimerization of acetic acid in several non-polar solvents using infrared spectroscopy. Kimtys and Balevicius [42] correlated changes in chemical shifts in  $^1\text{H}$  NMR spectra to self-association for a family of short-chain aliphatic carboxylic acids in cyclohexane at various concentrations and temperatures. The degree of dimerization was found to decrease with increasing temperature for all acids and increase by increasing the concentration up to 0.1 mole fraction of acid. A further increase in concentration resulted however in a monotonous decline in the chemical shift. This effect was discussed in terms of dimer interactions and polymerization, which decrease with acid dilution.

The fact that multimers may involve strong hydrogen bonding is well illustrated by the ESI ICR-MS spectra in figure 2.4. The analyses have been carried out on naphthenic acids extracted from a North Sea crude. As shown in the spectrum to the left, the peaks are distributed in three humps, which indicate presence of multimers. To confirm this assumption, the sample was exposed to *infrared multiphoton dissociation* (IRMPD) [43]. The obtained spectrum after such treatment (to the right) clearly shows enhanced formation of monomers, i.e. IR radiation breaks up intermolecular H-bonds bridging the monomers.

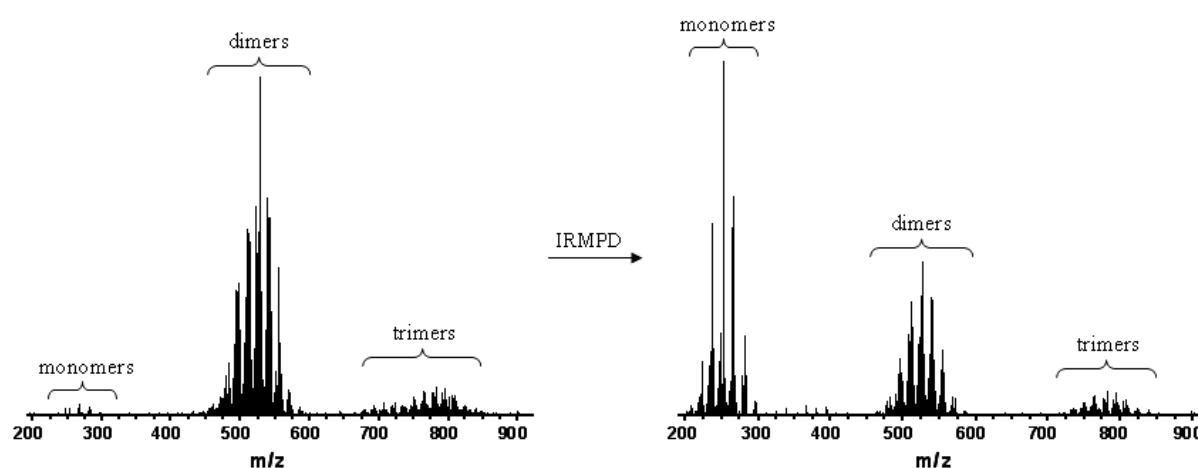


Figure 2.4: Naphthenic acids exposed to IR radiation.

Naphthenic acids in systems with oil and alkaline water may above certain concentrations also form larger aggregates in the hydrocarbon phase, such as inverted micelles (see chapter 2.2.3). This observation is reported by Horváth-Szabó and co-workers [44] from

a phase behaviour study of a sodium naphthenate/toluene/water system. Although the detailed composition range was not determined, the inverted micelles were found to coexist with the normal micellar phase almost all over its phase range.

### **2.2.3 Self-Association in Water**

Like in the oil phase, carboxylic acids are also found to dimerize in highly diluted aqueous solutions. By analyzing the set of data obtained by Goodman [39], Mukerjee [45] calculated that the self-association of fatty acids in water only involves two anions at a pH of 7.45. The dimerization constant was found to increase continuously with increasing hydrocarbon tail up to palmitic acid. A further increase of the chain length up to C<sub>18</sub> (stearic, oleic, and linoleic) gave however dimerization constants in the same order as palmitic acid. Although no definite explanation was ascribed to this striking phenomenon, Mukerjee speculates about the possibility of having a chain-coiling at sufficiently long chains, putting some of the methylene groups in an organic environment inside the curled-up structures. Suzuki and co-workers [46] investigated the effect of pressure on the dimerization of C<sub>1</sub>-C<sub>4</sub> aliphatic acids by means of electrical conductivity measurements. They considered two kinds of interactions to be of relevance; hydrogen bonding between carboxylic groups and hydrophobic interactions between alkyl chains. In the lower pressure region, H-bonds were found to dominate, and the dimerization increased with increasing pressure. At higher pressures, however, the contribution from alkyl chain interactions becomes more significant, and a minimum in the dimer dissociation constant was observed. The pressure at which this minimum appeared was found to decrease with increasing alkyl chain length due to stronger hydrophobic interactions. In a series of publications, Stenius [47-49] has studied the association of various fatty acid sodium salts in aqueous solutions at high ionic strength (3M NaCl). He found that small aggregates are formed by sodium alkanoates with more than 3 carbon atoms in the hydrocarbon chain. The aggregates consisted of 4 anions, irrespective of the hydrocarbon chain length. By increasing the temperature, the aggregates were found to increase slightly in size. Hydrophobic bonding was in all cases suggested to be the reason for the association. By excess Gibbs' energies calculations, Friman and Stenius [50] also found that the tendency of association decreases with increasing branching of the hydrocarbon moiety.

At higher concentrations of acid, larger aggregates, such as micelles, may also form. The concentration at which surfactants start to form micelles is known as the critical micelle

---

concentration (CMC). CMC is dependent on factors like molecular structure, e.g. the length of the hydrocarbon chain, electrolyte concentration as well as on physical conditions such as temperature and pH [51]. As for pre-micellar association, the micelle formation is favoured by an increase in the entropy [52]: water molecules near the hydrocarbon chain are more ordered than bulk water, causing a loss of entropy. By forming aggregates, the hydrophobic chains become less in contact with water and the entropy increases.

The shape of the formed aggregates can be predicted by the critical packing parameter (CPP), given by the following relation:

$$CPP = \frac{v}{l \cdot a} \quad (2.3)$$

where  $v$  is the volume and  $l$  the length of the hydrocarbon chain, respectively, while  $a$  is the cross-section area of the polar headgroup. The parameters used to calculate the CPP are illustrated in figure 2.5.

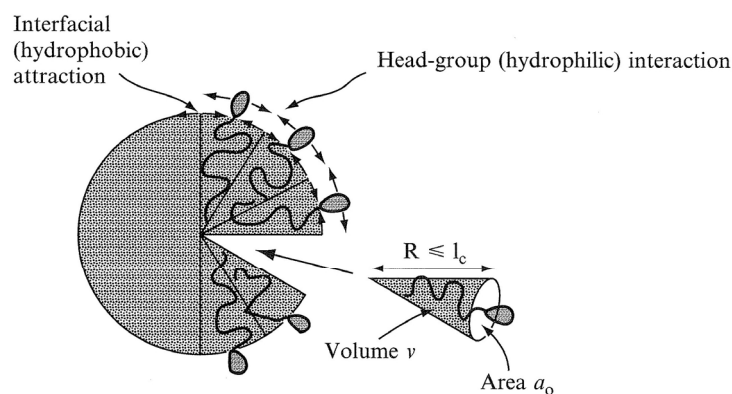


Figure 2.5: Illustration of the different parameters used to calculate the critical packing parameter (CPP) of surfactants in micelles [53].

Depending on the topology of the polar headgroup and the volume of the hydrocarbon moiety, different aggregate shapes will thus form, including micelles ( $CPP < 1/3$ ), rod-shaped aggregates ( $CPP \sim 1/3 - 1/2$ ), lamellar structures ( $1/2 \leq CPP \leq 1$ ), and inverted structures ( $CPP > 1$ ). The number of monomers in each micelle will also be lower for

branched surfactants than for more aliphatic ones. Micelles of naphthenic acids with cyclic units will thus contain less monomer than in the case of straight-chain fatty acids. For charged surfactants, like naphthenic acids under alkaline conditions, electrostatic repulsion between negatively charged carboxylic groups will favour the formation of spherical micelles. This tendency may however be altered by adding counterions to the solution, which brings about a compression of the electric double-layer and thus a reduction of the repulsion between equally charged molecules.

A common way to determine the CMC is to measure the change in surface tension (ST) as a function of surfactant concentration. Upon addition of surfactants to the aqueous phase, the surface tension decreases continuously until a constant value, reflecting the CMC, is reached. Above this concentration, any further added surfactants will take part in micelle formation, and hence the concentration of monomers remains constant. A relation between ST and the surfactant concentration is given by the Gibbs' adsorption equation [54]:

$$\frac{d\gamma}{d(\ln c)} = nk_B T \Gamma \quad (2.4)$$

where  $\gamma$  is the ST,  $c$  is the bulk concentration of surfactant,  $T$  is the temperature,  $\Gamma$  is the surface excess,  $k_B$  is the Boltzmann constant, and  $n$  is 1 for non-ionic surfactants and 2 for surfactants completely ionized at the surface. Hence, by plotting ST as a function of the logarithm of the concentration, this gives two linear curves, one for the descending ST in the pre-micellar region, according to equation 2.4, and one horizontal curve after the CMC is reached. The CMC of the given surfactant is found as the intersection point between these two linear relations. Figure 2.6 (a) displays some examples of CMC measurements carried out in alkaline solution (pH>11.5) on benzoic acid homologues with C<sub>4</sub>-C<sub>8</sub> alkyl chain length. As illustrated in figure 2.6 (b), the logarithm of the CMC decreases almost linear with increasing length of the hydrophobic tail, which is in accordance to findings also reported by other authors [55-57].



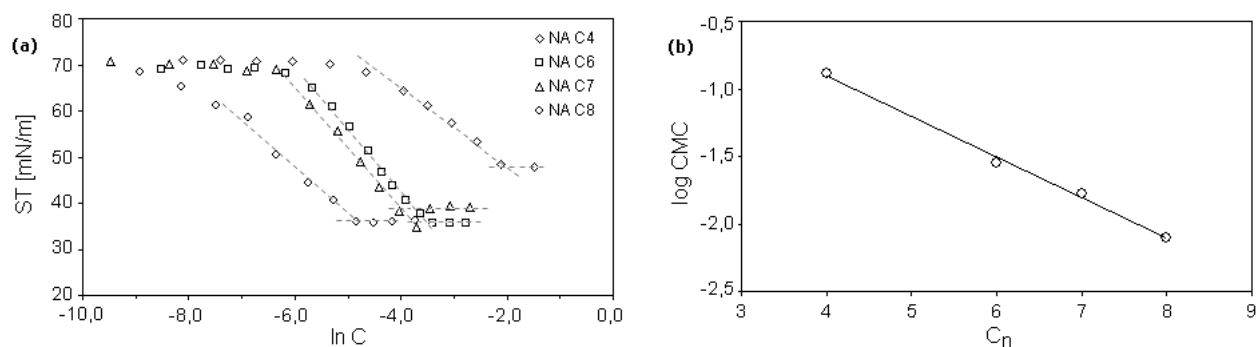


Figure 2.6: CMC of benzoic acid homologues with  $C_4$ - $C_8$  aliphatic chain (a), and  $\log$  CMC vs. carbon number for the series (b) (unpublished results).

At sufficiently high concentrations of fatty acid, other aggregates may also form, like liquid crystalline (LC) phases [58]. Under certain conditions, LC structures may accumulate at interfaces and stabilize emulsions [59-61], also in interplay with other polar crude oil fractions [62]. The correlation between LC phases and emulsion stability has been extensively reported by Friberg and co-workers [63-66].

#### 2.2.4 Interactions with other Fractions

Crude oil consists of a complex mixture of gaseous, liquid, and solid hydrocarbons with different degrees of polarity, in addition to small amounts of inorganic compounds [67]. Among the polar fractions one finds the asphaltenes and the resins, which are essential compounds for the stabilization of water-in-crude emulsions [68-74]. The stability depends on the size of the asphaltene aggregates, and it is believed that the resins act as asphaltene dispersants through an electron donor-acceptor mechanism or by interactions between polar sites on the molecules [75-78]. Since other amphiphilic compounds also have shown to be capable to disintegrate the asphaltenes through polar interactions [79-82], it is likely that also the naphthenic acids will take part in such a mechanism. Investigations of asphaltene-naphthenic acid interactions were carried out by Östlund and co-workers [83]. Using NMR and Near-IR spectroscopy, they found that the tendency of synthetic naphthenic acids to interact with asphaltenes from different North Sea crudes depended on the asphaltene type. Near-IR spectroscopy was also utilized by Auflem and co-workers [84] to follow the disintegration of asphaltene aggregates upon addition of different kinds of synthetic as well as indigenous naphthenic

acids/acid mixtures. The dispersion efficiency was found to depend on the naphthenic acid structure and concentrations.

The naphthenic acids may also interact with inorganic material existing in the crude, like different minerals arising from reservoir rocks. Depending on the system, the compounds may interact through different mechanisms, including polar, acid/base, and ion-binding interactions [85]. At certain conditions, adsorption of organic acids may alter the wettability of minerals completely from water to oil-soluble [86-88], and such particles and particle clusters may cause significant process problems, e.g. when the crude is being refined. The adsorption strength of carboxylic acids onto inorganic surfaces has been shown to depend on the chain length of the acids, according to a study of Zulling and Morse [89]. By measuring the adsorption of  $C_4$  to  $C_{18}$  straight chain fatty acid anion homologous from seawater (adjusted to pH 8) onto several carbonates such as calcite, aragonite, dolomite, and magnesite, they found that  $C_4$ - $C_{12}$  did not adsorb, while  $C_{14}$  -  $C_{18}$  adsorbed onto all surfaces. Within the latter range, the affinity to the surface increased with increasing alkyl chain length. Similar observations are also reported by Spildo and co-workers [90] who studied adsorption of benzoic acid and 4-heptyl benzoic acid on different silica substrates. In hydrocarbon solution, the 4-heptyl benzoic acid gave higher maximum adsorption than benzoic acid. Variations in the surface properties of the silica had no significant effect on the adsorption. Moreover, introduction of water (pH 7) resulted in enhanced adsorption. This effect was explained by adsorption of water molecules on the silica surface, which bridge the acid monomers and the surface together by hydrogen bonds.

### **2.3 Interfacial Behaviour of Naphthenic Acids**

A fundamental feature of amphiphilic molecules is their ability to adsorb onto interfaces and stabilize colloidal structures. For two immiscible liquids in contact, the molecules in the bulk phases are symmetrically surrounded by other molecules so that the molecular interactions in all directions are identical and the sum of all interacting forces is zero. At the interface, however, the molecules are affected by interactions from the two liquid sides, causing a net force towards the respective bulk phases. The molecules at the interface are thus forced towards the bulk phases, which in turn cause a minimizing of interfacial area. The interfacial tension (IFT) is probably the most commonly used parameter to measure the cohesive energy existing at a given interface. It may be

correlated to interfacial energy and the corresponding interfacial area by the following equation:

$$\gamma = \left( \frac{dG}{dA} \right)_{P,T} \quad (2.5)$$

where  $\gamma$  is the IFT,  $G$  is the interfacial Gibbs free energy, and  $A$  is the interfacial area at constant pressure  $P$  and temperature  $T$ . Hence, any factor which lowers  $G$ , like introducing interfacially active compounds, will also cause a lowering of the IFT.

When an interface between acidic oil and water is freshly formed, the IFT is very close to that of the pure liquids. Immediately after this, the interfacially active acid monomers will start to diffuse from the oil bulk towards the interface [91]. When reaching the interface, the IFT will decay until the equilibrium tension value is reached. After that point, since the adsorption of surfactants is a dynamic phenomenon, the flux of adsorption will be equal to the flux of desorption, according to equation 2.6:

$$\frac{d\Gamma_{eq}}{dt} = j_{ads} - j_{des} = 0 \quad (2.6)$$

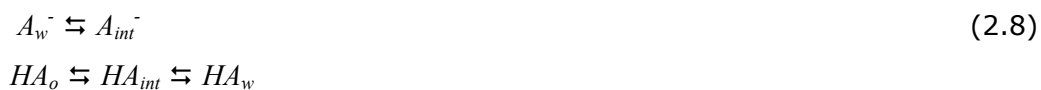
where  $\Gamma_{eq}$  is the interfacial concentration of surfactants at equilibrium,  $t$  is the time and  $j_{ads}$  and  $j_{des}$  are the fluxes of adsorption and desorption, respectively. The period of time  $dt$  during which the equilibrium is obtained may range from milliseconds to hours depending on the surfactant type and concentration [92].

Equilibration of acid monomers at the interface involves relaxation processes where the IFT normally decays exponentially with time, according to the following equation [93]:

$$\gamma = \gamma_{eq} + (\gamma_0 - \gamma_{eq}) e^{-kt} \quad (2.7)$$

The term  $\gamma_{eq}$  represents the interfacial tension at equilibrium,  $\gamma_0$  is the interfacial tension extrapolated to  $t \rightarrow 0$ ,  $t$  is the time, and  $k^{-1} = \tau$  is the relaxation time of the process. The relaxation period is assumed to include processes like reorientation of the molecules in the adsorption layer and solvation/desolvation of the adsorbed species.

At equilibrium, the interfacial concentration of monomers is also linked to the concentrations in the bulk media as illustrated by the following relations:



where  $HA$  and  $A^-$  represent naphthenic acids in undissociated and dissociated states, and the subscripts  $o$ ,  $int$ , and  $w$  indicate oil bulk, o/w interface, and water bulk, respectively. In order to describe the distribution of surfactants between the different phases mathematically, an appropriate adsorption isotherm is required. Adsorption models suiting different surfactant systems have been extensively reported by Fainerman and Miller [94-96].

Due to their tendency to accumulate at w/o interfaces, the naphthenic acids may contribute to stabilization of crude oil emulsions [8, 9, 11, 97]. The interfacial affinity is dependent on conditions like molecular structure, hydrophile-lipophile balance, concentrations, and the pH and the salinity of the aqueous phase. The w/o emulsions are formed during the transportation path from the reservoir to the topside processing facilities due to pressure gradients which cause sufficient mechanical energy to disperse co-produced water as droplets into the crude. Due to the continuous drop in pressure, gases like carbon dioxide are released from the mixture, causing an increase in pH and hence a higher degree of dissociation of the naphthenic acids at the interface. As the dissociated acids possess higher affinity towards the interface than the corresponding undissociated ones, the emulsion stability may increase.

The fact that the IFT decreases with increasing pH may however also be benefited from, like in enhanced oil recovery, where alkaline solutions are injected into reservoirs in order to lower capillary forces and hence mobilize residual oil [98-102]. For very low tensions, several authors [103-107] have reported that the IFT goes through an ultralow minimum at a specific pH value before a steep increase is observed. For acidic model and crude oil-water systems, Rudin and Wasan [106, 107] ascribed this effect to a simultaneous adsorption of ionized and unionized acids, causing an optimum packing of surfactants at the interface. Similar explanations were also given by Touhami and co-workers [108].

### 3 Formation and Inhibition of Metal Naphthenates

#### 3.1 Background

Deposition of metal naphthenates in process facilities is from an operational point of view one of the most serious issues related to the production of acidic crudes. The problem arises from pressure drop and degassing of carbon dioxide during the transport of the fluids from the reservoir to the topside, leading to dissociation of naphthenic acids at the interface between the crude and the co-produced water. Consequently, the naphthenic acids may react with metal cations in the water to form naphthenates. These electrochemically neutral compounds might then start to agglomerate in the oil phase, normally in combination with inorganic materials, and further adhere and accumulate to process unit surfaces. This may lead to costly shutdown periods during which the deposits have to be removed. Metal naphthenate deposition in topside facilities is becoming a common problem in a number of fields where acidic crudes are being processed, including fields in West Africa [1, 109] and on the Norwegian continental shelf [1, 110]. Naphthenate deposits in a separator vessel (West African oil field) during clean out are illustrated in figure 3.1.



*Figure 3.1: Naphthenate deposits in a separator vessel during clean out (left picture). Naphthenate collected from the separator (right picture). Reproduced with permission from OilPlus, UK.*

This chapter deals with the mechanisms which are suggested to be of relevance for metal naphthenate formation and inhibition. In addition, some recent findings on naphthenate composition are reported.

### 3.2 Reaction Mechanisms

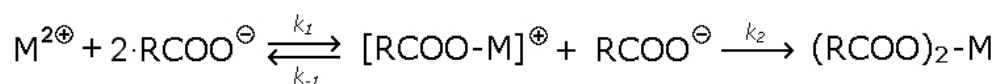
Basically, there are two main approaches to how the naphthenic acids may react with cations to form metal naphthenates. The first and more traditional one is a reaction between water-soluble acids and cations in the aqueous bulk. This was e.g. considered by Havre [111], who studied the reaction between different synthetic naphthenic acids and calcium ions in alkaline aqueous solution using near infrared spectroscopy, and by correlating changes in optical density to the formation and growth of naphthenate particles. However, at normal operational conditions, the fraction of acids showing significant solubility in water only accounts for a limited part of the total amount of naphthenic acids: the major part, consisting of larger molecules, is preferably oil-soluble and will rather tend to accumulate at the o/w interface. According to this, and by taking into account the tremendously large interfaces created when co-produced water is emulsified with the crude oil during the transport from the reservoir to the topside, it is obvious that the contact and the interactions between the compounds *across* the interface may lead to a second approach, i.e. based on interfacial reactions.

Interfacial interactions between fatty acids and metal cations have been a subject of several studies, both for air-water [112-117] and for oil-water systems [118-122]. Wolstenholme [112] postulated the following four types of interactions depending on the pH of the aqueous phase; i) induced dipole-ion interactions between undissociated acids and cations, ii) induced dipole-basic ion aggregate interactions between undissociated acids and metal-hydroxide complexes, iii) ion-basic ion aggregate interactions between dissociated acid molecules and metal-hydroxide complexes, and iv) ion-ion interactions between dissociated acids and free cations. The coulombic forces which induce interactions between dissociated acid monomers and metal cations may either establish an electric double layer or a chemical reaction between the compounds, depending on concentrations, the pH of the aqueous phase, and the valency and the degree of hydration of the metal cations. For systems consisting of water, stearic acid, and calcium ions, Pilpel and Enever [115-117] measured the changes in viscosity of the water surface with time over a range of pH values, temperatures, areas per molecule, and concentrations. They concluded that the interfacial reaction involves the following stages:

- Diffusion of  $\text{Ca}^{2+}$  into the interface;
- Reaction between  $\text{Ca}^{2+}$  and ionized carboxyl groups;
- Subsequent structural reorientation in the mixed calcium stearate and fatty acid film, leading possibly to:
- Further reaction between  $\text{Ca}^{2+}$  and stearate ions due to the removal of steric hindrance.

However, as a result of having two liquid phases, the o/w interfacial affinity will be defined by the hydrophilic-lipophilic balance of the formed product, and not only the water solubility as in the case of air-water surface measurements. Hence, the more hydrophobic compounds will tend to migrate into oil bulk solution rather than remain at the interface.

When naphthenic acids and divalent cations react at the o/w interface, it is reasonable to suppose that the process involves two reaction steps where the acid monomers sequentially bind to one cation, according to the reactions in scheme 3.1:



*Scheme 3.1: Reaction between naphthenic acids ( $\text{RCOO}^-$ ) and divalent cation ( $\text{M}^{2+}$ ), where  $\{k_1, k_2\}$  and  $\{k_{-1}\}$  represent the reaction rate constants of the forward and the reverse steps, respectively.*

The rate of naphthenate formation will thus depend on the stability of the positive monovalent complex. For fast reactions, the occurrence of the intermediate complex might be neglected as the two monomers will bind almost simultaneously. This is likely the normal case for bulk reactions due to high chain-flexibility and free diffusion. However, when the monomers are distributed at an interface, their location is much more fixed, and effects like steric hindrance might thus have a reducing impact on the reaction rate or even counteract a completion of the reaction to 2:1 complexes.

Formation of 1:1 positively charged complexes of carboxylic acids and divalent cations has been considered in several previous studies. By performing electrokinetic potential measurements, Albers and Overbeek [123] observed that water droplets in benzene

stabilized by oleates of various multivalent metal ions were positively charged. Later McLaughlin and co-workers [124] found that divalent cations adsorbed on phosphatidylserin gave rise to positively charged surfaces. Berg and Claesson [125] measured the forces between a mica surface covered by 1:1 eicosylamine and docosanedioic acid and divalent salt solutions of calcium and cadmium. They assumed that a model in which one calcium ion binds one acid monomer is reasonable since the hydrocarbon tail of the amine in between the carboxylic groups brings about a large average distance between the negatively charged species. A more definite conclusion was given by Bloch and Yun [126]. They argued that only 1:1 complexes should be taken into account because the conformation of one divalent cation with two fatty acid chains cannot exist in the surface layer. Kovalchuk and co-workers [127], on the other hand, considered both 1:1 and 1:2 complexes of divalent cations and fatty acids by treating the possibilities theoretically on the basis of the Poisson-Boltzmann equation.

A 1:1 binding of cation and acid may lower the IFT as the surfactants penetrate deeper into the interfacial layer, forming a complex that is neither soluble in the water nor in the oil phase. The electrostatic repulsion between the positively charged species may also be lowered by the co-addition of a considerable amount of anions. On the other hand, if the reaction in scheme 3.1 is fully switched to the right, more hydrophobic compounds are formed which most likely will tend to migrate away from the interface and towards the oil bulk, as also argued by Jennings [128]. Formation of positively charged mono-acid complexes was suggested to be the reason for the permanent reduction of the IFT observed in papers I and III.

The rate of naphthenate formation will, in addition to steric conditions between acid monomers at the interface, also depend on the interfacial affinity of the cations. It is well established that small cations are more strongly hydrated than larger ones. Hence, the hydration water surrounding the cation may create an energy barrier against adsorption towards the interface [129-131] and thus lower the reaction rate, as discussed in papers I-III.



### 3.3 Naphthenate Inhibition

In order to reduce the extent of naphthenate formation, chemical mixtures of various compositions are nowadays commonly injected into the well stream. Naphthenate deposition is a problem only if the aqueous pH exceeds the pKa of the naphthenic acids. Anything which keeps the pH low, like injecting short-chain organic acids, may thus hinder formation of naphthenates [132]. In addition, acid demulsifiers consisting of acetic acid in an aromatic solvent mixture, and non-acid demulsifiers consisting of ethoxylates and alcohol, have shown to reduce deposition significantly [133]. The main mechanism behind naphthenate inhibition by using non-ionic surfactants is likely a competitive process which takes place at the interface. Ethoxylates are highly interfacially active and have normally a much higher affinity towards the o/w interface than naphthenic acids. Consequently, they may occupy the interface and thus hinder the naphthenic acids to reach it and to further react with the cations. In addition, it is reasonable to assume a dilution mechanism to take place. As pointed out earlier, the lifetime of positively charged 1:1 complexes of naphthenic acid and divalent cations is among other factors that depend on the interfacial conditions. Due to lateral steric hindrance, 2:1 complexes of branched structures will be less favoured than more aliphatic ones. A similar effect is also achieved by introducing surfactants with large polar headgroups, as illustrated in figure 3.2. First, this will cause an increased average intermolecular distance between the naphthenic acid monomers. Second, due to inhibitors located in between the acid monomers, the naphthenic acids also have to restructure in the interfacial layer in order to complete the reaction. Consequently, this will slow down the rate of step 2 of the reaction given in scheme 3.1.

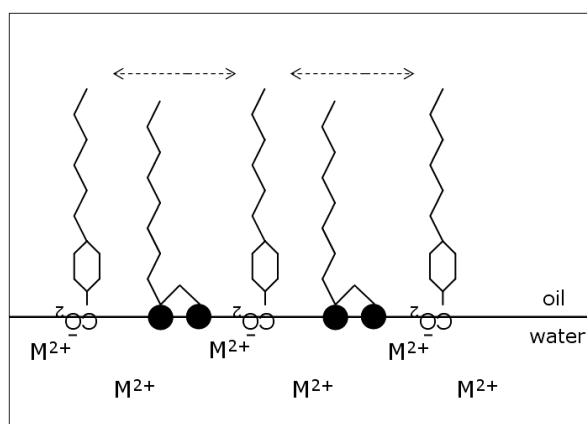


Figure 3.2: Surfactants distributed between the naphthenic acid monomers may hinder/inhibit metal naphthenate to form.

The effect on the reaction between naphthenic acids and divalent cations upon addition of different surfactants used as basis compounds for naphthenate inhibitors was investigated in paper III and paper V.

### **3.4 Naphthenate Composition - Recent Discoveries**

The composition of naphthenic acids found in naphthenate deposits from different sources may differ, as pointed out by Gallup and co-workers [133, 134]. From a characterization study of a soap-sludge from an Indonesian field, they found naphthenate consisting of long-chain fatty acid and sodium. According to the authors, this is contrary to studies from other fields, where naphthenate has shown to comprise predominantly cyclic naphthenic acid structures in combination with calcium. More recently, Baugh and co-workers [135, 136] also demonstrated that naphthenic acids causing naphthenate deposits do not necessarily resemble the majority of the naphthenic acids existing in the crude. By characterizing a deposit sample acquired from an offshore installation located on the Norwegian continental shelf, they found exciting results, indicating that a narrow family of 4-protic acids in the molecular weight range 1227-1235 g/mol is the main contributor to naphthenate deposition. Allegedly, similar observations have also been found by analyzing deposits from other fields, including UK sector and West Africa.

The discovery of the 4-protic naphthenic acids was the motivation behind the work reported in paper IV. In that study, naphthenic acids were isolated from a deposit collected from a West African offshore installation and further characterized by means of FT-IR, NMR, and ESI FT-ICR Mass spectroscopy. The main advantage in the study was the very high mass accuracy (<1 ppm) and the resolving power of the mass spectrometer, allowing for the unambiguous assignment of elemental formulas of singly charged ions (see chapter 4.4.3). Hence, no further analyses were required to prove the elemental formula of the compound. As shown in paper IV, the same narrow acid family discovered previously was also found in the West African sample. Hence, the finding further supports the assumption that the 4-protic acid family is indeed a universal characteristic of oilfield naphthenate deposits.

By taking into account all the different naphthenic acid structures existing in crude oil, it is evident that the 4-protic acids have to possess quite unique physico-chemical properties in order to form naphthenate deposits so selectively. One of these properties, as further disclosed in paper IV, is their very high affinity towards the o/w interface;

---

concentrations of only  $10^{-6}$ - $10^{-5}$  M acid lower the IFT between hexadecane-toluene (9-1vol) and water (pH 9) from 52 mN/m (pure interface) down to 12 mN/m. Compared with findings in paper III, naphthenic acids extracted from crude oil cause, under the same experimental conditions, a lowering of the IFT of less than 30 units at 2000 times as high concentration. Another interesting aspect regarding the 4-protic acids is their potential ability to form polymer-like structures in contact with multivalent cations. As a result of having four carboxylic groups, the acid monomers may be bridged together by the cations to form extended networks. This is in deep contrast to normal monoprotic acids, which are only able to form distinct particles.

Formation of networks, in addition to the large molecular structure, are likely reasons why the calcium product of the  $C_{80}$  naphthenic acids tends to stick onto solid surfaces. The sticky behaviour of calcium naphthenate of the  $C_{80}$  acids compared to calcium naphthenate of a monoprotic acid is well illustrated in figure 3.3. The naphthenates were formed at the oil (toluene) – water (pH 9 and  $CaCl_2$ ) interface and dispersed into the oil phase upon stirring. The sample to the left contains calcium naphthenate of the  $C_{80}$  acids. As indicated, the product tends to adhere as a film at the surface of the glass bottle. This behaviour is very different compared to the calcium naphthenate formed by a monoprotic synthetic naphthenic acid, as illustrated by the sample to the right.

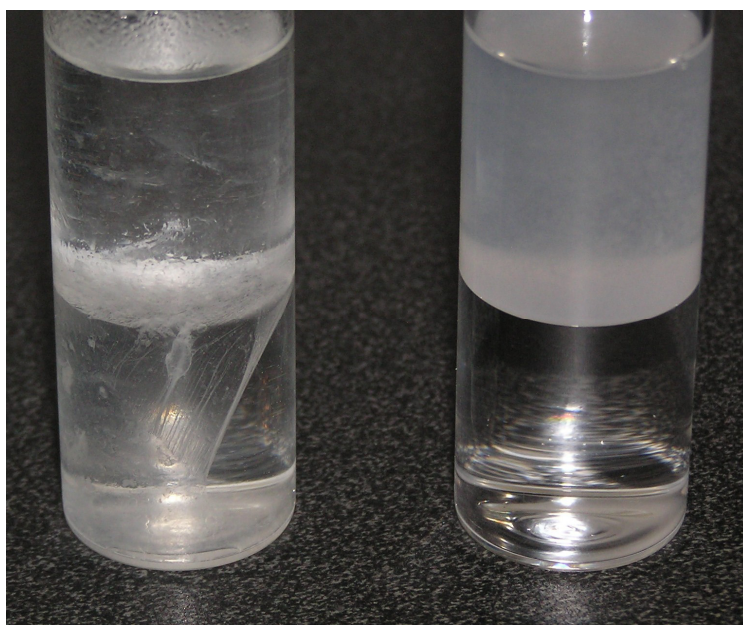


*Figure 3.3: Picture of oil-water systems with calcium naphthenate of the  $C_{80}$  naphthenic acids (sample to the left) and of *p*-(*n*-dodecyl) benzoic acid (sample to the right). The picture clearly illustrates the different consistency of the formed products.*

## 4 Experimental Techniques

The following chapter gives a brief summary of the theory behind the most essential techniques that have been utilized in the experimental work, including physico-chemical techniques (4.1-4.3) and analytical characterization techniques (4.4).

### 4.1 Pendant Drop Technique

Through the past, several experimental techniques have been developed with the purpose to measure surface and interfacial tensions. This includes the Wilhelmy's plate method, different kinds of ring and rotating drop tensiometry, techniques based on capillary rise, method of drop counting etc. The technique mostly used for dynamic IFT measurements nowadays is probably the pendant drop technique, where liquid boundary tension is determined from the shape of drops without any direct contact.

Figure 4.1 displays a sketch of the CAM 200 pendant drop equipment (KSV Instruments) which has been used in the thesis. The instrument includes a CCD video camera with telecentric optics, a frame grabber, and a LED based background light source. The resolution is 512 x 512 pixels and the frame interval is between 40 ms and 1000 s. The LEDs are housed in a reflective sphere which integrates their light and directs it towards the sample. The light is also strobed and monochromatic, and all these features help to assure sharp images.

The pendant drop technique has a number of advantages compared to other techniques developed to determine surface and interfacial tensions. First, very accurate ( $\pm 0.15\%$  or less) boundary tension measurements can be made [137]. Second, the measurements might be made rapidly and, since no direct contact exists, successive measurements may be carried out without disturbing the interface.

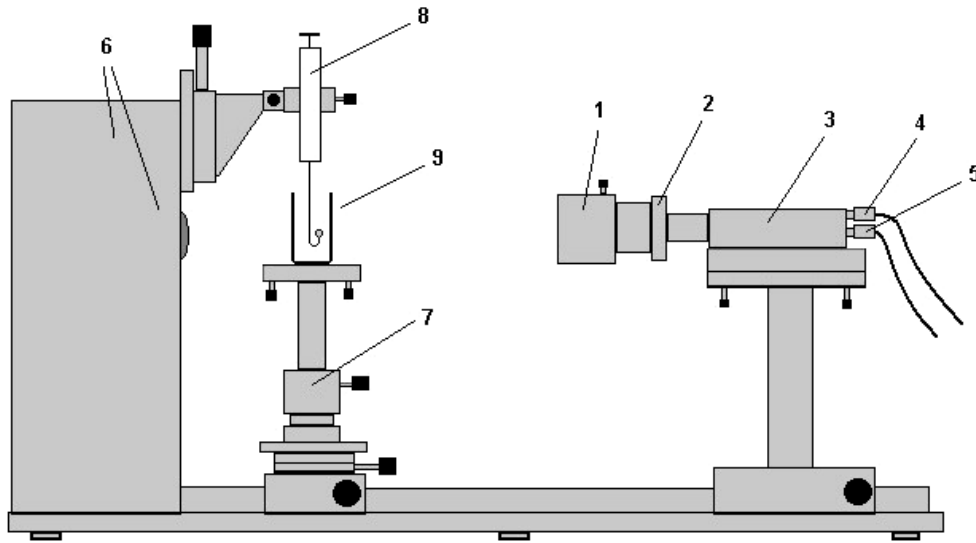


Figure 4.1: A sketch of the CAM 200 equipment. The instrument and the setup include (1) camera lens zoom, (2) lens aperture adjustment, (3) a CCD camera, (4) light synchronizing cable, (5) video out cable, (6) light source and interface unit, (7) stage for sample, (8) syringe with a pendant drop, and (9) transparent liquid chamber.

The first studies involving the pendant drop technique were performed by measuring characteristic drop diameters and interpreting them according to various tables [138]. Later, computer technology has made it possible to obtain direct measurements through drop-shape analysis by co-ordinating the data to suitable mathematical equations. The theory behind the method has frequently been given in the literature [137, 139-141].

A relation between drop shape and interfacial tension may be given by introducing the classical Young-Laplace equation:

$$\Delta P = \gamma \left( \frac{1}{R_1} + \frac{1}{R_2} \right) \quad (4.1)$$

where  $\Delta P$  is the pressure difference across the drop interface,  $\gamma$  is the interfacial tension, and  $R_1$  and  $R_2$  are the radii of curvature. In the absence of external forces other than gravity, the difference in pressure is linear to the ascending forces:

$$\Delta P = \Delta P_0 + (\Delta \rho)gz \quad (4.2)$$

where  $\Delta P_0$  is the pressure difference at a selected datum plane,  $\Delta\rho$  is the difference in the densities of the two bulk phases,  $g$  is the gravity, and  $z$  is the vertical distance between the datum plane and a given point. A sketch of a pendant drop including symbols and dimensions is shown in figure 4.2.

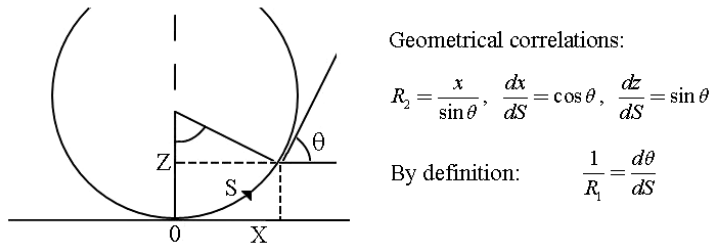


Figure 4.2: A pendant drop including geometrical correlations.

By combining equation 4.1 and 4.2, and by introducing the geometrical correlations given in figure 4.2, the following relation appears:

$$\frac{d\theta}{dS} = \frac{2}{R_0} + \frac{(\Delta\rho)g}{\gamma} z - \frac{\sin \theta}{x} \quad (4.3)$$

In most cases it is appropriate to transform  $x$ ,  $z$ , and  $S$  into the dimensionless coordinates  $x'$ ,  $z'$ , and  $S'$  by dividing by  $R_0$ . This results in the following three dimensionless first-order differential equations:

$$\frac{dx'}{dS'} = \cos \theta \quad \frac{dz'}{dS'} = \sin \theta \quad \frac{d\theta}{dS'} = 2 + \alpha \cdot z' - \frac{\sin \theta}{x'} \quad (4.4)$$

where the term  $\alpha = (\Delta\rho)g \cdot R_0^2 \cdot \gamma^{-1}$  constitutes the shape factor of the pendant drop. Thus, for any pendant drop where the densities of the two liquids in contact are known, the interfacial tension  $\gamma$  can be calculated by iterating the above equations simultaneously.

## 4.2 Langmuir Technique

The Langmuir equipment is one of the most commonly used methods to measure physico-chemical properties of monolayers of water insoluble amphiphiles adsorbed onto air-water surfaces under different experimental conditions. This includes information about molecular area, intermolecular interactions, and film resistance against mechanical rupture, e.g. in the case of fatty acid model systems [142-146] or systems involving indigenous film forming compounds [147-149], as also reported in paper IV.

The amphiphilic molecules are normally spread onto the water surface using an appropriate spreading solvent. The solvent has to possess several properties. First, in order to spread spontaneously, the spreading coefficient of the solvent onto the subphase has to be positive. The solvent must also disperse the film forming molecules well to ensure that the amphiphiles are in a monomeric state at the surface. Moreover, it is essential that the solvent is chemically inert with respect to the film forming material and the subphase, and it has to be adequately volatile so as to evaporate completely within a reasonable short time (minutes).

The Langmuir equipment consists of a shallow rectangular trough in which the liquid subphase is added, and two moving barriers for adjusting the area. The surface pressure is normally measured by means of the Wilhelmy method [150]. A typical experimental setup is illustrated schematically in figure 4.3.

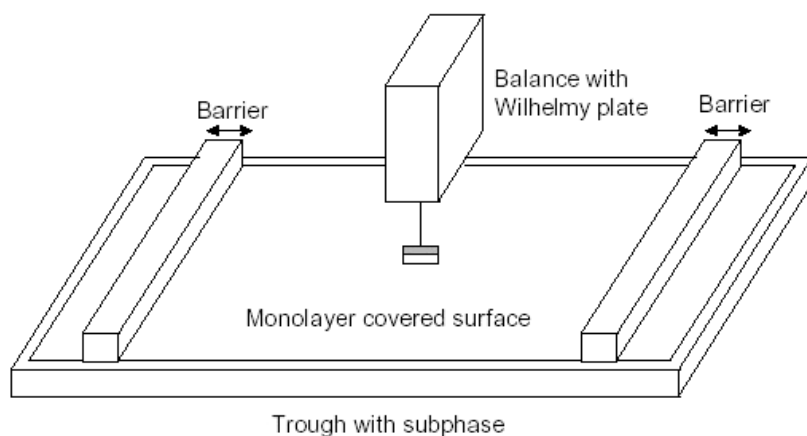


Figure 4.3: A sketch of the Langmuir technique and its main components.

A normal measurement is carried out by placing the barriers out at the edges of the trough (max. area) and by pouring the liquid phase up to the rim. The Wilhelmy plate is hanged on the balance at a distance above the surface so that the plate becomes partially immersed by the liquid. The amphiphiles are then spread onto the surface. After solvent evaporation, the barriers are set to move with a given speed creating continuously smaller area. By sufficient compression, the amphiphiles will start to interact, causing an increase in the surface pressure  $\Pi$  according to equation 4.5:

$$\Pi = \gamma_0 - \gamma \quad (4.5)$$

where  $\gamma_0$  and  $\gamma$  is the surface tension in absence and in presence of a monolayer, respectively. Hence, by plotting  $\Pi$  versus molecular area, the properties of and the interactions in the film as the area gradually becomes smaller can be followed.

At the beginning of the compression, the area per molecule is large and molecular-molecular interactions are only weak. This state is normally referred to as gaseous (G). By a further compression, the film goes then through some kind of liquid state, expanded (LE) or condensed (LC), depending on the compressibility of the monolayer [151]. The liquid condensed state is characterized by relatively low compressibility and area per molecule at a value just moderately higher than the molecular cross section. On the other hand, if the film is highly compressible, e.g. due to irregularities in the hydrophobic moiety causing difficulty in close packing, the state is termed as liquid expanded. If the molecules are able to adhere very strongly to each other through van der Waals forces, the liquid state may be followed by a solid state (S) by compressing the molecules even closer. This state gives rise to a steep linear region in the  $\Pi$ -A isotherm. To attain a solid state, the film forming material has to comprise molecules with very regular structure.

At a specific point, the resistance of the monolayer will reach its maximum and film collapse occurs. This point is observed as a sharp break in the isotherm. In general, the collapse pressure is the highest surface pressure to which a monolayer can be compressed before rupture and fragmentation of the film forming material sets in.

As already noted, the presence of the different phases is strongly dependent on the molecular structure of the amphiphiles. Normally, the transition between a liquid and solid state is detectible only for model systems. A good example of such a system is

---



stearic acid spread onto acidic water. A plot of  $\Pi$  versus molecular area is displayed in figure 4.4, together with illustrations of the different phases.

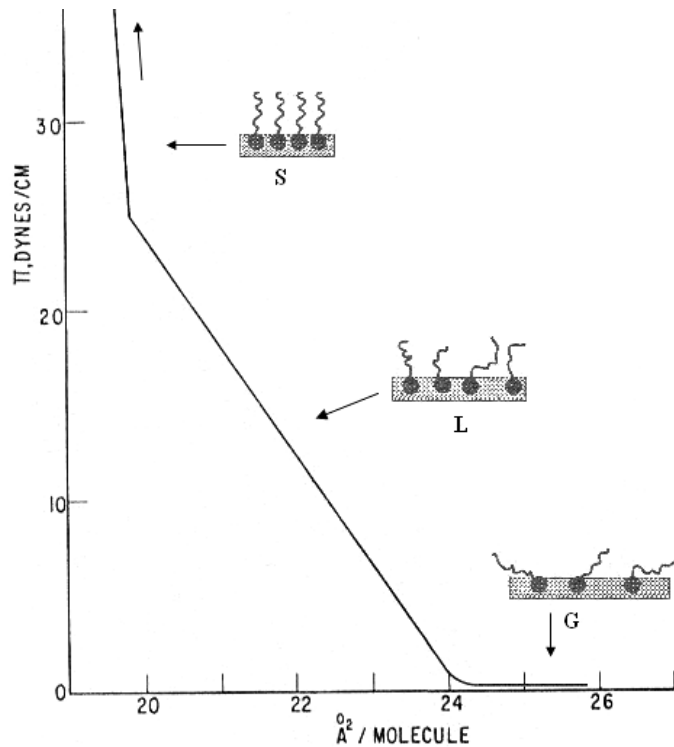


Figure 4.4: Surface pressure-area isotherm for stearic acid onto acidic aqueous surface, illustrating the different film phases.

Recently, instrumental modifications have also made it possible to utilize the Langmuir technique to study properties of surfactant films at liquid-liquid interfaces [152]. By introducing a second liquid phase, the interfacial properties of the film will be a function of the hydrophilic-lipophilic balance of the amphiphiles. In contrast to air-water systems, very hydrophobic compounds will thus be forced into oil bulk solution rather than squeezed together at the interface and, as a consequence, the density of amphiphiles will be lower than at an air-water surface. According to emulsion stability, this will give a more realistic approach.

The liquid-liquid Langmuir system has been used e.g. by Ese and co-workers in their investigations of the film forming properties of interfacially active crude oil fractions [153]. In paper II, the technique was also used to measure the stability of metal naphthenate films formed at the o/w interface.

The main difference between the air-liquid and the liquid-liquid system is the design of the trough. A drawing of the liquid-liquid trough is given in figure 4.5. As illustrated, the barriers have to contain holes to allow the flow of the light phase as the compression of the interface proceeds. The experiments are performed by first pouring the heavy phase into the trough up to level 1. The Wilhelmy plate is then placed onto the liquid as to measure the surface tension before the subphase is covered by the light phase till the plate is totally immersed.

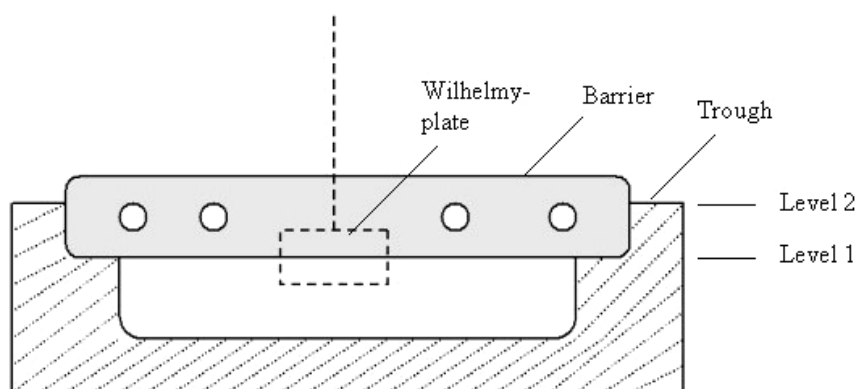


Figure 4.5: Cross sectional drawing of the Langmuir trough for liquid-liquid measurements.

### 4.3 Near Infrared Spectroscopy

The application of near infrared (NIR) spectroscopy as an analytical as well as a physico-chemical characterization tool has during the last decades increased progressively. The increasing popularity is due to several advantages such as speed, simplicity, multiplicity of analysis from a single spectrum, and low sample volumes. In that regard, the use of methods based on fibre optics has extended the area of NIR application.

The NIR spectroscopic region extends from 780 to 2500 nm. When the light is exposed to a liquid sample, the light is transmitted through the liquid, absorbed by the different molecules, and/or scattered by particles or aggregates existing in the solution. One of the main advantages using NIR spectroscopy in colloidal systems is the ability to gain information about the physical state of particles in the solution. Due to scattering, the NIR spectra will display baseline elevation depending on the size and the number of particles. This phenomenon has frequently been benefited from to qualitatively study aggregation or disintegration of crude oil fractions [84, 154], or to estimate the sizes of different kinds of particles [155-158]. In paper V, NIR spectroscopy was used to monitor the formation, growth, and inhibition of calcium naphthenate particles in o/w systems under different experimental conditions.

In the following section, a brief description of the theory behind light scattering in the near infrared region is given. For a more detailed theoretical background, the work of Kerker [159] and Mullins [160] are recommended.

Light scattering may be divided into wavelength dependent and wavelength independent. The first model cover systems where the size of the particles is large compared to the wavelength of the incident light, while the latter may be used if the particles are of comparable sizes to or smaller than the wavelength of the light. If the particle size fits the criteria  $r/\lambda \leq 0.05$ , where  $r$  is the particle radius and  $\lambda$  is the wavelength of the incident light, the particles are so small that the electromagnetic field it experiences is uniform over the particle (according to Rayleigh). By also assuming slightly lossy and dielectric particles, the following relation for the scattering cross section may be introduced:

$$\sigma_{sc} = \frac{2^7 \pi^5 r^6}{3 \lambda^4} \left( \frac{n^2 - 1}{n^2 + 2} \right)^2 \quad (4.6)$$

where  $r$  is the particle radius,  $\lambda$  the wavelength of the incident light,  $\pi = 3.14\dots$ , and  $n$  is the ratio of the dispersed phase to the continuous phase index of refraction. Hence, in the Rayleigh limit, since the scattering is proportional to the 6th power of the radius, fewer but larger particles will contribute more to the scattering than the same mass of smaller ones. The premise for the above expression is that the sample is sufficiently diluted so that no multiple scattering occurs.

Within the Rayleigh limit the light extinction can be considered as a sum of the scattering and the absorbance:

$$\sigma_{tot} = \sigma_{sc} + \sigma_{abs} \quad (4.7)$$

where  $\sigma_{tot}$ ,  $\sigma_{sc}$ , and  $\sigma_{abs}$  are the total, scattering and absorption cross-sections, respectively. The scattering and the absorption cross-sections result in an exponential extinction of the transmitted light:

$$\frac{I}{I_0} = \exp(-N\sigma_{tot}) \quad (4.8)$$

where  $I_0$  and  $I$  are the intensities of the incident and the transmitted light, respectively, and  $N$  is the number of particles. The light intensities and the number of particles in a given total cross-section may be related to optical density  $OD$  by the following equation:

$$OD = \log\left(\frac{I_0}{I}\right) = 0.434N\sigma_{tot} \quad (4.9)$$

As already noted, the effect of multiple scattering is not accounted for in the above equations. In case of multiple scattering, the scattering and absorption cannot be treated separately.

## 4.4 Analytical Characterization Tools

The following section presents briefly the theoretical basis behind the spectroscopic methods used to characterize naphthenic acids acquired from a metal naphthenate deposit in paper IV.

### 4.4.1 FT-IR Spectroscopy

Infrared (IR) radiation refers broadly to that part of the electromagnetic spectrum between the visible and microwave regions. The fraction of the infrared region of most use for structure determination lies between the wavelengths 2.5 and 25  $\mu\text{m}$ , which in terms of wavenumber corresponds to 4000 and 400  $\text{cm}^{-1}$ . Electromagnetic radiation in this region corresponds to the separation between adjacent vibrational energy states in organic molecules. Absorption of a photon of infrared radiation excites a molecule from its lowest, or ground, vibrational state to a higher one. There are two primary types of molecular vibrations: stretching and bending. A stretching vibration is a rhythmical movement along the bond axis such that the interatomic distance is increasing or decreasing. A bending vibration may consist of a change in bond angle between bonds with a common atom or the movements of a group of atoms with respect to the remainder of the molecule without movement of the atoms in the group with respect to one another. For example, twisting, rocking, and torsional vibrations involve a change in bond angles with reference to a set of coordinates arbitrarily set up within the molecule.

Only those vibrations that results in a rhythmical net change in the dipole moment of the molecule are observed in the IR spectrum. The alternating electric field, produced by the changing charge distribution accompanying a vibration, couples the molecule vibration with the oscillating electric field of the electromagnetic radiation. For polyatomic molecules, the vibrations involve complex movement of their constituent atoms. Hence, such molecular vibrations tend to be anharmonic, i.e. non-symmetric vibrations about the equilibrium position. The energy  $E_{vi}$  of the  $i^{\text{th}}$  vibrational mode is given by:

$$E_{vi} = \left( v_i + \frac{1}{2} \right) h c \nu_{0i} - \left( v_i + \frac{1}{2} \right)^2 h c \nu_{0i} x_i \quad (4.10)$$

where  $\nu_{0i}$  is the fundamental vibration frequency of the  $i^{\text{th}}$  mode,  $\nu_i$  is the vibrational quantum number,  $h$  is the Planck's constant,  $c$  is the velocity of light, and  $x_i$  is the anharmonic constant. For diatomic molecules,  $x_i$  is zero and the molecule may be treated as a simple harmonic oscillator.

Because of the non-symmetric vibrations of polyatomic molecules the theoretical number of fundamental vibrations (absorption frequencies) will seldom be observed. Overtones, i.e. multiples of a given frequency, and combination tones, i.e. sum of two other vibrations, increase the number of bands, whereas other phenomena reduce the number of bands. The latter includes fundamental frequencies that fall outside the 4000 and 400  $\text{cm}^{-1}$  region, bands that are too weak to be observed, fundamental vibrations that are so close that they coalesce etc.

#### **4.4.2 NMR Spectroscopy**

The phenomenon of nuclear magnetic resonance (NMR) was first observed in 1946 [161, 162]. Since then, it has grown enormously in power and versatility, conspicuously after the late 1970s with the introduction of Fourier transform (FT) NMR spectroscopy on a routine basis.

The basis for NMR spectroscopy is that some atomic nuclei have a nuclear spin ( $I$ ), and the presence of a spin makes these nuclei behave rather like bar magnets. By immersing the atoms in a static magnetic field ( $B_0$ ) the nuclear magnets can orient themselves in  $2I+1$  ways. Examples of nuclei possessing non-zero spin are  $^1\text{H}$ ,  $^{13}\text{C}$ ,  $^{15}\text{N}$ ,  $^{19}\text{F}$ , and  $^{31}\text{P}$ . The most important in the application of NMR spectroscopy are  $^1\text{H}$  and  $^{13}\text{C}$ , both having spins of  $1/2$ . These nuclei can thus take up one of only two orientations, a low energy orientation aligned with the applied field and a high energy orientation opposed to the applied field. If then an oscillating magnetic field in form of a radio frequency (r.f.) pulse is applied for a short time orthogonal to  $B_0$ , some of the nuclei in the low energy state are tipped into the transverse plane, i.e. to the high energy state. The absorption or emission of electromagnetic radiation by the nuclear spins cause transitions between the two energy states, spin-up and spin down, and the specific frequency at which a given type of nuclei absorbs is given by the Larmor equation:

$$\omega_0 = \gamma \cdot B_0 \tag{4.11}$$

where  $\omega_0$  is the Larmor angular frequency,  $\gamma$  the gyromagnetic ratio of the nuclei, and  $B_0$  the strength of the magnetic field. Since the application of a resonant r.f. pulse affects the spin system, there must subsequently be a process of returning to equilibrium. This involves exchange of energy between the spin system and its surroundings. Such a process is called spin-lattice relaxation, and the rate at which equilibrium is restored is characterized by the spin-lattice or longitudinal relaxation time, T1. The spins do not only exchange energy with the surrounding lattice, but also among themselves. This is generally a faster process than spin-lattice relaxation, and is characterized by the spin-spin relaxation time, T2. The relaxation processes induce a voltage that can be detected by a suitably tuned coil of wire, amplified, and the signal displayed as the free induction decay (FID). This gives rise to characteristic spectra, which are functions of several factors, like the type of nucleus, the chemical environment of the nucleus, and on the spatial location in the magnetic field if that field is not uniform everywhere.

#### **4.4.3 ESI FT-ICR Mass Spectroscopy**

The introduction of electrospray ionization (ESI) in the late 1980s presented a new opportunity for polar molecules in petroleum streams [163]. ESI coupled to high-field Fourier transform ion cyclotron resonance mass spectroscopy (FT-ICR MS) offers a powerful tool for detailed chemical characterization of heteroatomic species in crude oils [164] and crude oil distillates [163] as well as humic materials [165-167].

In ESI, a large positive or negative potential (1000-5000 V) is applied to generate ions, negative or positive. The generated ions are transferred to the ICR cell for excitation and detection of the sample compounds. Positive-ion electrospray (i.e., protonation) ionizes basic nitrogen compounds whereas negative-ion electrospray (i.e., deprotonation) ionizes petroleum acids and weakly acidic, neutral nitrogen compounds but hydrocarbons are not ionized. Hence, polar heteroatomic compounds are detected selectively despite the predominately nonpolar hydrocarbon matrix of petroleum samples, eliminating the need for pre-chromatographic isolation.

In the ICR cell, a high magnetic field is required to resolve and identify the excited sample molecules. The cell has also to be evacuated, typically down to  $10^{-9}$  to  $10^{-10}$  torr, to present the absence of collision. An ion of mass  $m$  and charge  $q$  in a spatially uniform magnetic field  $B_0$  experiences a Lorentz force which causes the ion trajectory to bend

such that it rotates in a plane perpendicular to the magnetic field axis. This unperturbed cyclotron frequency,  $\omega$ , is expressed as:

$$\omega = \frac{qB_0}{m} \quad (4.12)$$

The ions adopting a circular path are then trapped on a detector plate, with a radius of which depends on their mass-to-charge ratio. Hence, a group of ions of a given mass-to-charge ratio will always orbit at the same frequency, regardless of velocity or kinetic energy. From equation 4.12, taking the first derivative with respect to  $m$ , yields:

$$\frac{d\omega}{dm} = \frac{-qB_0}{m^2} \quad (4.13)$$

or

$$\left| \frac{m}{\Delta m} \right| = \left| \frac{qB_0}{m\Delta\omega} \right| \quad (4.14)$$

where  $\Delta m$  stands for the peak width at some fixed fraction of the peak height (usually 50%). Therefore, mass resolving power ( $m/\Delta m$ ) increases in proportion with magnetic field ( $B_0$ ). Hence, increase of high magnetic field increases mass resolving power (and thus mass accuracy) resulting in the improved separation and decrease of peak coalescence. Moreover, the maximum number of trapped ions increases with the square of the magnetic field. Thus, the higher the magnetic field, the more ions can be trapped in the cell.

Initially ion cyclotron rotation is incoherent and any charge induced on one trapping plate will be balanced by a charge on the other plate, resulting on average in a cancellation of signals. Because of this, ion detection is preceded by excitation by means of an applied electric field, which brings the ion packet to coherence. As the ions are excited the radius of orbit increases and the ions eventually generate an ion current on the detector plate. The ion current is then subjected to fast Fourier transform (FT) for extraction of the detected frequencies which are then directly converted to mass-to-charge by calibration.



## 5 Main Results

The following section summarizes the main results from the five papers presented in this thesis. In paper I the pendant drop equipment was utilized to study the effect on the dynamic interfacial tension (IFT) of an oil droplet containing a synthetic naphthenic acid in an aqueous solution (pH 9.0) upon addition of different divalent cations. It was found that the dynamic IFT responded very differently depending on the type of added cation. The effect is due to different cation sizes and thus different degree of cation hydration, which affects the interfacial affinity of the cations and thus their reactivity with the dissociated acid monomers. Paper II reports stability measurements of naphthenate films formed at the o/w interface using the Langmuir technique. Measurements were carried out on three different synthetic naphthenic acids and the same divalent cations as in paper I. The film stability was found to depend on the type of cation, naphthenic acid structure, and the pH of the aqueous phase. In paper III, several more naphthenic acids, model as well as indigenous acids, were introduced to the system reported in paper I. The reactivity across the o/w interface was found to depend on the naphthenic acid structure, type of divalent cation (as discussed in paper I and II), and the pH of the aqueous phase. In addition, an example of how introduction of oil-soluble non-ionic surfactants affects the interfacial reaction is given. Paper IV consists of two parts. The first part covers a characterization study of naphthenic acids isolated from a metal naphthenate deposit, while the second part reports some investigations of interfacial properties of the isolated acids using the pendant drop and the Langmuir technique. The deposit was found to consist of a narrow family of 4-protic naphthenic acids with molecular weights around 1230 g/mol where the determined mass of 1231.0707 g/mol fits the elemental formula of  $C_{80}H_{142}O_8$ . The acids are highly interfacially active and form Langmuir monolayers at the air-water surface with a stability which increases with increasing concentration of calcium ions in the aqueous subphase at high pH. In paper V, near infrared (NIR) spectroscopy was used to monitor the formation and growth of calcium naphthenate particles in o/w systems. The naphthenate particles were formed at the o/w interface and dispersed into the oil phase upon stirring. It was shown that the particle formation and growth depended on the naphthenic acid structure, concentrations of reactants, and the pH of the aqueous phase. Moreover, the effect of adding different oil-soluble surfactants used as basis compounds in naphthenate inhibitors was investigated.

## Paper I

Deposition of metal naphthenates in process facilities is today one of the most challenging separation issues. It is thus of great interest to increase the knowledge of the mechanisms behind naphthenate formation in order to reduce future problems. Since production of crude oil normally also involves co-production and further emulsification of water, it is assumed that the large interfaces created between the two liquids may lead to interfacial reactions between oil-soluble naphthenic acids and multivalent cations in the brine.

In the first paper the pendant drop technique was used to investigate interactions between a synthetic naphthenic acid (p-(n-dodecyl) benzoic acid) and four different divalent cations ( $\text{Ba}^{2+}$ ,  $\text{Sr}^{2+}$ ,  $\text{Mg}^{2+}$ ,  $\text{Ca}^{2+}$ ) across a model o/w interface. The theory behind the technique is described in chapter 4.1. The model oil consisted of 1-9 volume ratio of toluene-hexadecane while a buffer solution of pH 9.0 was used as water phase. The experiments were conducted by forming an oil droplet containing dissolved naphthenic acid in the aqueous solution and by capturing the drop profile (with a camera speed of 1 pic/sec) continuously upon addition of the divalent cations. The changes in IFT were then correlated to plausible reaction mechanisms.

Plots of IFT versus time are given in figures 5.1 for 0.1mM naphthenic acid and (a) 1:1 and (b) 1:3 concentration ratios of acid and cations. The cations were added after 180 seconds. As indicated, this caused a sudden decline in the IFT for  $\text{Mg}^{2+}$ ,  $\text{Ca}^{2+}$ , and  $\text{Sr}^{2+}$ . At the lowest concentration ratio, the drop in IFT was then followed by an almost equal increase with an ascending rate in the order  $\text{Sr}^{2+} > \text{Ca}^{2+} > \text{Mg}^{2+}$ . At higher concentration of cations, the initial drop in the IFT is deeper in all three cases. The curves of  $\text{Ca}^{2+}$  and  $\text{Sr}^{2+}$  then elevate to a level some units above the starting IFT. The curve of  $\text{Mg}^{2+}$ , on the other hand, deviates from the others by showing a permanent decline in the IFT. For both concentration ratios, addition of  $\text{Ba}^{2+}$  does not cause any preliminary drop in the IFT. The curve rises spontaneously and equilibrates at a tension value around 35-40 mN/m, which is about 10-15 units below the value of the pure o/w interface.

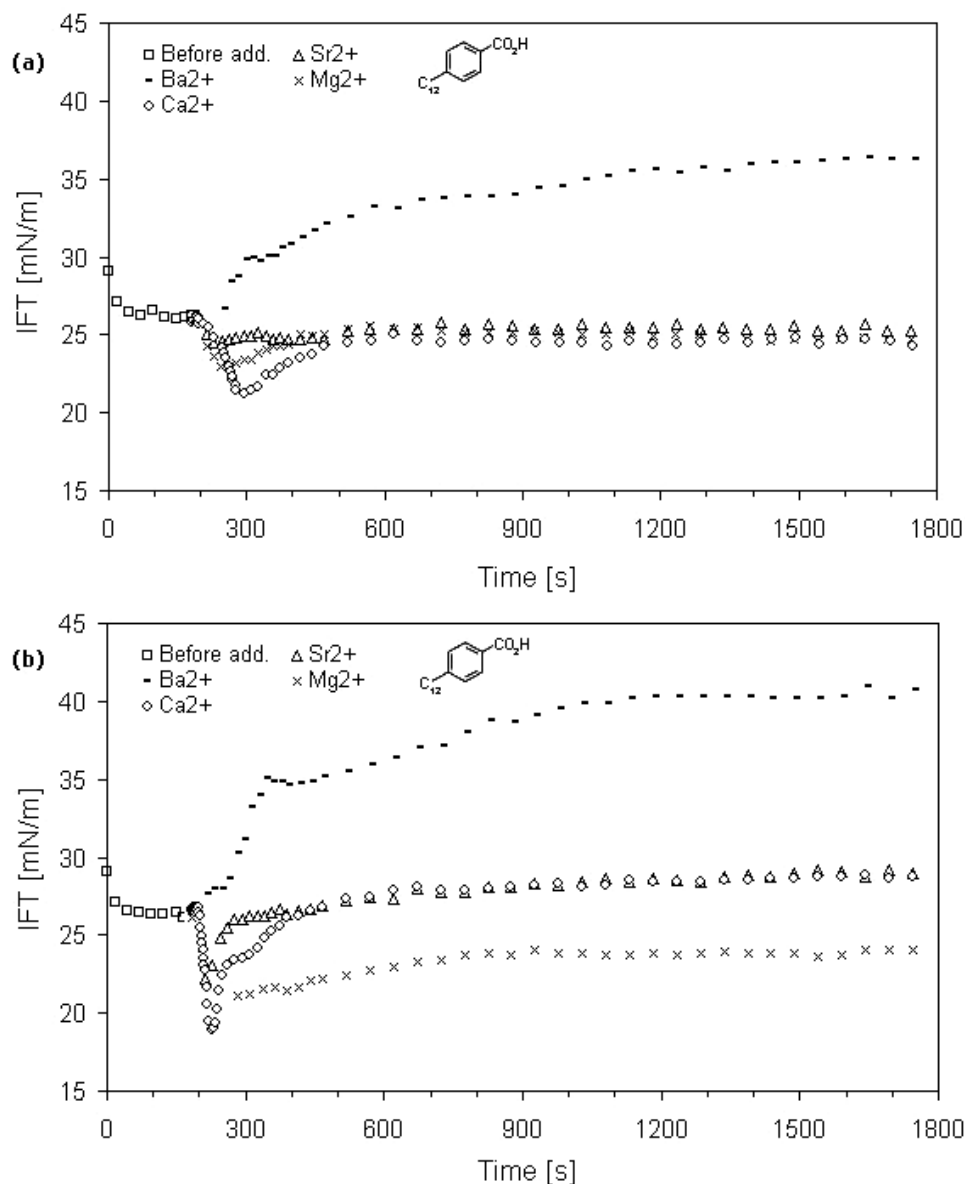


Figure 5.1: Dynamic IFT upon addition of divalent cations for (a) 1:1 concentration ratio of cation and acid, and (b) 3:1 concentration ratio of cation and acid.

In order to explain the observed effects of adding various cations it is necessary to consider the interfacial conditions for the different systems. As discussed in chapter 3.2, it is reasonable to suppose that interfacial reactions between naphthenic acids and divalent cations involve two reaction steps with sequential binding of two acid monomers to the cation. The steep decline in the IFT as observed in all cases except of  $Ba^{2+}$  reflects an increasing density of naphthenic acids at the interface, which is caused by electrostatic attraction forces exerted by the cations upon the dissociated acid monomers. The compounds may then react, according to the equation in scheme 3.1 in

chapter 3.2, to form either 1:1 or 2:1 complexes of acid and cation. The 2:1 complexes are likely less interfacially active. Hence, the monotonous increase in the IFT probably reflects a completion of the reaction, where the complexes migrate away from the interface and into oil bulk solution. As pointed out in section 3.2, the affinity of the cations toward the interface is dependent on the degree of hydration. For the divalent cations under study, the degree of hydration increases in the order  $Ba^{2+} < Sr^{2+} < Ca^{2+} < Mg^{2+}$ , according to decrease in ionic size. Consequently,  $Ba^{2+}$  will likely adsorb more densely at the interface than the other cations, causing a higher converting rate to 2:1 complexes. The reaction is too quick to give any initial drop in the IFT under the present experimental conditions.  $Mg^{2+}$ , on the other hand, is strongly hydrated which brings about a barrier against adsorption and thus a much lower reaction rate. The permanent decline in the IFT is thus probably due to interfacial coverage of the intermediate in scheme 3.1, i.e. magnesium-monoacid complexes, which possess higher interfacial activity than the corresponding 2:1 complexes. Since  $Ca^{2+}$  and  $Sr^{2+}$  are less hydrated than  $Mg^{2+}$ , the monovalent complexes will be converted to 2:1 complexes at a higher rate and, as observed, the curves of IFT versus time ascend steeper.

## **Paper II**

In this paper, the stability of o/w interfacial films of metal naphthenate against compression was investigated using the Langmuir technique with a trough designed for liquid-liquid interfaces. Formation of interfacial films that are resistant against mechanical rupture is an essential property when it comes to the stability of w/o emulsions. Under certain conditions, the naphthenic acids and their salts may contribute to film stabilization.

Three synthetic naphthenic acids with different structure were used in the study. The acids were dissolved in pure n-decane to a concentration of 0.5mM. The water phase consisted of ultrapure water (pH 5.6) or ultrapure water buffered to pH 8.0 by using sodium tetraborate and hydrochloric acid. Chloride salts of  $Mg^{2+}$ ,  $Ca^{2+}$ ,  $Sr^{2+}$ , and  $Ba^{2+}$  were dissolved into the water to a concentration of 10mM.

Figures 5.2-5.4 display some examples of interfacial pressure (IP) – area isotherms obtained from different systems; figures 5.2 (a) and (b) p-(n-dodecyl) benzoic acid at pH 5.6 and 8.0, respectively, figures 5.3 and 5.4 4-n-dodecylcyclohexane carboxylic acid and 5 $\beta$ (H)-cholanolic acid at pH 5.6, respectively. The interface was compressed at a

---

constant barrier-speed of 5 mm/min. Generally, in the beginning of the compression, the IP increases slightly as the barriers move towards smaller area. Gradually, the curves become steeper and the IP increases as the acid monomers in the interfacial layer start to interact. At a given point, however, the curves bend off, which indicates collapse of the film as it is reaching its maximum IP. After this the monolayer is broken and the film forming material is fragmented into bulk solution. A further compression has thus only a small influence on the IP.

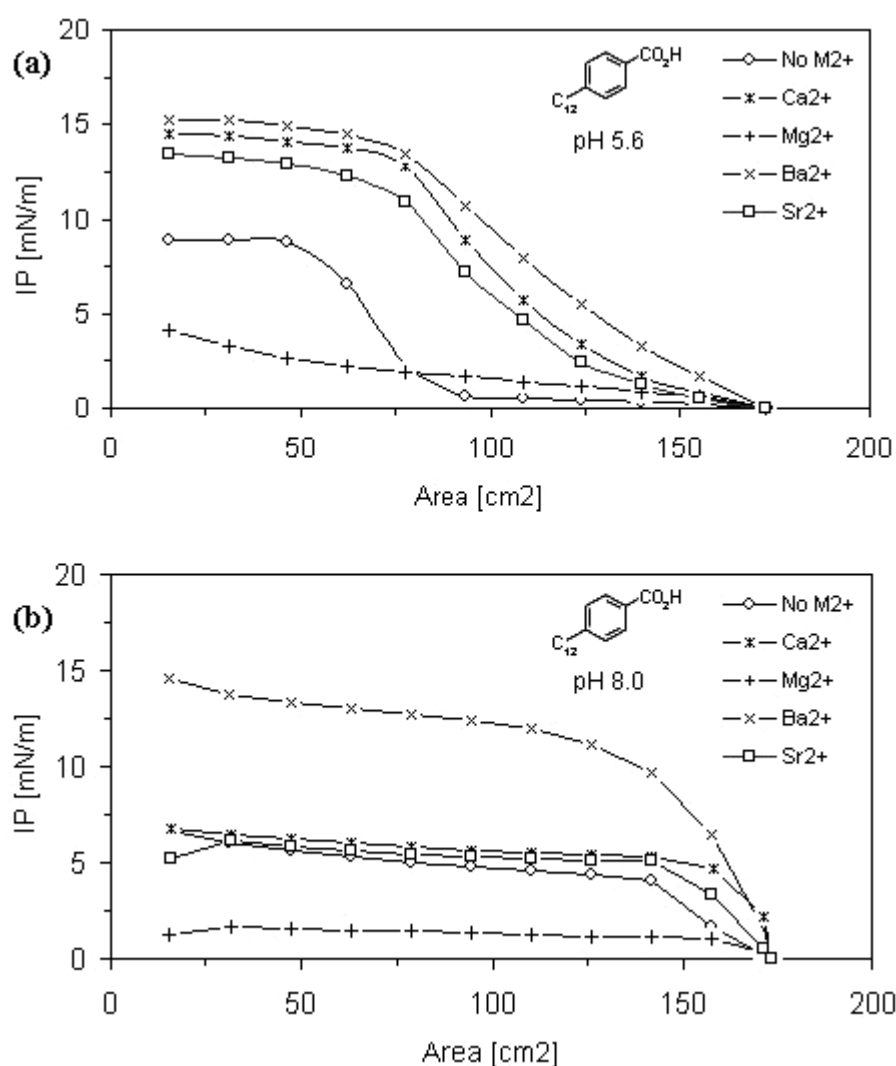


Figure 5.2: Interfacial pressure vs. area for *p*-(*n*-dodecyl) benzoic acid in presence of different divalent cations in the subphase at (a) pH 5.6, and (b) pH 8.0.

As indicated by comparing figures 5.2 (a) and (b), elevating the pH from 5.6 to 8.0 brings about quite different isotherms. First, the increase in pressure sets in at an earlier stage at the higher pH and the curves ascend steeper. Second, higher IP is generally

reached at pH 5.6 than at pH 8.0. All these effects are ascribed to the increase in naphthenic acid dissociation. Dissociated moieties have a larger molecular area than undissociated ones, and repulsion between charged molecules cause a less compressible film. Furthermore, higher degree of dissociation increase the solubility in water, and more of the film forming material is dissolved into the aqueous phase by compression.

Introducing different naphthenic acid structures also affects the shape of the pressure-area isotherms, as demonstrated by comparing figure 5.2 (a) with figures 5.3-5.4. Because of the condensed versus the aromatic ring, 4-n-dodecylcyclohexane carboxylic acid will be less soluble in water than the p-(n-dodecyl) benzoic acid. Hence, less of the film material is squeezed into the subphase and higher IP is reached. 5 $\beta$ (H)-cholanolic acid, on the other hand, has a quite bulky structure due the four fused rings. Consequently, the monomers become less compressible than the two other acids and less stable films are formed. Complementary, the bulky structure may also counteract 2:1 interactions of acids and cations due to large lateral distance between the carboxylic groups.

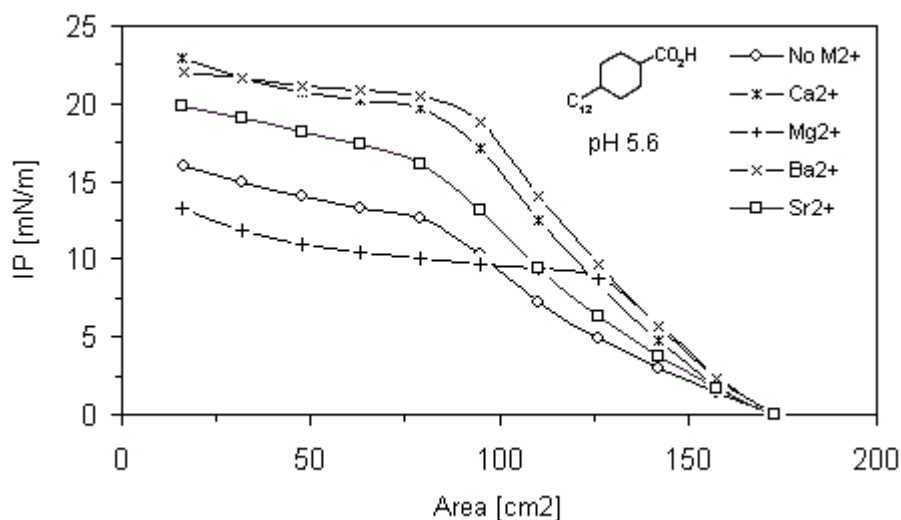


Figure 5.3: Compression isotherms of films of 4-n-dodecylcyclohexane carboxylic acid and various divalent cations at pH 5.6.

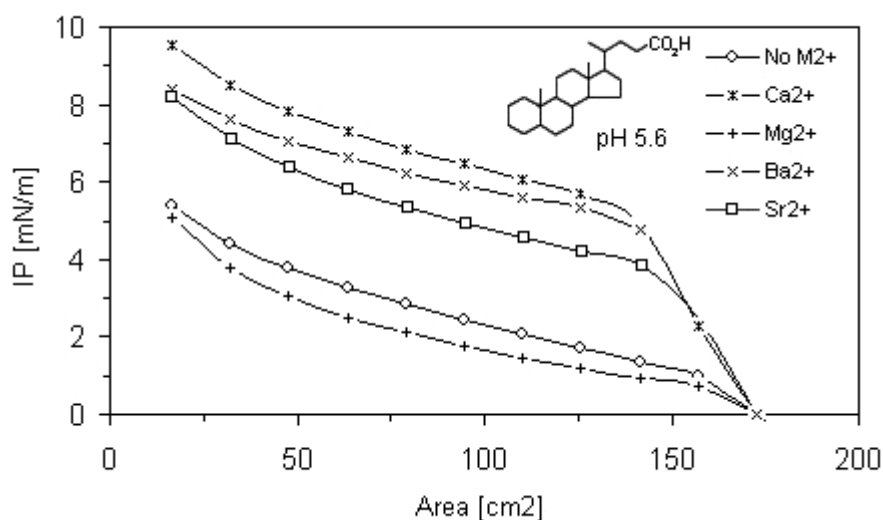


Figure 5.4: Compression isotherms of films of 5 $\beta$ (H)-cholanolic acid and various divalent cations at pH 5.6.

As observed in all figures, the films of Mg<sup>2+</sup> are generally much less stable than the films of the other divalent cations. As also discussed in paper I, Mg<sup>2+</sup> is the smallest and thus the most hydrated cation and the hydration water causes a barrier against interfacial adsorption. Hence, the magnesium ions will only interact slightly with the naphthenic acids, either through formation of 1:1 complexes or by establishing an electrostatic double layer. Accordingly, the film becomes more soluble and less stable against compression.

### Paper III

The third paper is a direct continuation of the work reported in paper I. A total of eight synthetic naphthenic acids and four indigenous acid mixtures were introduced and their interactions with the divalent cations were measured by the same experimental technique. In addition, blends of non-ionic oil-soluble surfactants were added in order to investigate how they affected the local interactions. These molecules are also potential candidates for naphthenate inhibitors.

Figures 5.5-5.7 display examples of dynamic IFT upon addition of divalent cations for two different synthetic naphthenic acids (4-n-dodecylcyclohexane carboxylic acid, fig.

5.5, and 6-heptylnaphthalene-2-carboxylic acid, fig. 5.6), and one indigenous acid mixture acquired from a North Sea crude (fig. 5.7).

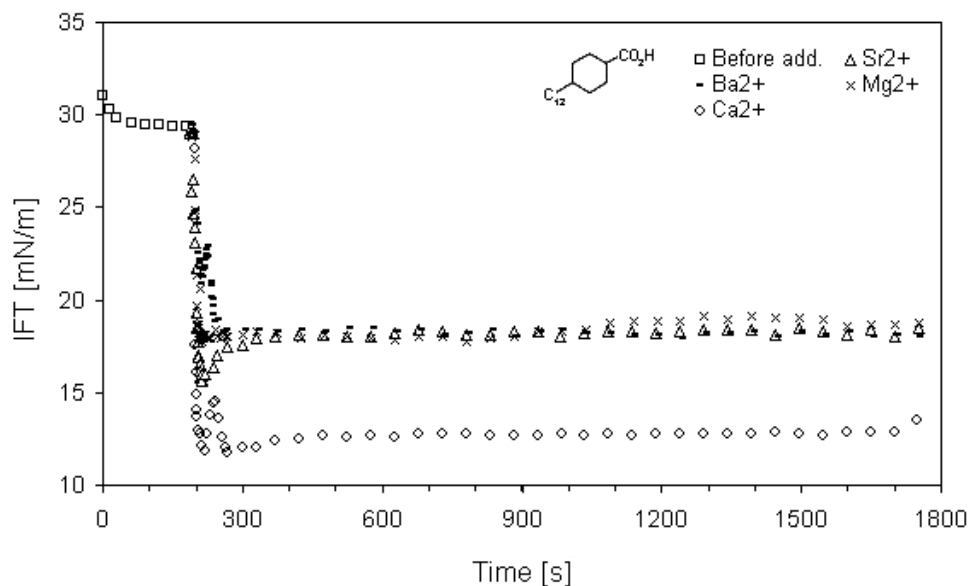


Figure 5.5: Dynamic IFT upon addition of divalent cations for 4-n-dodecylcyclohexane carboxylic acid.

As shown in figure 5.5, the naphthenic acid with a single condensed ring is less interfacially active than the corresponding structure with aromatic ring (reported in paper I) as it equilibrates at a higher tension value even though the concentration is ten times as high. Contrary to the system involving the aromatic acid, addition of all the cations resulted in a permanent decline in the IFT. This indicates coverage of highly interfacially active complexes in all cases. The explanation for this is twofold. First, due to the condensed ring, the acid will penetrate less into the interfacial layer than the acid with aromatic ring, causing a longer interfacial distance between the cations and the carboxylic groups and more well-defined interfaces. Second, due to the conformation of the ring, the lateral distance between acid monomers will also be longer, which may hinder 2:1 complexes of acids and cations to form. The reason for the permanent lowering of the IFT is thus a higher coverage of acid monomers at the interface, which likely are bond in a 1:1 ratio to the divalent cations. Since this effect is caused by the acid structure, all the added cations will influence in a similar way.



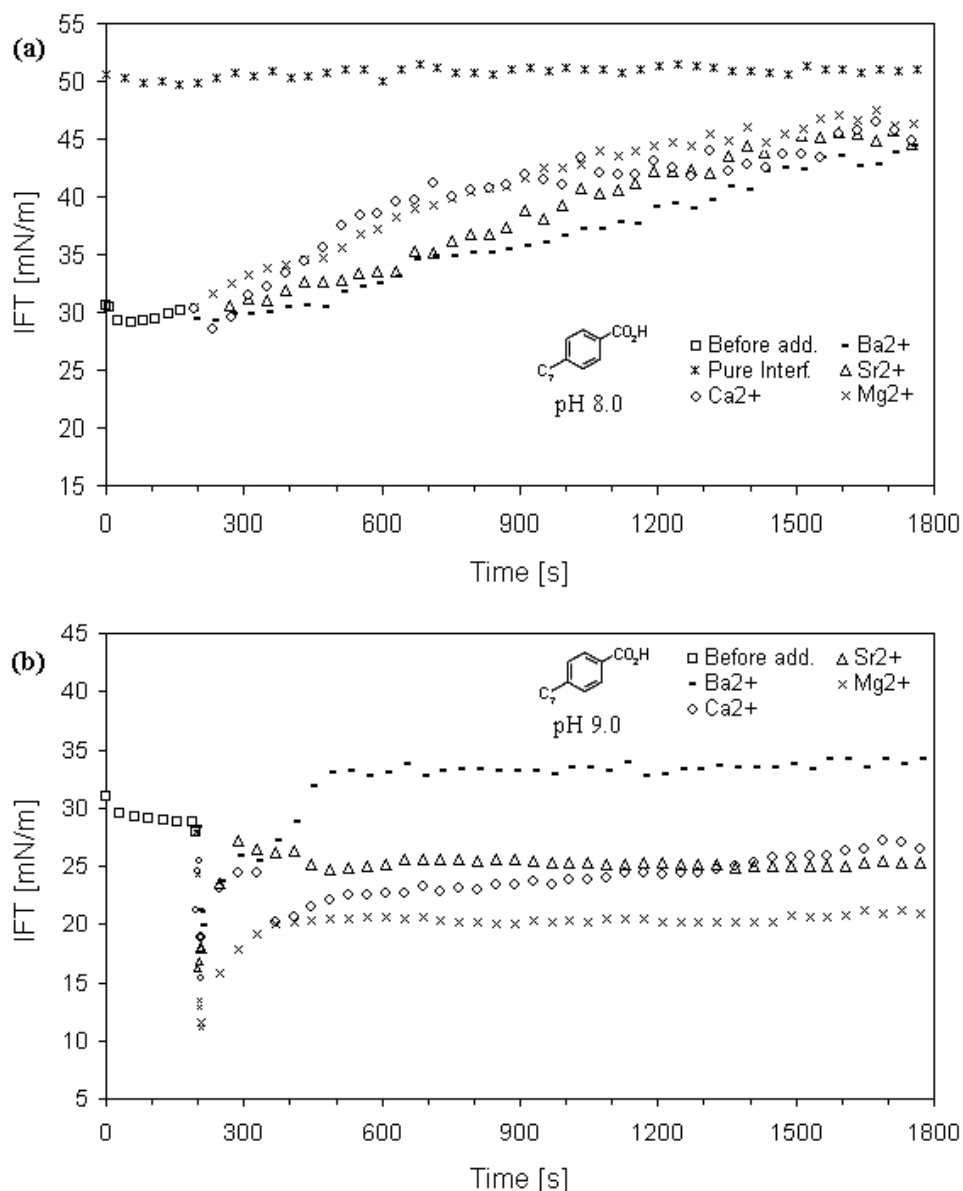


Figure 5.6: Dynamic IFT upon addition of divalent cations for 6-heptylnaphthalene-2-carboxylic acid at (a) pH 9.0 and (b) pH 8.0.

Figure 5.6 shows plots of dynamic IFT upon addition of the divalent cations for an oil-water system of heptylnaphthalene-2-carboxylic acid. Due to high water solubility at pH 9.0 (a), experiments were also performed at pH 8.0 (b) to lower the degree of dissociation. Consequently, higher concentrations of acid and cations were required to obtain the desired starting IFT level of 25-30 mN/m. As in the case of the single aromatic ring structure in paper I, addition of Ba<sup>2+</sup> caused the highest IFT level, followed by Sr<sup>2+</sup>/Ca<sup>2+</sup> and Mg<sup>2+</sup>. However, because of a lower degree of dissociation and hence longer lateral distance between charged carboxylic groups, the rate of formation of 2:1

complexes becomes lower. This is the reason why an initial decline in the IFT now is observed also in the case of  $\text{Ba}^{2+}$ .

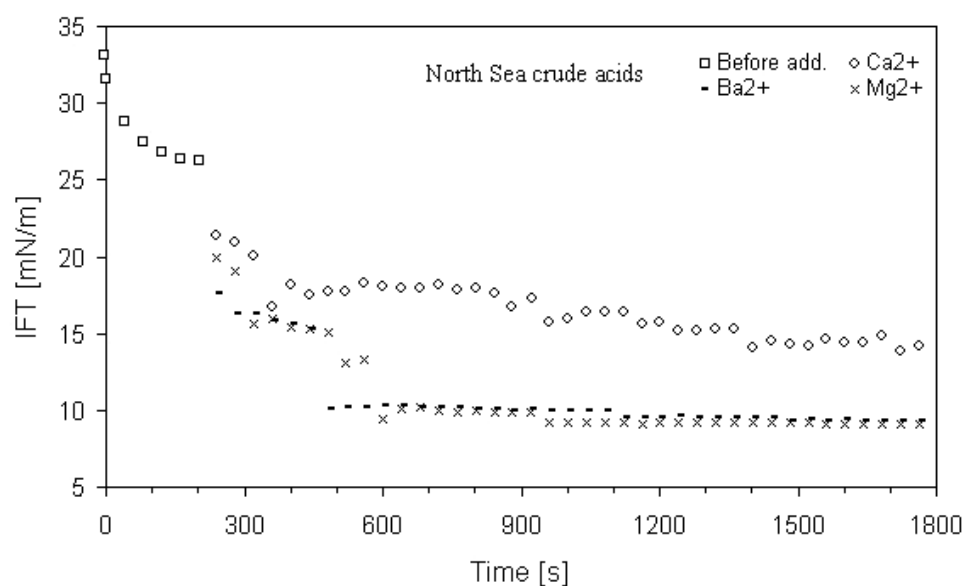


Figure 5.7: Dynamic IFT upon addition of divalent cations for naphthenic acids extracted from a North Sea crude.

Results from measurements performed on one of the acid fractions extracted from a North Sea crude are given in figure 5.7. After addition of cations, the IFT shows a step-wise progress until it equilibrates 10-15 units below the starting value. The step-wise curve is likely a result of a combination of two processes. First, since the mixture is polydisperse, small molecules will be the first ones to reach the interface due to higher diffusion rate. Gradually, however, the smallest molecules will be replaced by larger molecules. Due to their higher water solubility, the low-molecular weight species will cross the o/w interface and dissolve into the aqueous phase. A stepwise adsorption of monomers to the interface might thus occur. Second, for polydisperse acid mixtures, more dynamic processes are taking place at the interface than for monodisperse acids and a longer time is normally needed for the system to equilibrate. The sequential steps in IFT might thus refer to temporary states of equilibrium before the final equilibrium is reached as the curves flatten out. At this state, the interface is covered by a film comprising more interfacially active molecules in combination with the divalent cations.

## Paper IV

Deposition and accumulation of metal naphthenates in process facilities is a huge problem for many companies producing highly acidic crudes. Recent discoveries from analyses of deposits from various fields have indicated that the deposition mainly is caused by a narrow family of 4-protic naphthenic acids with high molecular weights. The motivation behind the work reported in the fourth paper has been to check this finding by analyzing a deposit sample acquired from a West African field. In addition, the extracted acids were introduced to systems with oil and water in order to investigate how they behave interfacially under different conditions. The interfacial properties are of essential importance when it comes to the formation of metal naphthenates.

### Characterization study

The naphthenic acids bound as naphthenates were isolated and then characterized by means of IR, NMR, and high resolution ESI ICR mass spectroscopy. The techniques are described in chapter 4.4. Figure 5.8 displays NMR spectra of the sample. Typically, NMR spectra of petroleum and petroleum fractions contain broad overlapping peaks due to the complexity and high number of isomers in the samples [168-170]. However, for the fraction isolated from the deposit, the  $^{13}\text{C}$ -NMR spectra show a single peak in the carboxylic acid region and well resolved peaks in the aliphatic region. The  $^1\text{H}$ -NMR spectra show four distinct regions, indicating the type of hydrogen. Neither spectra show any sign of aromatic carbon.

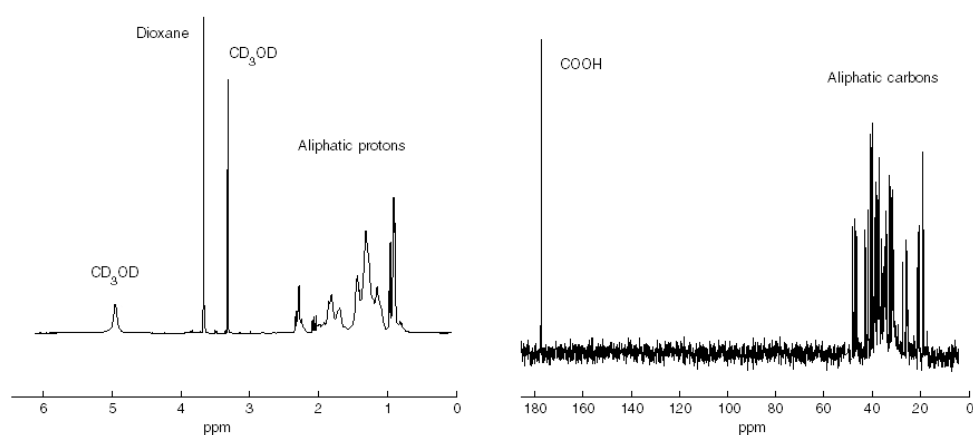


Figure 5.8:  $^1\text{H}$  (left) and  $^{13}\text{C}$  (right) NMR spectra of the naphthenic acid sample.

The indication from the NMR study that the sample comprises well-defined structures was further supported by the obtained ESI FT-ICR MS spectrum given in figure 5.9. As indicated, the sample is totally dominated by molecules with molecular weights around 1230 g/mol. Because of the ultrahigh resolution of the mass spectrometer, the elemental formula of the molecule given by the main peak in the spectrum could be found directly without any further verification. The molecular weight of 1230.0627 amu is consistent with the ion  $C_{80}H_{141}O_8^-$ , which refers to a compound with the elemental formula of  $C_{80}H_{142}O_8$ .

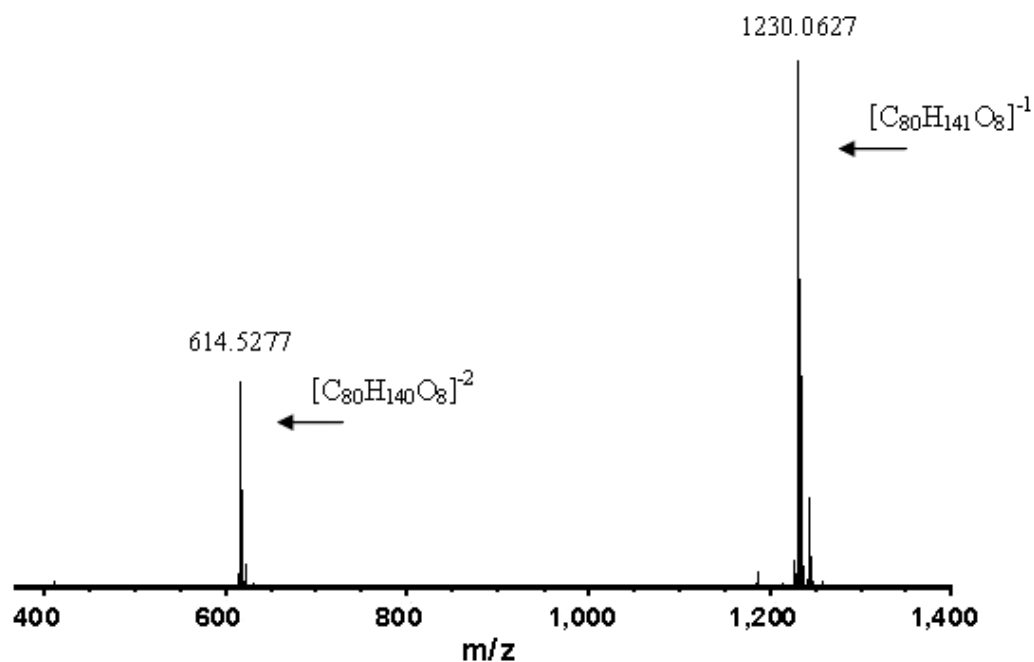


Figure 5.9: ESI FT-ICR MS spectrum of the naphthenic acid sample.

A common way to calculate average molecular weight based on NMR data is to integrate the peaks in the spectra to find the molar ratios between the different elements. For the NMR spectra in figure 5.8, this gives  $C/O = 10.2$  and  $C/H = 0.58$ . Moreover, for fatty acids, it is normal to assume one carboxylic group per molecule since monoprotic acids generally are predominating. For the naphthenic acid sample, this gives an average molecular weight of 313 g/mol, which is far below the weight determined in the MS spectrum. However, assuming four carboxylic groups per molecule, the molecular weight is 1252 g/mol, which is close to the MS results. Hence, this indicates that the  $C_{80}H_{142}O_8$  compound is an acid comprising four carboxylic groups. The peak appearing at 614.5277 amu in figure 5.9 represents double-charged molecules, i.e. deprotonation of two carboxylic groups ( $z=2$ ). The results are in good agreement to the findings recently

reported by Baugh and co-workers [135, 136]. Hence, their suggestion that the 4-protic naphthenic acids are a general characteristic of naphthenate deposits is further supported.

### **Interfacial properties**

The second part of the study focused on the interfacial behaviour of the isolated C<sub>80</sub> naphthenic acids. Measurements of o/w interfacial activity were carried out using the CAM200 pendant drop equipment while monolayer properties at different conditions were investigated by means of the Langmuir technique.

#### Interfacial (o/w) activity

The naphthenic acid was dissolved in toluene and diluted by n-hexadecane to a 1-9 volume ratio. The naphthenic acid concentration was calculated using the molecular weight of 1230 g/mol. The aqueous phase consisted of ultra-pure water (pH 5.6), phosphate buffer of pH 7.0, or borate buffer of pH 9.0. In figure 5.10, dynamic IFT is plotted for systems of (a) 0.010mM naphthenic acid and different pH levels, and (b) pH 9.0 and different naphthenic acid concentrations. As indicated in figure (a), the IFT becomes lower the higher the pH as more carboxylic groups dissociate at the interface. The rate of the IFT decrease is also clearly concentration dependent, as observed from the plots in figure (b); by lowering the concentration of naphthenic acid from 0.010 mM to 0.0075 mM and further to 0.005 mM, the slope of the descending curve (-dy/dt) gradually becomes smaller although the IFT in all cases is lowered about 40 units compared to the pure o/w interface. At the lowest concentration level, on the other hand, the IFT decreases only a few units during the time under consideration.

As the coverage of the interface is more complete by naphthenic acids, the curves slightly bend off. This is likely due to intermolecular interactions and reorientation of the molecules in the interfacial layer, which affect the rate of equilibration. For longer observation times, the curves representing the three highest concentrations suddenly flatten out and show further an almost constant IFT. This appears at a well-defined equilibrium IFT value ( $\sim 12$  mN/m), as illustrated by the overlapping curves. Well-defined equilibrium tensions are rarely found for naphthenic acids, but have frequently been observed for larger molecules, such as peptides [171, 172]. The anomalous behaviour is

likely a result of the high molecular weight and the four carboxylic groups, making the  $C_{80}$  acid structure much more extensive than for normal monoprotic naphthenic acids.

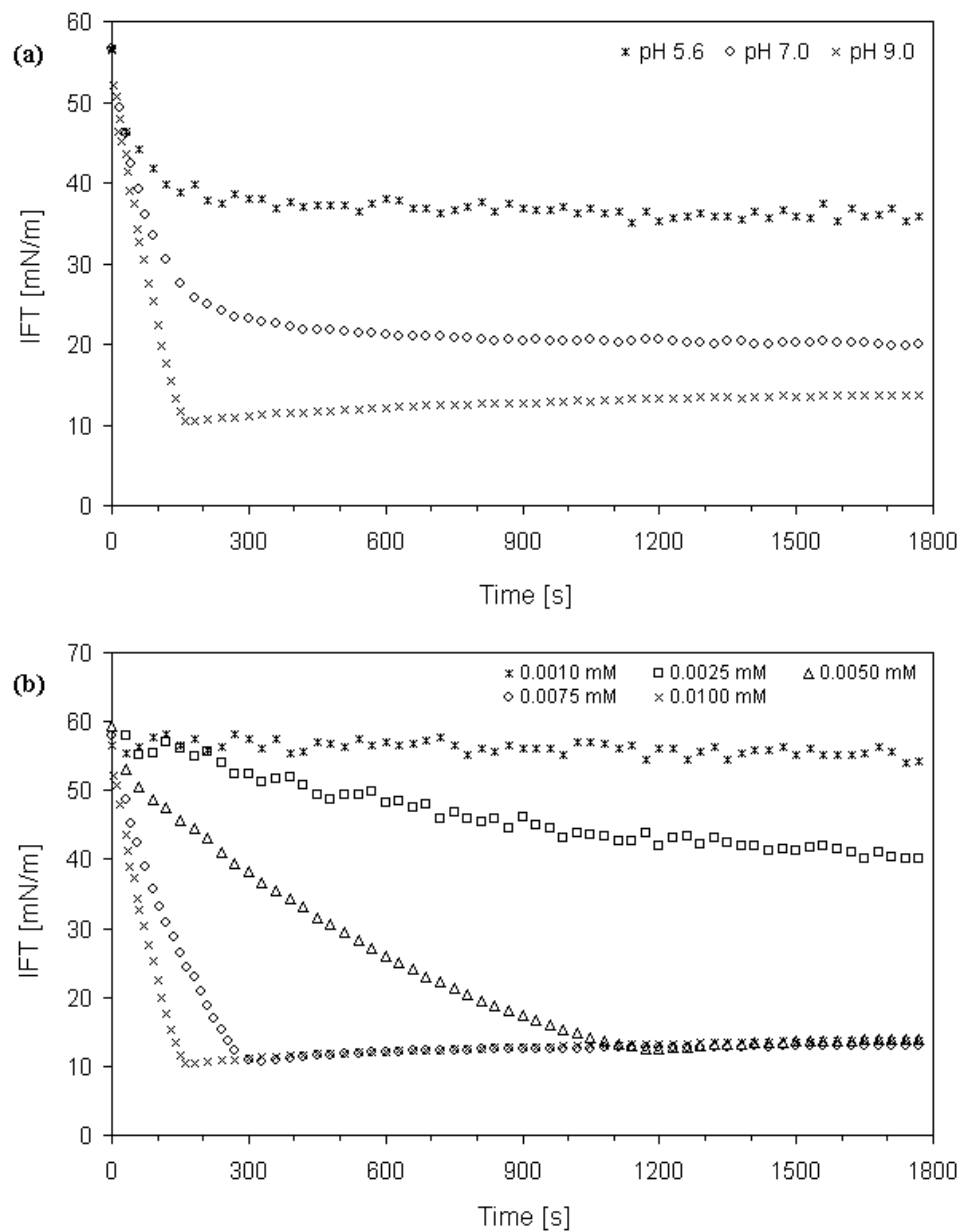


Figure 5.10: Dynamic IFT for an o/w interface of the  $C_{80}$  naphthenic acids as a function of (a) pH (0.010mM acid), and (b) concentration (pH 9.0).

### Langmuir monolayer properties

Toluene was used as spreading solvent for the naphthenic acid. The naphthenic acid concentration was calculated using the molecular weight of 1230 g/mol. The subphase consisted of ultrapure water (pH 5.6), pH adjusted water using hydrochloric acid (pH 2.3) and sodium hydroxide (pH 11.6), or buffered water using sodium borate and hydrochloric acid (pH 9.2). Calcium chloride was dissolved at different concentrations. The experimental procedure is described in chapter 4.2.

Surface pressure-area isotherms at different pH levels of the aqueous subphase are given in figure 5.11 (a). As observed, the surface pressure (SP) is reaching a higher value by elevating the pH. This is a result of electrostatic repulsion between dissociated carboxylic groups. At pH 2.3, 5.6, and 11.6, the pH effect is rather small with regard to changes in area/molecule when the pressure starts to increase. In the case of pH 9.2, on the other hand, the rise in pressure sets in at an earlier stage. This is due to the ionized carboxylic groups, which, due to electrostatic repulsion, require larger area than the corresponding molecules in an undissociated state. The reason why this effect is missing at pH 11.6 is most likely because of dissolution into water; at such high pH, the naphthenic acid monomers become completely dissociated, resulting in an enhanced water solubility and hence loss of initial film material. The surface concentration of naphthenic acids will thus be lower than at the beginning of the experiment and, accordingly, the obtained molecular area will be lower. The considerable solubility in water at high pH is also well illustrated in figure 5.11 (b), where relative area loss ( $A/A_0$ ) is plotted versus time at a constant surface pressure of 10 mN/m. As indicated, the lower the pH the more stable is the film. Even at slightly alkaline solution, the film becomes very unstable and approximately 60% of the initial area is lost within 10 minutes.

The film stability at high pH is increased by adding calcium ions to the subphase, as demonstrated by the stability isotherms at pH 11.6 in figure 5.12 (b). The dissociated molecules may thus react with  $\text{Ca}^{2+}$  at the surface to form less soluble calcium naphthenate. Hence, as illustrated by the pressure-area isotherms in figure 5.12 (a), less of the film material is lost due to dissolution and the onset area increases. A notable observation in figure 5.12 (b) is the uneven shapes of the curves, especially in the case of  $10^{-2}$  M  $\text{CaCl}_2$ . As noted in chapter 3.4, because of having four reactive carboxylic groups, the monomers may be cross-linked together by the divalent cations to make The

---

film stability at high pH is increased by adding calcium ions to the subphase, as demonstrated by the stability isotherms at pH 11.6 in figure 5.12 (b). The dissociated molecules may thus react with  $\text{Ca}^{2+}$  at the surface to form less soluble calcium naphthenate. Hence, as illustrated by the pressure-area isotherms in figure 5.12 (a), less of the film material is lost due to dissolution and the onset area increases. A notable observation in figure 5.12 (b) is the uneven shapes of the curves, especially in the case of  $10^{-2}$  M  $\text{CaCl}_2$ . As noted in chapter 3.4, because of having four reactive carboxylic groups, the monomers may be cross-linked together by the divalent cations to make

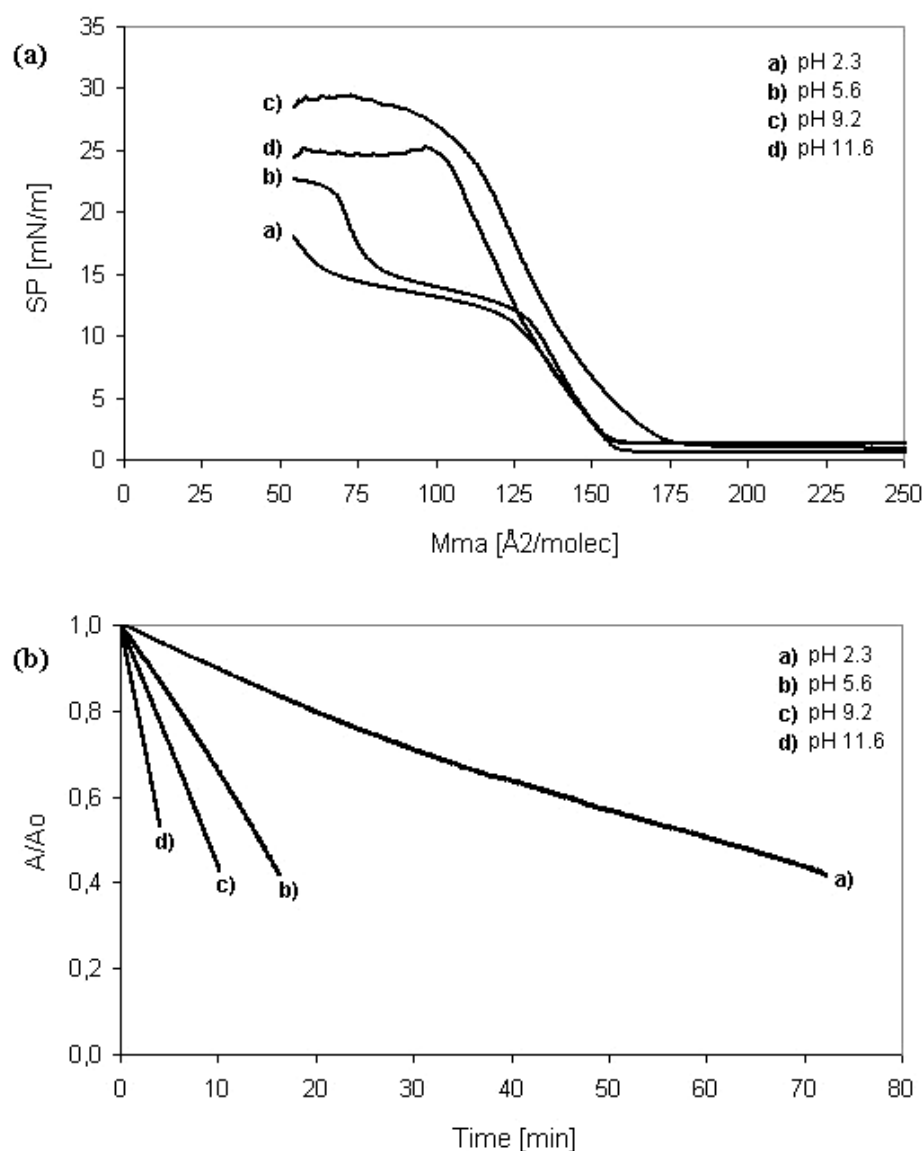


Figure 5.11: Langmuir monolayers of the  $C_{80}$  naphthenic acids at different pH levels, (a) compression isotherms, and (b) stability isotherms at constant surface pressure of  $10 \text{ mN/m}$ .



some kind of polymeric structure. A likely reason for the uneven shape is thus a subsequent fragmentation of the network of acid monomers and calcium ions forming the naphthenate network layer.

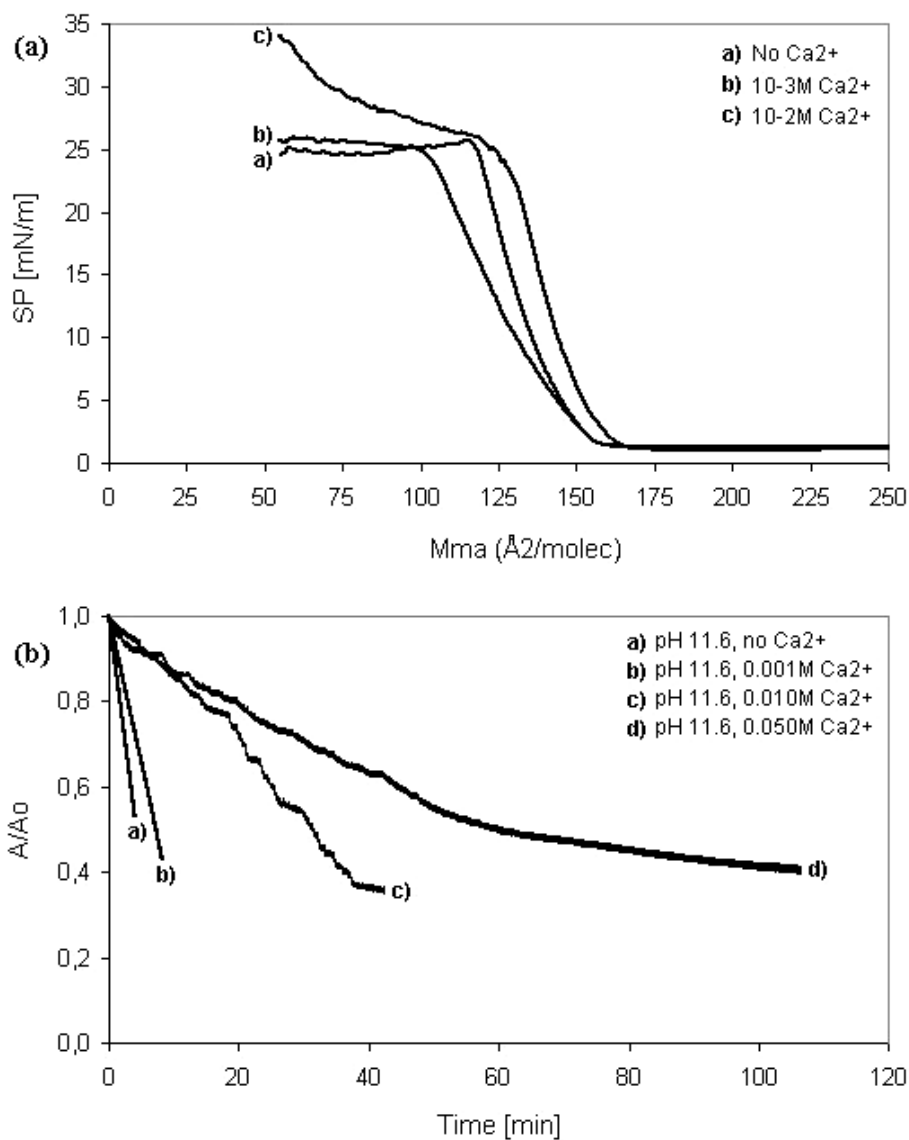


Figure 5.12: Langmuir monolayers of the  $C_{80}$  naphthenic acids and  $Ca^{2+}$  at pH 11.6, (a) compression isotherms, and (b) stability isotherms at constant surface pressure of 10 mN/m.

Considering the undissociated state of the naphthenic acids, the surface pressure starts to increase at a molecular area of about 160 Å<sup>2</sup>/molecule. The high area reflects the extensive molecular structure of the  $C_{80}$  acids, comprising four surface-active headgroups. The carboxylic groups alone do however not cover the entire area, as the

molecular area of saturated monomeric long-chain fatty acids is around  $20 \text{ \AA}^2/\text{molecule}$  [150]. Hence, it is likely that the carboxylic groups are separated by hydrocarbon units.

## **Paper V**

In paper V, a new experimental setup based on near infrared (NIR) spectroscopy for online studies of formation, growth, and inhibition of calcium naphthenate particles in o/w systems was reported. The aim of the work was to investigate how particle formation and growth depended on different conditions such as the naphthenic acid structure, the concentrations of reactants, and the pH of the aqueous phase. Moreover, different oil-soluble surfactants, which are basis compounds for metal naphthenate inhibitors, were added in order to study their effect on the particle formation. In paper I-III, these effects were investigated by means of interfacial tension measurements correlated to interfacial reactions.

The naphthenic acids and the oil-soluble surfactants were dissolved in toluene at different concentrations. The water phase consisted of ultra-pure water or borate buffer solutions of pH 8.0 and 9.0. A 1:1 volume ratio of water and toluene containing naphthenic acid was then poured into a glass bottle to a total volume of 80 ml. The oil and the water phase were continuously stirred according to the experimental setup illustrated in figure 5.13. By injecting a solution of dissolved  $\text{CaCl}_2$  into the aqueous phase, the reaction between dissociated naphthenic acids and  $\text{Ca}^{2+}$  at the interface was initiated. The naphthenate particles formed at the o/w interface were then dispersed into the oil bulk solution upon stirring and the changes in optical density (OD) caused by light-scattering by particles were continuously monitored using a fibre optic NIR sampling probe. Since only the scattering contribution was of interest, the reference spectrum of pure toluene was subtracted from all the naphthenate solution spectra.

To follow the formation and growth of particles as a function of time, the change in OD at one specific wavenumber ( $9500 \text{ cm}^{-1}$ ) was considered. The square root of the OD was then plotted versus time. The reason for plotting the square root of OD is that the OD, within the Rayleigh regime ( $r/\lambda \leq 0.05$ ), depends on the sixth power of the particle radius and thus the square of the particle volume. Hence, change in the square root of OD can serve as a measurement of change in the particle volume.

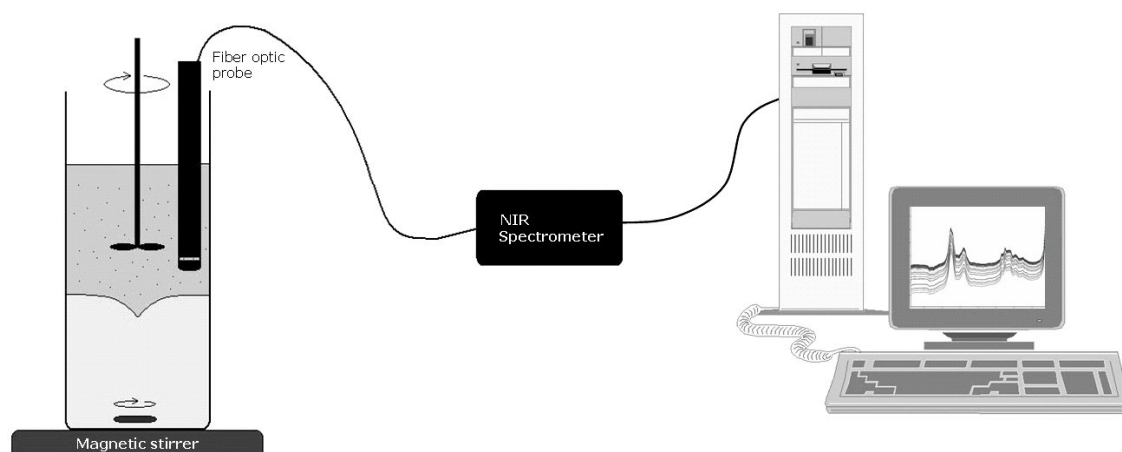


Figure 5.13: A sketch of the experimental setup used in the NIR spectroscopic study.

Figures 5.14-5.15 show plots of square root of OD vs. time for naphthenate solutions consisting of particles of a single naphthenic acid obtained at different acid concentrations (fig. 5.14) and particles of different naphthenic acid structures obtained at pH 9.0 (fig. 5.15). As clearly indicated in figure 5.14, the OD increases more rapidly the higher the concentration of naphthenic acid since more particles are formed at the interface. As shown in figure 5.15, the naphthenic acids with aromatic rings are also forming particles at a higher rate and with a larger volume than the acid with condensed ring. The reason for this is the higher interfacial affinity which causes a higher density of acid monomers at the o/w interface. Due to the aromatic rings and the  $\pi$ -bonds between them, the acid monomers will pack more densely at the interface than the acid with condensed ring, favouring interfacial formation of 2:1 complexes of acid and  $\text{Ca}^{2+}$ . Monomers with two aromatic rings will pack even denser than monomers with only one ring, causing a higher reaction rate as demonstrated by comparing the slopes of the ascending curves at the beginning of the experiments. These findings are in good agreement to what observed and discussed in paper III.

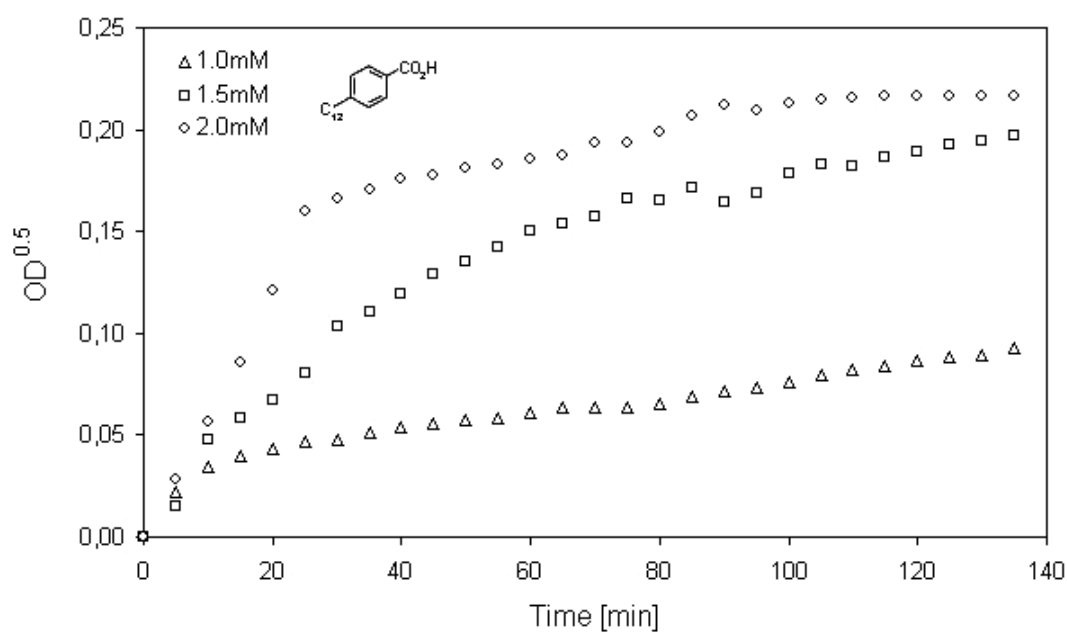


Figure 5.14: Square root of OD vs. time for naphthenate solutions containing particles of the aromatic single-ring naphthenic acid, obtained at different acid concentrations. The concentration of  $\text{Ca}^{2+}$  is twice the concentration of acid.

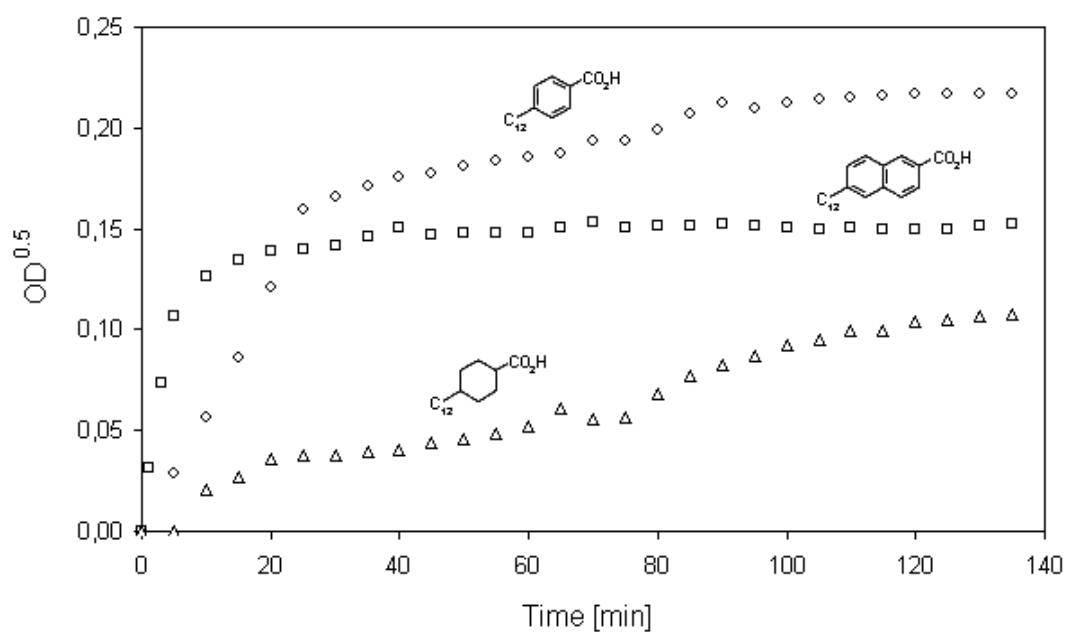


Figure 5.15: Square root of OD vs. time for naphthenate solutions containing particles of different naphthenic acid structures. The concentrations of acid and  $\text{Ca}^{2+}$  are 2mM and 4mM, respectively.

Figure 5.16 shows plots of square root of OD vs. time for naphthenate solutions containing particles of the aromatic single-ring naphthenic acid (2mM) in addition of 50ppm of three different oil-soluble surfactants (A-C). As indicated, addition of all the surfactants causes a lowering of the OD as compared to the system without additives. Surfactant A, which, according to figure 5.17 is more interfacially active than C, also causes a lower particle volume. However, the most interesting observation is that surfactant B, which is highly water soluble compared to A and C, causes a lower OD than the more interfacially active A. Due to the low o/w interfacial affinity, it is unlikely that the mechanism is interfacial dilution of the acid monomers. To verify the partitioning of B into water, the surface tension (ST) of bulk water was measured for two different systems at different times; (1) water pH 9.0 in contact with oil (1:1 vol.) containing 50ppm of B, and (2) water pH 9.0 in contact with oil (1:1 vol.) containing 2mM of naphthenic acid and 50ppm of B upon addition of  $\text{Ca}^{2+}$ . The ST of the aqueous phase of system (1) was found to descend with time, indicating dissolution of B into water. For system (2), on the other hand, the ST of the water phase remained constant at the value of pure water ( $\sim 72\text{mN/m}$ ). Hence, surfactant B do not partition into the aqueous solution when naphthenate particles are present in the oil phase. Possible reasons for the lower OD in presence of B are interactions between the particles and the reactants, i.e. between B and the naphthenic acid and/or  $\text{Ca}^{2+}$ , or interactions between B and the particles, causing disintegrating into smaller aggregates. The assumption about smaller particles was further supported by measuring the particle size of systems both in presence and in absence of B.

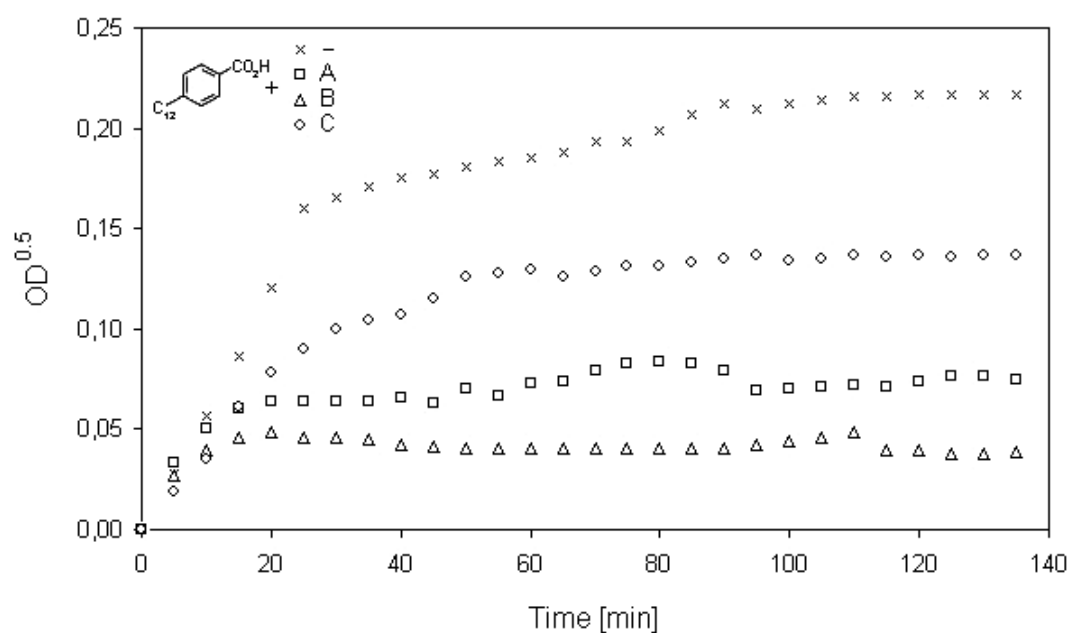


Figure 5.16: Square root of OD vs. time for naphthenate solutions in addition of different surfactants.

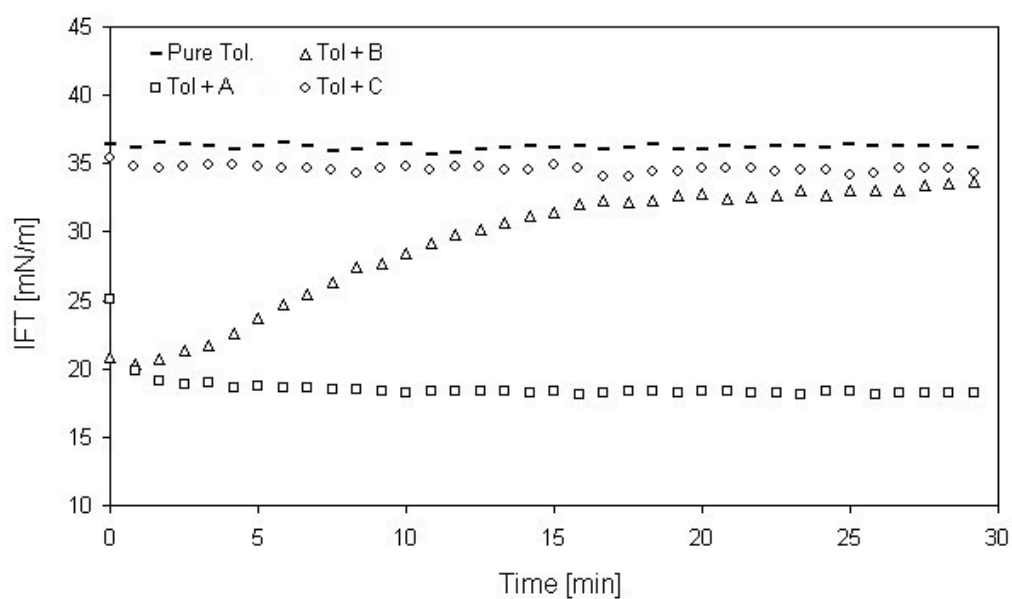


Figure 5.17: Dynamic interfacial tensions for toluene-water (pH 9.0) in presence of 50ppm of the different surfactants in the toluene phase.

## 6 Summary and Conclusions

The main focus in this thesis has been towards interfacial properties of naphthenic acids and metal naphthenates in oil-water systems. The reaction between naphthenic acids, synthetic as well as indigenous, and various divalent cations ( $\text{Ba}^{2+}$ ,  $\text{Sr}^{2+}$ ,  $\text{Ca}^{2+}$ ,  $\text{Mg}^{2+}$ ), which occur naturally in the co-produced water, has been followed using the pendant drop technique and by correlating changes in dynamic interfacial tension to plausible reaction mechanisms. The results have been interpreted by considering the interfacial reaction to proceed through two steps with subsequent binding of acid monomers to the divalent cation. This model is reasonable due to the limited flexibility of the naphthenic acids at the interface compared to the behaviour in bulk solution. Hence, steric hindrance among acid monomers, as caused by bulky structures, may affect the rate of naphthenate formation as the lifetime of the intermediate of the reaction, i.e. the 1:1 complex of acid and cation, will increase. A similar effect is also achieved by adding oil-soluble non-ionic surfactant mixtures to the systems. These compounds will, due to high interfacial affinity, dilute the acids at the interface and cause longer lateral distance between the reactive carboxylic groups. Interfacial coverage of 1:1 complexes of acid and cation is believed to be the reason behind the permanent reduction in the IFT observed for certain systems. A completion of the reaction to 2:1 stoichiometric complexes will, on the other hand, lead to an increase in the IFT due to migration of less interfacially active product away from the interface and into the oil bulk solution. It has also been clearly demonstrated that the divalent cations may react differently depending on degree of hydration. Strongly hydrated cations, like  $\text{Mg}^{2+}$ , will be less preferable towards the o/w interface than less hydrated cations, like  $\text{Ba}^{2+}$ . Consequently, an energy barrier against adsorption is created, which may hinder a completion of the reaction to 2:1 complexes.

The stability of films of different naphthenic acids and divalent cations ( $\text{Ba}^{2+}$ ,  $\text{Sr}^{2+}$ ,  $\text{Ca}^{2+}$ ,  $\text{Mg}^{2+}$ ) at o/w interfaces has been investigated using the Langmuir technique with a trough designed for liquid-liquid systems. The film stability against compression was shown to depend on naphthenic acid structure, type of divalent cation, and the pH of the aqueous phase. In all cases,  $\text{Mg}^{2+}$  caused the less stable films. This is due to the high degree of hydration of the magnesium ions, which, as discussed in paper I and III, hinder them to adsorb at the o/w interface and further react with the naphthenic acids. Hence, the charged complexes will be forced into the aqueous solution upon film compression. Furthermore, naphthenic acids with branched structures have generally shown to form

---

less stable films in combination with the divalent cations than acids comprising aliphatic structures. This is due to steric reasons, as highly branched molecules will not pack in so defined and dense layers than more aliphatic ones.

By analyzing naphthenic acids isolated from a naphthenate deposit, a narrow family of 4-protic naphthenic acids with molecular weights around 1230 g/mol has been detected. The finding is similar to what recently discovered from other fields. These acids were found to be very interfacially active compared to the majority of naphthenic acids existing in the crude. This property is believed to be one of the main reasons why the 4-protic acids are found to dominate in naphthenate deposits, and is a further indication of that the naphthenic acids react at the o/w interface. The ability of 4-protic acids to form Langmuir monolayers at different subphase compositions was also investigated. The acids were found to have a large molecular area compared to normal fatty acids. This reflects the extensive molecular structure consisting of four carboxylic groups which likely are bridged together by hydrocarbon chains. Under alkaline conditions, the film stability increased by adding calcium ions to the aqueous phase due to the formation of less water soluble calcium naphthenate at the surface. Because of having four carboxylic groups, the acid monomers may be cross-linked together by  $\text{Ca}^{2+}$  to form extensive networks, which is very different compared to normal monoprotic acids. In addition to the high interfacial activity, this is likely a further reason for the predominant occurrence of the 4-protic acids in the deposits.

A new experimental setup based on near infrared (NIR) spectroscopy has been utilized to online follow the formation and growth of naphthenate particles in o/w systems. The particles were formed at the interface and dispersed into the oil phase upon stirring. The method has shown to be suitable to follow the particle formation and growth qualitatively under different experimental conditions.



---

## 7 References

1. Rousseau, G., Zhou, H., and Hurtevent, C., *Calcium carbonate and naphthenate mixed scale in deep-offshore fields*. In *SPE Oilfield Scale Symposium*, SPE68307, (2001), Aberdeen, UK.
2. Madill, R. E. A., Orzechowski, M. T., Chen, G., Brownlee, B. G., and Bunce, N. J., *Preliminary risk assessment of the wet landscape option for reclamation of oil sands mine tailings: bioassays with mature fine tailings pore water*, *Environmental Toxicology*, **16** (2001) 197-208.
3. Kamaluddin, M., and Zwiazek, J. J., *Naphthenic acids inhibit root water transport, gas exchange and leaf growth in aspen (*Populus tremuloides*) seedlings*, *Tree Physiology*, **22** (2002) 1265-1270.
4. Rogers, V. V., Wickstrom, M., Liber, K., and MacKinnon, M. D., *Acute and subchronic mammalian toxicity of naphthenic acids from oil sands tailings*, *Toxicological Sciences*, **66** (2002) 347-355.
5. Piehl, R. L., *Naphthenic acid corrosion in crude distillation units*, *Mater Performance*, **27** (1988) 37-43.
6. Babaian-Kibala, E., Craig, H. L., Rusk, G. L., Blanchard, K. V., Rose, T. J., Uehlein, B. L., Quinter, R. C., and Summers, M. A., *Naphthenic acid corrosion in refinery settings*, *Mater Performance*, **32** (1993) 50-55.
7. Slavcheva, E., Shone, B., and Turnbull, A., *Review of naphthenic acid corrosion in oil refining*, *British Corrosion Journal*, **34** (1999) 125-131.
8. Acevedo, S., Escobar, G., Ranaudo, M. A., Khazen, J., Borges, B., Pereira, J. C., and Méndez, B., *Isolation and characterization of low and high molecular weight acidic compounds from Cerro Negro extraheavy crude oil. Role of these acids in the interfacial properties of the crude oil emulsions*, *Energy & Fuels*, **13** (1999) 333-335.
9. Goldszal, A., Bourrel, M., Hurtevent, C., and Volle, J.-L., *Stability of water in acidic crude oil emulsions*. In *The 3rd International Conference on Petroleum Phase Behavior and Fouling*, (2002), New Orleans, USA.
10. Ese, M.-H., and Kilpatrick, P. K., *Stabilization of water-in-oil emulsions by naphthenic acids and their salts: model compounds, role of pH, and soap:acid ratio*, *Journal of Dispersion Science and Technology*, **25** (2004) 253-261.
11. Pathak, A. K., and Kumar, T., *Study of indigenous crude oil emulsions and their stability*. In *Proceedings of PETROTECH-95, Technology trends in oil industry*, (1995), New Dehli.
12. Brient, J. A., Wessner, P. J., and Doyle, M. N., *Naphthenic acids* In *Encyclopedia of Chemical Technology* (Kirk-Othmer, Ed.), (1995), John Wiley & Sons, New York.
13. Seifert, W. K., *Carboxylic acids in petroleum and sediments*, *Fortschritte der Chemie Organischer Naturstoffe*, **32** (1975) 1-49.

- 
14. Mediaas, H., Grande, K. V., Hustad, B. M., Rasch, A., Rueslåtten, H. G., and Vindstad, J. E., *The Acid-IER Method - a method for selective isolation of carboxylic acids from crude oils and other organic solvents*. In *5th SPE Oilfield Scale Symposium*, SPE 80404, (2003), Aberdeen, UK.
  15. Laredo, G. C., Lopez, C. R., Alvarez, R. E., and Cano, J. L., *Naphthenic acids, total acid number and sulfur content profile characterization in Isthmus and Maya crude oils*, *Fuel*, **83** (2004) 1689-1695.
  16. Jaffe, R., and Gallardo, M. T., *Application of carboxylic acid biomarkers as indicators of biodegradation and migration of crude oils from the Maracaibo Basin, Western Venezuela*, *Organic Geochemistry*, **20** (1993) 973-984.
  17. Behar, F. H., and Albrecht, P., *Correlations between carboxylic acids and hydrocarbons in several crude oils. Alteration by biodegradation*, *Organic Geochemistry*, **6** (1984) 597-604.
  18. Meredith, W., Kelland, S.-J., and Jones, D. M., *Influence of biodegradation on crude oil acidity and carboxylic acid composition*, *Organic Geochemistry*, **31** (2000) 1059-1073.
  19. Nascimento, L. R., Reboucas, L. M. C., Koike, L., de A.M Reis, F., Soldan, A. L., Cerqueira, J. R., and Marsaioli, A. J., *Acidic biomarkers from Albacora oils, Campos Basin, Brazil*, *Organic Geochemistry*, **30** (1999) 1175-1191.
  20. Watson, J. S., Jones, D. M., and Swannell, R. P. J., *Formation of carboxylic acids during biodegradation of crude oil* In *In Situ Bioremediation of Petroleum Hydrocarbon and other Organic Compounds* (B. C. Alleman and A. Leeson, Eds.), (1999), Battelle Press, Columbus, Ohio, USA.
  21. Watson, J. S., Jones, D. M., Swannell, R. P. J., and van Duin, A. C. T., *Formation of carboxylic acids during aerobic biodegradation of crude oil and evidence of microbial oxidation of hopanes*, *Organic Geochemistry*, **33** (2002) 1153-1169.
  22. Dzidic, I., Somerville, A. C., Raia, J. C., and Hart, H. V., *Determination of naphthenic acids in California crudes and refinery wastewaters by fluoride ion chemical ionization mass spectrometry*, *Analytical Chemistry*, **60** (1988) 1318-1323.
  23. Fan, T.-P., *Characterization of naphthenic acids in petroleum by fast-atom-bombardment mass-spectrometry*, *Energy & Fuels*, **5** (1991) 371-375.
  24. Wong, D. C. L., van Compernelle, R., Nowlin, J. G., O'Neal, D. L., and Johnson, G., *Use of supercritical fluid extraction and fast ion bombardment mass spectrometry to identify toxic chemicals from a refinery effluent adsorbed onto granular activated carbon*, *Chemosphere*, **32** (1996) 1669-1697.
  25. Hsu, C. S., Dechert, G. J., Robbins, W. K., and Fukuda, E. K., *Naphthenic acids in crude oil characterized by mass spectrometry*, *Energy & Fuels*, **14** (2000) 217-223.
  26. Gabryelski, W., and Froese, K. L., *Characterization of naphthenic acids by electrospray ionization high-field asymmetric waveform ion mobility mass spectrometry*, *Analytical Chemistry*, **75** (2003) 4612-4623.
-

- 
27. St. John, W. P., Rughani, J., Green, S. A., and McGinnis, G. D., *Analysis and characterization of naphthenic acids by gas chromatography-electron impact mass spectroscopy of tert.- butyldimethylsilyl derivatives*, *Journal of Chromatography A*, **807** (1998) 241-251.
  28. Holowenko, F. M., MacKinnon, M. D., and Fedorak, P. M., *Characterization of naphthenic acids in oil sands wastewaters by gas chromatography-mass spectroscopy*, *Water Research*, **36** (2002) 2843-2855.
  29. Koike, L., Reboucas, L. M. C., Reis, F. d. A., Marsaioli, A. J., Richnow, H. H., and Michaelis, W., *Naphthenic acids from crude oils of Campos Basin*, *Organic Geochemistry*, **18** (1992) 851-860.
  30. Seifert, W. K., and Teeter, R. M., *Identification of polycyclic naphthenic, mono-, and diaromatic crude oil carboxylic acids*, *Analytical Chemistry*, **42** (1970) 180-189.
  31. Tomczyk, N. A., Winans, R. E., Shinn, J. H., and Robinson, R. C., *On the nature and origin of acidic species in petroleum. 1. Detailed acid type distribution in a California crude oil*, *Energy & Fuels*, **15** (2001) 1498-1504.
  32. Rudzinski, W. E., Oehlers, L., Zhang, Y., and Najera, B., *Tandem mass spectrometric characterization of commercial naphthenic acids and a Maya crude oil*, *Energy & Fuels*, **16** (2002) 1178-1185.
  33. Qian, K., Robbins, W. K., Hughey, C. A., Cooper, H. J., Rodgers, R. P., and Marshall, A. G., *Resolution and identification of elemental compositions for more than 3000 crude acids in heavy petroleum by negative-ion microelectrospray high-field Fourier Transform ion cyclotron resonance mass spectrometry*, *Energy & Fuels*, **15** (2001) 1505-1511.
  34. Hughey, C. A., Rodgers, R. P., Marshall, A. G., Qian, K., and Robbins, W. K., *Identification of acidic NSO compounds in crude oils of different geochemical origins by negative ion electrospray Fourier transform ion cyclotron resonance mass spectroscopy*, *Organic Geochemistry*, **33** (2002) 743-759.
  35. Reinsel, M. A., Borkowski, J. J., and Sears, J. T., *Partition coefficients for acetic, propionic, and butyric acids in a crude oil/water system*, *Journal of Chemical and Engineering Data*, **39** (1994) 513-516.
  36. Havre, T. E., Sjöblom, J., and Vindstad, J. E., *Oil-water partitioning and interfacial behaviour of naphthenic acids*, *Journal of Dispersion Science and Technology*, **24** (2003) 789-801.
  37. Kocherginsky, N. M., and Grishchenko, A. B., *Mass transfer of long chain fatty acids through liquid-liquid interface stabilized by porous membrane*, *Separation and Purification Technology*, **20** (2000) 197-208.
  38. Pohl, H. A., Hobbs, M. E., and Gross, P. M., *Electric polarization of carboxylic acids in dilute solutions of nonpolar solvents. I. The relation of electric polarization to the association of carboxylic acids in hydrocarbon solvents*, *Journal of Chemical Physics*, **9** (1941) 408-414.
  39. Goodman, D. S., *The distribution of fatty acids between n-heptane and aqueous phosphate buffer*, *Journal of the American Chemical Society*, **80** (1958) 3887-3892.
-

- 
40. Takeda, K., Yamashita, H., and Akiyama, M., *Dimerization of some carboxylic acids in organic phases*, Solvent Extraction and Ion Exchange, **5** (1987) 29-53.
  41. Fujii, Y., Yamada, H., and Mizuta, M., *Self-association of acetic acid in some organic solvents*, Journal of Physical Chemistry, **92** (1988) 6768-6772.
  42. Kimtys, L. L., and Balevicius, V. J., *Self-association of carboxylic acids as studied by proton NMR spectroscopy*, Advances in Molecular Relaxation and Interaction Processes, **15** (1979) 151-161.
  43. Rodgers, R. P., Hendrickson, C. L., Emmett, M. R., Marshall, A. G., Greaney, M., and Qian, K., *Molecular characterization of petroporphyrins in crude oil by electrospray ionization Fourier transform ion cyclotron resonance mass spectrometry*, Canadian Journal of Chemistry, **79** (2001) 546-551.
  44. Horváth-Szabó, G., Masliyah, J., and Czarnecki, J., *Phase behavior of sodium naphthenates, toluene and water*, Journal of Colloid and Interface Science, **242** (2001) 247-254.
  45. Mukerjee, P., *Dimerization of anions of long-chain fatty acids in aqueous solutions and the hydrophobic properties of the acids*, Journal of Physical Chemistry, **69** (1965) 2821-2827.
  46. Suzuki, K., Taniguchi, Y., and Watanabe, T., *Effect of pressure on the dimerization of carboxylic acids in aqueous solution*, Journal of Physical Chemistry, **77** (1973) 1918-1922.
  47. Stenius, P., *Association equilibria and micelle formation of fatty acid sodium salts. I. A survey of potentiometric measurements on salts with 2-6 carbon atoms at high ionic strength*, Acta Chemica Scandinavica, **25** (1971) 2232-2250.
  48. Stenius, P., *Association equilibria and micelle formation of fatty acid sodium salts. II. An investigation of straight-chain salts by vapour pressure osmometry*, Acta Chemica Scandinavica, **27** (1973) 3435-3451.
  49. Stenius, P., *Association equilibria and micelle formation of fatty acid sodium salts. III. The association of sodium butyrate at 40° in 3M NaCl*, Acta Chemica Scandinavica, **27** (1973) 3452-3466.
  50. Friman, R., and Stenius, P., *Association equilibria and micelle formation of fatty acid sodium salts. V. Investigation of branched chain salts by vapour pressure osmometry*, Acta Chemica Scandinavica A, **32** (1978) 289-296.
  51. Theander, K., and Pugh, R.-J., *The influence of pH and temperature on the equilibrium and dynamic surface tension of aqueous solutions of sodium oleate*, Journal of Colloid and Interface Science, **239** (2001) 209-216.
  52. Somasundaran, P., Ananthapadmanabhan, K. P., and Ivanov, J. B., *Dimerization of oleate in aqueous solutions*, Journal of Colloid and Interface Science, **99** (1984) 128-135.
  53. Israelachvili, J., *Intermolecular and surface forces, with applications to colloidal and biological systems*, (1985), Academic Press, London.
  54. Gibbs, J. W., *The collected works of J. Willard Gibbs*, (1928), Longmans, Green and Co., New York.
  55. Gu, T., and Sjöblom, J., *Surfactant structure and its relation to the Krafft point, cloud point and micellization: Some empirical relationships*, Colloids and Surfaces, **64** (1992) 39-46.
-

- 
56. Yamabe, T., and Moroi, Y., *Micelle formation of anionic surfactant with divalent counterion of separate electric charge*, Journal of Colloid and Interface Science, **215** (1999) 58-63.
  57. Knag, M., Sjöblom, J., Øye, G., and Gulbrandsen, E., *A quartz crystal microbalance study of the adsorption of quaternary ammonium derivatives on iron and cementite*, Colloids and Surfaces A, **250** (2004) 269-278.
  58. Horváth-Szabó, G., Czarnecki, J., and Masliyah, J., *Liquid crystals in aqueous solutions of sodium naphthenates*, Journal of Colloid and Interface Science, **236** (2001) 233-241.
  59. Skurtveit, R., Sjöblom, J., and Høiland, H., *Emulsions under elevated temperature and pressure conditions. I. The model system water-hexadecanoic acid-sodium hexadecanoate-decane at 70°C*, Journal of Colloid and Interface Science, **133** (1989) 395-403.
  60. Horváth-Szabó, G., Czarnecki, J., and Masliyah, J., *Sandwich structures at oil-water interfaces under alkaline conditions*, Journal of Colloid and Interface Science, **253** (2002) 427-434.
  61. Horváth-Szabó, G., Masliyah, J., and Czarnecki, J., *Emulsion stability based on phase behavior in sodium naphthenates containing systems: gels with a high organic solvent content*, Journal of Colloid and Interface Science, **257** (2003) 299-309.
  62. Havre, T. E., and Sjöblom, J., *Emulsion stabilization by means of combined surfactant multilayer (D-phase) and asphaltene particles*, Colloids and Surfaces A, **228** (2002) 131-142.
  63. Friberg, S., *Liquid crystalline phases in emulsions*, Journal of Colloid and Interface Science, **37** (1971) 291-295.
  64. Friberg, S., Mandell, L., and Larsson, M., *Mesomorphous phases, a factor of importance for the properties of emulsions*, Journal of Colloid and Interface Science, **29** (1969) 155-161.
  65. Friberg, S., Jansson, P. O., and Cedreberg, E., *Surfactant association structure and emulsion stability*, Journal of Colloid and Interface Science, **55** (1976) 614-623.
  66. Friberg, S., and Solans, C., *Surfactant association structures and the stability of emulsions and foams*, Langmuir, **2** (1986) 121-126.
  67. Speight, J. G., *The Chemistry and Technology of Petroleum*, 3 ed., (1998), Marcel Dekker, Inc., New York.
  68. Sjöblom, J., Urdahl, O., Børve Nordli, K. G., Mingyuan, L., Saeten, J. O., Christy, A. A., and Gu, T., *Stabilization and destabilization of water-in-crude oil emulsions from the Norwegian Continental Shelf. Correlation with model systems*, Advances in Colloid and Interface Science, **41** (1992) 241-271.
  69. Førdedal, H., Midttun, Ø., Sjöblom, J., Kvalheim, O. M., Schildberg, Y., and Volle, J.-L., *A multivariate screening analysis of W/O emulsions in high external electric fields as studied by means of dielectric time domain spectroscopy. II. Model emulsions stabilized by interfacially active fractions from crude oils*, Journal of Colloid and Interface Science, **182** (1996) 117-125.
  70. Førdedal, H., Schildberg, Y., Sjöblom, J., and Volle, J.-L., *Crude oil emulsions in high electric fields as studied by dielectric spectroscopy. Influence of interaction between commercial and indigenous surfactants*, Colloids and Surfaces A, **106** (1996) 33-47.
-

- 
71. Sjöblom, J., Johnsen, E. E., Westvik, A., Bergflødt, L., Auflem, I. H., Havre, T. E., and Kallevik, H., *Colloid chemistry in sub sea petroleum and gas processing*. In *The 2nd International Conference on Petroleum and Gas Phase Behaviour and Fouling*, (2000), Copenhagen, Denmark.
  72. Kilpatrick, P. K., and Spiecker, P. M., *Asphaltene Emulsions* In *Encyclopedic Handbook of Emulsion Technology* (J. Sjöblom, Ed.), (2001), Marcel Dekker, Inc., New York.
  73. Aske, N., Kallevik, H., and Sjöblom, J., *Water-in-crude oil emulsion stability studied by critical electric field measurements. Correlation to physico-chemical parameters and near-infrared spectroscopy*, *Journal of Petroleum Science & Engineering*, **36** (2002) 1-17.
  74. Sjöblom, J., Aske, N., Auflem, I. H., Brandal, Ø., Havre, T. E., Sæther, Ø., Westvik, A., Johnsen, E. E., and Kallevik, H., *Our current understanding of water-in-crude oil emulsions. recent characterization techniques and high pressure performance*, *Advances in Colloid and Interface Science*, **100-102** (2003) 399-473.
  75. Koots, J. A., and Speight, J. G., *Relation of petroleum resins to asphaltenes*, *Fuel*, **54** (1975) 179-184.
  76. McLean, J. D., and Kilpatrick, P. K., *Effect of asphaltenes solvency on stability of water-in-crude-oil emulsions*, *Journal of Colloid and Interface Science*, **189** (1997) 242-253.
  77. McLean, J. D., and Kilpatrick, P. K., *Effects of asphaltene aggregation in model heptane-toluene mixtures on stability of water-in-oil emulsions*, *Journal of Colloid and Interface Science*, **196** (1997) 23-34.
  78. Merino-Garcia, D., and Andersen, S. I., *Thermodynamic characterization of asphaltene-resin interaction by microcalorimetry*, *Langmuir*, **20** (2004) 4559-4565.
  79. Gonzalez, G., and Middea, A., *Peptization of asphaltene by various oil soluble amphiphiles*, *Colloids and Surfaces*, **52** (1991) 207-217.
  80. Chang, C.-L., and Fogler, S. H., *Stabilization of asphaltenes in aliphatic solvents using alkylbenzene-derived amphiphiles. 2. Study of the asphaltene-amphiphile interactions and structures using Fourier Transform infrared spectroscopy and small-angle X-ray scattering techniques*, *Langmuir*, **10** (1994) 1758-1766.
  81. Chang, C.-L., and Fogler, S. H., *Peptization and coagulation of asphaltenes in apolar media using oil-soluble polymers*, *Fuel Science & Technology International*, **14** (1996) 75-100.
  82. Merino-Garcia, D., and Andersen, S. I., *Interaction of Asphaltenes with Nonylphenol by Microcalorimetry*, *Langmuir*, **20** (2004) 1473-1480.
  83. Östlund, J.-A., Nyden, M., Auflem, I. H., and Sjöblom, J., *Interactions between asphaltenes and naphthenic acids*, *Energy & Fuels*, **17** (2003) 113-119.
  84. Auflem, I. H., Havre, T. E., and Sjöblom, J., *Near infrared study on the dispersive effects of amphiphiles and naphthenic acids on asphaltenes in model heptane-toluene mixtures*, *Colloid and Polymer Science*, **280** (2002) 695-700.
  85. Buckley, J. S., and Liu, Y., *Some mechanisms of crude oil/brine/solid interactions*, *Journal of Petroleum Science & Engineering*, **20** (1998) 155-160.
-

- 
86. McCaffery, F. G., and Mungan, N., *Contact angle and interfacial tension studies of some hydrocarbon-water-solid systems*, Journal of Canadian Petroleum Technology, **9** (1970) 185-196.
  87. Lowe, A. C., Phillips, M. C., and Riddiford, A. C., *Wetting of carbonate surfaces by oil and water*, Journal of Canadian Petroleum Technology, **12** (1973) 33-40.
  88. Thomas, M. M., Clouse, J. A., and Longo, J. M., *Adsorption of organic compounds on carbonate minerals. 1. Model compounds and their influence on mineral wettability*, Chemical Geology, **109** (1993) 201-213.
  89. Zullig, J. J., and Morse, J. W., *Interaction of organic acids with carbonate mineral surfaces in seawater and related solutions: I. Fatty acid adsorption*, Geochimica et Cosmochimica Acta, **52** (1988) 1667-1678.
  90. Spildo, K., Høiland, H., and Olsen, M. K., *Adsorption of benzoic and 4-heptylbenzoic acid on different silica substrates from organic and aqueous solution*, Journal of Colloid and Interface Science, **221** (2000) 124-132.
  91. Davies, J. T., and Rideal, E. K., *Adsorption at Liquid Interfaces (Chapter 4)* In *Interfacial Phenomena* (1961), Academic Press, New York and London.
  92. Eastoe, J., and Dalton, J. S., *Dynamic surface tension and adsorption mechanisms of surfactants at the air-water interface*, Advances in Colloid and Interface Science, **85** (2000) 103-144.
  93. Van Hunsel, J., Bleys, G., and Joos, P., *Adsorption kinetics at the oil/water interface*, Journal of Colloid and Interface Science, **114** (1986) 432-441.
  94. Fainerman, V. B., Makievski, A. V., and Miller, R., *Surfactant adsorption isotherms considering molecular reorientation or aggregation at liquid/fluid interfaces*, Reviews in Chemical Engineering, **14** (1998) 373-407.
  95. Miller, R., and Fainerman, V. B., *Surfactant adsorption layers at liquid-fluid interfaces*, (2001), Academic Press, San Diego, California.
  96. Fainerman, V. B., and Miller, R., *Thermodynamics of adsorption of surfactants at the fluid interfaces*, Studies in Interface Science, **13** (2001) 99-188.
  97. Strassner, J. E., *Effect of pH on interfacial films and stability of crude oil-water emulsions*, Journal of Petroleum Technology, **20** (1968) 303-312.
  98. Cooke, C. E., Jr., Williams, R. E., and Kolodzie, P. A., *Oil recovery by alkaline waterflooding*, Journal of Petroleum Technology, **26** (1974) 1365-1374.
  99. Chan, M., and Yen, T. F., *A chemical equilibrium model for interfacial activity of crude oil in aqueous alkaline solution: the effects of pH, alkali and salt*, Canadian Journal of Chemical Engineering, **60** (1982) 305-308.
  100. Chiwetelu, C. I., Hornof, V., and Neale, G. H., *Interaction of aqueous caustic with acidic oils*, Journal of Canadian Petroleum Technology, **28** (1989) 71-78.
  101. Nasr-El-Din, H. A., and Taylor, K. C., *Dynamic interfacial tension of crude oil/alkali/surfactant/surfactant systems*, Colloids and Surfaces, **66** (1992) 23-37.
  102. Chatterjee, J., and Wasan, D. T., *A kinetic model for dynamic interfacial tension variation in an acidic oil/alkali/surfactant system*, Chemical Engineering Science, **53** (1998) 2711-2725.
-

- 
103. Chiwetelu, C. I., Hornof, V., and Neale, G. H., *A dynamic model for the interaction of caustic reagents with acidic oils*, *AIChE Journal*, **36** (1990) 233-241.
  104. Chiwetelu, C. I., Hornof, V., and Neale, G. H., *Mechanisms for the interfacial reaction between acidic oils and alkaline reagents*, *Chemical Engineering Science*, **45** (1990) 627-638.
  105. Ramakrishnan, T. S., and Wasan, D. T., *A model for interfacial activity of acidic crude oil/caustic systems for alkaline flooding*, *Society of Petroleum Engineers Journal*, **23** (1983) 602-612.
  106. Rudin, J., and Wasan, D. T., *Mechanism of lowering interfacial tension in alkali/acidic oil systems. 1. Experimental studies*, *Colloids and Surfaces*, **68** (1992) 67-79.
  107. Rudin, J., and Wasan, D. T., *Mechanism of lowering interfacial tension in alkali/acidic systems. 2. Theoretical studies*, *Colloids and Surfaces*, **68** (1992) 81-94.
  108. Touhami, Y., Hornof, V., and Neale, G. H., *Dynamic interfacial tension behavior of acidified oil/surfactant-enhanced alkaline systems. 1. Experimental studies*, *Colloids and Surfaces A*, **132** (1998) 61-74.
  109. Poggese, G., Hurtevent, C., and Buchart, D., *Multifunctional chemicals for West African deep offshore fields*. In *SPE Oilfield Scale Symposium*, SPE74649, (2002), Aberdeen, UK.
  110. Dyer, S. J., Graham, G. M., and Arnott, C., *Naphthenate scale formation - examination of molecular controls in idealised systems*. In *SPE 5th International Symposium on Oilfield Scale*, SPE 80395, (2003), Aberdeen, UK.
  111. Havre, T. E., *Near infrared spectroscopy as a method for studying the formation of calcium naphthenate*, *Colloid and Polymer Science*, **282** (2004) 270-279.
  112. Wolstenholme, G. A., and Schulman, J. H., *Metal-monolayer interactions in aqueous systems: I. Interaction of monolayers of long-chain polar compounds with metal ions in the underlying solution*, *Transactions of the Faraday Society*, **46** (1950) 475-487.
  113. Durham, K., *Interaction of monolayers of branched-chain fatty acids with calcium ions in the underlying solutions*, *Journal of Applied Chemistry*, **5** (1955) 686-692.
  114. Durham, K., *Molecular interaction in mixed monolayers of fatty acids*, *Journal of Applied Chemistry*, **8** (1958) 724-728.
  115. Enever, R. P., and Pilpel, N., *Reaction between stearic acid and calcium ions at the air-water interface using surface viscometry*, *Transactions of the Faraday Society*, **63** (1967) 781-792.
  116. Enever, R. P., and Pilpel, N., *Reaction between stearic acid and calcium ions at the air/water interface using surface viscometry. II. Mixed films of octadecanol and stearic acid*, *Transactions of the Faraday Society*, **63** (1967) 1559-1566.
  117. Pilpel, N., and Enever, R. P., *Reaction between stearic acid and calcium ions at the air/water interface using surface viscometry. III. Mechanism*, *Transactions of the Faraday Society*, **64** (1968) 231-237.
  118. Chifu, E., Sálájan, M., Demeter-Vodnár, I., and Tomoaia-Cotisel, M., *Fatty acid films at the benzene/water interface*, *Revue Roumaine de Chimie*, **32** (1987) 683-691.
-



- 
119. Flipsen, J. A. C., van der Hijden, H. T. W. M., Egmond, M. R., and Verheij, H. M., *Action of cutinase at the triolein-water interface. Characterization of interfacial effects during lipid hydrolysis using the oil-drop tensiometer as a tool to study lipase kinetics*, *Chemistry and Physics of Lipids*, **84** (1996) 105-115.
  120. Hoppe, A., and Theimer, R. R., *Titrimetric test for lipase activity using stabilized triolein emulsions*, *Phytochemistry*, **42** (1996) 973-978.
  121. Demeter-Vodnár, J., Sálájan, M., and Lowy, D. A., *Kinetic study of the diffusion and adsorption of fatty acids at the benzene-water interface*, *Journal of Colloid and Interface Science*, **183** (1996) 424-430.
  122. Touhami, Y., Hornof, V., and Neale, G. H., *Dynamic interfacial tension behavior of acidified oil/surfactant-enhanced alkaline systems. 2. Theoretical studies*, *Colloids and Surfaces A*, **133** (1998) 211-231.
  123. Albers, W., and Overbeek, J. T. G., *Stability of emulsions of water in oil. I. The correlation between electrokinetic potential and stability*, *Journal of Colloid Science*, **14** (1959) 501-509.
  124. McLaughlin, S., Mulrine, N., Gresalfi, T., Vaio, G., and McLaughlin, A., *Adsorption of divalent cations to bilayer membranes containing phosphatidylserine*, *Journal of General Physiology*, **77** (1981) 445-473.
  125. Berg, J. M., and Claesson, P. M., *Forces between carboxylic acid layers in divalent salt solutions*, *Thin Solid Films*, **178** (1989) 261-270.
  126. Bloch, J. M., and Yun, W., *Condensation of monovalent and divalent metal ions on a Langmuir monolayer*, *Physical Review A*, **41** (1990) 844-862.
  127. Kovalchuk, V. I., Zholkovskiy, E. K., Bondarenko, N. P., and Vollhardt, D., *Dissociation of fatty acid and counterion binding at the Langmuir monolayer deposition: theoretical considerations*, *Journal of Physical Chemistry B*, **105** (2001) 9254-9265.
  128. Jennings, H. Y. Jr., *A study of caustic solution-crude oil interfacial tensions*, *Society of Petroleum Engineers Journal*, **15** (1975) 197-202.
  129. Marra, J., and Israelachvili, J., *Direct measurements of forces between phosphatidylcholine and phosphatidylethanolamine bilayers in aqueous electrolyte solutions*, *Biochemistry*, **24** (1985) 4608-4618.
  130. Yazdani, M., Yu, H., and Zografi, G., *Ionic interactions of fatty acid monolayers at the air/water interface*, *Langmuir*, **6** (1990) 1093-1098.
  131. Ederth, T., and Claesson, P. M., *Forces between carboxylic acid surfaces in divalent electrolyte solutions*, *Journal of Colloid and Interface Science*, **229** (2000) 123-128.
  132. Goldszal, A., Hurtevent, C., and Rousseau, G., *Scale and naphthenate inhibition in deep-offshore fields*. In *SPE Oilfield Scale Symposium*, SPE74661, (2002), Aberdeen, UK.
  133. Gallup, D. L., *Soap sludges: aggravating factors and mitigation measures*. In *6th SPE Oilfield Scale Symposium*, SPE87471, (2004), Aberdeen, UK.
-

- 
134. Gallup, D. L., Smith, P. C., Chipponeri, J., Abuyazid, A., and Mulyono, D., *Formation & mitigation of "metallic soap" sludge, Attaka, Indonesia field*. In *SPE International Conference on Health, Safety and Environment in Oil and Gas Exploration and Production*, SPE73960, (2002), Kuala Lumpur, Malaysia.
  135. Baugh, T. D., Wolf, N. O., Mediaas, H., Vindstad, J. E., and Grande, K. V., *Characterization of a calcium naphthenate deposit - The ARN acid discovery*, Preprints - American Chemical Society, Division of Petroleum Chemistry, **49** (2004) 274-276.
  136. Baugh, T. D., Grande, K. V., Mediaas, H., Vindstad, J. E., and Wolf, N. O., *The discovery of high molecular weight naphthenic acids (ARN Acid) responsible for calcium naphthenate deposits*. In *7th SPE Oilfield Scale Symposium*, SPE93011, (2005), Aberdeen, UK.
  137. Ambwani, D. S., and Fort, T. Jr., *Pendant drop technique for measuring liquid boundary tensions*, *Surface and Colloid Science*, **11** (1979) 93-119.
  138. Stauffer, C. E., *The measurement of surface tension by the pendant drop technique*, *Journal of Physical Chemistry*, **69** (1965) 1933-1938.
  139. Andreas, J. M., Hauser, E. A., and Tucker, W. B., *Boundary tension by pendant drops*, *Journal of Physical Chemistry*, **42** (1938) 1001-1019.
  140. Rotenberg, Y., Boruvka, L., and Neumann, A. W., *Determination of surface-tension and contact-angle from the shapes of axisymmetric fluid interfaces*, *Journal of Colloid and Interface Science*, **93** (1983) 169-183.
  141. Boucher, E. A., Evans, M. J. B., and Jones, T. G. J., *The computation of interface shapes for capillary systems in a gravitational field*, *Advances in Colloid and Interface Science*, **27** (1987) 43-79.
  142. Goddard, E. D., *Monolayer properties of fatty acids. IV. Influence of cation at high pH*, *Journal of Colloid and Interface Science*, **24** (1967) 297-309.
  143. Tomoaia-Cotisel, M., Zsako, J., Mocanu, A., Lupea, M., and Chifu, E., *Insoluble mixed monolayers. III. The ionization characteristics of some fatty acids at the air/water interface*, *Journal of Colloid and Interface Science*, **117** (1987) 464-476.
  144. Pezron, E., Claesson, P. M., Berg, J. M., and Vollhardt, D., *Stability of arachidic acid monolayers on aqueous salt solutions*, *Journal of Colloid and Interface Science*, **138** (1990) 245-254.
  145. Yazdani, M., Yu, H., Zografi, G., and Kim, M. W., *Divalent cation-stearic acid monolayer interactions at the air/water interface*, *Langmuir*, **8** (1992) 630-636.
  146. Avila, L. V. N., Saraiva, S. M., and Oliveira, J. F., *Stability and collapse of monolayers of stearic acid and the effect of electrolytes in the subphase*, *Colloids and Surfaces A*, **154** (1999) 209-217.
  147. Ese, M.-H., *Langmuir film properties of indigenous crude oil components. Influence of demulsifiers*, (1999), doctoral thesis, Department of Chemistry, University of Bergen, Norway.
  148. Gundersen, S. A., Ese, M.-H., and Sjöblom, J., *Langmuir surface and interface films of lignosulfonates and kraft lignins in the presence of electrolyte and asphaltenes: correlation to emulsion stability*, *Colloids and Surfaces A*, **182** (2001) 199-218.
-

- 
149. Zhang, L. Y., Lawrence, S., Xu, Z., and Masliyah, J. H., *Studies of Athabasca asphaltene Langmuir films at air-water interface*, Journal of Colloid and Interface Science, **264** (2003) 128-140.
  150. Gaines, G. L., *Insoluble monolayers at liquid-gas interfaces*, (1966), Interscience, New York.
  151. Birdi, K. S., *Lipid and biopolymer monolayers at liquid interfaces*, (1989), Plenum Press, New York.
  152. Murray, B. S., and Nelson, P. V., *A novel Langmuir trough for equilibrium and dynamic measurements on air-water and oil-water monolayers*, Langmuir, **12** (1996) 5973-5976.
  153. Ese, M.-H., Galet, L., Clause, D., and Sjöblom, J., *Properties of Langmuir surface and interfacial films built up by asphaltenes and resins. Influence of chemical demulsifiers*, Journal of Colloid and Interface Science, **220** (1999) 293-301.
  154. Aske, N., Kallevik, H., Johnsen, E. E., and Sjöblom, J., *Asphaltene aggregation from crude oils and model systems studied by high-pressure NIR spectroscopy*, Energy & Fuels, **16** (2002) 1287-1295.
  155. Gossen, P. D., MacGregor, J. F., and Pelton, R. H., *Composition and particle diameter for styrene/methyl methacrylate copolymer latex using UV and NIR spectroscopy*, Applied Spectroscopy, **47** (1993) 1852-1870.
  156. Frake, P., Gill, I., Luscombe, C. N., Rudd, D. R., Waterhouse, J., and Jayasorriya, U. A., *Near-infrared mass median particle size determination of lactose monohydrate, evaluating several chemometric approaches*, Analyst, **123** (1998) 2043-2046.
  157. Santos, A. F., Lima, E. L., and Pinto, J. C., *In-line evaluation of average particle size in styrene suspension polymerizations using near-infrared spectroscopy*, Journal of Applied Polymer Science, **70** (1998) 1737-1745.
  158. Pasikatan, M. C., Steele, J. L., Spillman, C. K., and Haque, E., *Near infrared reflectance spectroscopy for online particle size analysis of powders and ground materials*, Journal of Near Infrared Spectroscopy, **9** (2001) 153-164.
  159. Kerker, M., *The scattering of light and other electromagnetic radiation* In *Physical Chemistry. A Series of Monographs* (E. M. Loebel, Ed.), (1969), Academic Press, New York.
  160. Mullins, O. C., *Asphaltenes in crude oil: Absorbers and/or scatters in the near-infrared region?*, Analytical Chemistry, **62** (1990) 508-514.
  161. Purcell, E. M., Torrey, H. C., and Pound, R. V., *Resonance absorption by nuclear magnetic moments in a solid*, Physical Review, **69** (1946) 37-38.
  162. Bloch, F., *Nuclear induction*, Physical Review, **70** (1946) 460-474.
  163. Zhan, D., and Fenn, J. B., *Electrospray mass spectrometry of fossil fuels*, International Journal of Mass Spectrometry, **194** (2000) 197-208.
  164. Marshall, A. G., and Rodgers, R. P., *Petroleomics: The next grand challenge for chemical analysis*, Accounts of Chemical Research, **37** (2004) 53-59.
  165. Kim, S., Simpson, A. J., Kujawinski, E. B., Freitas, M. A., and Hatcher, P. G., *High resolution electrospray ionization mass spectrometry and 2D solution NMR for the analysis of DOM extracted by C18 solid phase disk*, Organic Geochemistry, **34** (2003) 1325-1335.
-

- 
166. Kujawinski, E. B., *Electrospray ionization Fourier transform ion cyclotron resonance mass spectrometry (ESI FT-ICR MS): characterization of complex environmental mixtures*, *Environmental Forensics*, **3** (2002) 207-216.
167. Stenson, A. C., Landing, W. M., Marshall, A. G., and Cooper, W. T., *Ionization and fragmentation of humic substances in electrospray ionization Fourier transform-ion cyclotron resonance mass spectrometry*, *Analytical Chemistry*, **74** (2002) 4397-4409.
168. Williams, R. B., *Nuclear magnetic resonance in petroleum analytical research*, *Spectrochimica Acta*, **14** (1959) 24-44.
169. Clutter, D. R., Petrakis, L., Stenger, R. L., and Jensen, R. K., *Nuclear magnetic resonance spectrometry of petroleum fractions. Carbon-13 and proton nuclear magnetic resonance characterizations in terms of average molecule parameters*, *Analytical Chemistry*, **44** (1972) 1395-1405.
170. Urdahl, O., Brekke, T., and Sjöblom, J., *Carbon-13 N.M.R. and multivariate statistical analysis of adsorbed surface-active crude oil fractions and the corresponding crude oils*, *Fuel*, **71** (1992) 739-746.
171. Middelberg, A. P. J., Radke, C. J., and Blanch, H. W., *Peptide interfacial adsorption is kinetically limited by the thermodynamic stability of self association*, *Proceedings of the National Academy of Sciences of the United States of America*, **97** (2000) 5054-5059.
172. Wang, L., Atkinson, D., and Small, D. M., *Interfacial properties of an amphipathic  $\alpha$ -helix consensus peptide of exchangeable apolipoproteins at air/water and oil/water interfaces*, *Journal of Biological Chemistry*, **278** (2003) 37480-37491.
-

Papers I and II are not included due to copyright restrictions.

Øystein Brandal  
Ann-Mari Dahl Haneseth  
Johan Sjöblom

## Interactions between synthetic and indigenous naphthenic acids and divalent cations across oil–water interfaces: effects of addition of oil-soluble non-ionic surfactants

Received: 15 February 2005  
Accepted: 5 April 2005  
© Springer-Verlag 2005

Electronic Supplementary Material Supplementary material is available for this article at <http://dx.doi.org/10.1007/s00396-005-1343-0>

Øystein Brandal (✉)  
A.-M. D. Haneseth · J. Sjöblom  
Ugelstad Laboratory, Department of  
Chemical Engineering, Norwegian  
University of Science and Technology,  
7491 Trondheim, Norway  
E-mail: [oystein.brandal@chemeng.ntnu.no](mailto:oystein.brandal@chemeng.ntnu.no)  
Tel.: +47-7-3550339  
Fax: +47-7-3594080

**Abstract** Interactions between naphthenic acids and divalent metal cations across model oil–alkaline water interfaces were investigated by correlating changes in dynamic interfacial tension (IFT), to plausible reaction mechanisms. The measurements were carried out by using a CAM 200 optical instrument, which is based on the pendant drop technique. The naphthenic acids used were synthesised model compounds as well as commercial acid mixtures from crude distillation and extracted acid fractions from a North Sea crude oil. The divalent cations involved  $\text{Ca}^{2+}$ ,  $\text{Mg}^{2+}$ ,  $\text{Sr}^{2+}$ , and  $\text{Ba}^{2+}$ , which are all common in co-produced formation water and naphthenate deposits. The results show that the dynamic IFT strongly depends on naphthenic acid structure, type of divalent cation, and the concentration of the compounds as well as the pH of the aqueous phase. Introducing divalent cations to systems involving saturated naphthenic acids caused mostly a permanent lowering of the IFT. The decline in IFT is due to electrostatic attraction

forces across the interface between the cations in the aqueous phase and the carboxylic-groups at the o/w interface, which cause a higher interfacial density of naphthenic acid monomers. The permanent lowering in IFT is likely due to formation of positively charged monoacid complexes, which possess high interfacial activity. On the other hand, in the case of the aromatic model compounds, the cations affected the IFT differently. This is mainly discussed in light of degree of cation hydration and steric conditions. Various oil-soluble non-ionic surfactant mixtures were also introduced to systems involving a model naphthenic acid and  $\text{Ca}^{2+}$  in order to investigate how the interfacial competition affected the local interactions. Based on the behaviour of dynamic IFT, probable inhibition mechanisms are discussed.

**Keywords** Naphthenic acid · Metal naphthenate · Non-ionic surfactant · Pendant drop · Dynamic interfacial tension · Interfacial reaction

### Introduction

The naturally occurring naphthenic acids in crude oil are complex mixtures consisting of saturated and aromatic rings connected by aliphatic chains [1, 2]. The acids show polydispersity in stoichiometry and molecular weight

[2–5] and due to the complex distribution of different structures, the physico–chemical behaviour of naphthenic acids is quite different from normal fatty acids.

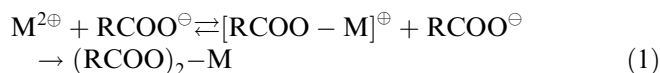
From an operational point of view in crude production, the naphthenic acids are causing several problems. Since they are amphiphilic molecules, they may

accumulate at water–oil interfaces and stabilize emulsions [6–9], which in turn cause enhanced separation problems. When the pH of the co-produced water increases due to release of CO<sub>2</sub> during fluid transportation from the reservoir to the topside, the acid monomers dissociate at the water–oil interface, making them even more interfacially active. In combination with the co-produced formation brine, the dissociated carboxylic groups may also react with cations in the brine to form metal soaps/naphthenates. At certain conditions, these metal soaps can stabilize foams and emulsions [10, 11]. In addition, naphthenates may precipitate during the processing [12–14], mainly in topside facilities like heat exchangers and separators, which may lead to the worst scenarios in cleaning processes and regular production shutdowns.

### Reaction mechanisms

Basically, there are two main approaches, how the naphthenic acids may react with cations to form metal naphthenates. The first and more traditionally one is a reaction between water-soluble acids and cations in the water bulk. The fraction of the acids with the lowest molecular weight is soluble in the aqueous phase, even at pH values near the pKa. However, normally this accounts only for a limited part of the total amount of naphthenic acids: the major part, consisting of larger molecules, is preferably oil-soluble at normal operational conditions and will rather be accumulated at the oil–water interface. According to this, and by taking into account the tremendously large interfaces created when the formation water is emulsified with the crude oil during the transport from the reservoir to the topside, it is obvious that the contact and the interactions between the compounds across the interface may lead to the second approach, i.e. interfacial reactions.

When naphthenic acids and divalent cations react at oil–water interfaces, it is reasonable to suppose that the process involve two reaction stages where the acid monomers sequentially bind to one cation, according to Eq. 1



The rate of formation of naphthenate will thus depend on the stability of the positive monovalent complex. For fast reactions, the occurrence of the intermediate might be neglected as the two monomers will bind almost simultaneously. This is likely the normal case for bulk reactions due to high chain-flexibility and free diffusion. However, when the monomers are distributed at an interface, their location is much more fixed, and effects

like steric hindrance might thus have a reducing impact on the reaction rate or even counteract 2:1 structures to form. Consequently, this would increase the lifetime of the intermediate complex.

Formation of positively charged metal–mono-acid complexes has also been discussed in earlier studies, e.g., by Albers and Overbeek [15] in their investigations in correlating emulsion stability to electrokinetic potential. Later McLaughlin et al. [16] found that divalent cations adsorbed on phosphatidylserin gave rise to positively charged surfaces. A 1:1 binding of cation and acid would probably lower the IFT as the surfactants penetrate deeper into the interfacial layer. On the other hand, if Eq. 1 is fully switched to the right, more hydrophobic structures are formed, which most likely will tend to migrate away from the interface and towards the oil bulk [17]. This is especially the case if multiacidic naphthenates are formed. These electrochemically neutral structures might then accumulate and start to agglomerate in the oil phase, normally in combination with inorganic materials like clay and scale, and further adhere to surfaces of the process units. Naphthenate deposits are becoming a common problem in a number of fields where highly acidic crude oils are processed, like in West Africa [12, 18] and in the North Sea [18, 19]. An improved basic understanding of how the naphthenic acids react to form naphthenates is thus of essential importance for future elimination of related problems.

### Naphthenate inhibition

In order to reduce the extent of naphthenate formation, chemical mixtures of various compositions are nowadays commonly injected into the well stream. Naphthenate deposition is a problem only if the aqueous pH exceeds the pKa of the naphthenic acids. Anything which keeps the pH low, like injecting short-chain organic acids, may thus avoid naphthenate to form [20]. In addition, acid demulsifiers, consisting of acetic acid in an aromatic solvent mixture, and non-acid demulsifiers, consisting of ethoxylates and alcohol, have shown to reduce deposition significantly [21]. The main mechanism behind naphthenate inhibition by using non-ionic surfactants is likely a competitive process, which takes place at the interface. Etoxylates are highly interfacially active and have normally a much higher affinity towards water–oil interfaces than naphthenic acids. Consequently, they may occupy the interface and thus hinder the naphthenic acids to reach it and to further react with the cations. In addition, it is reasonable to assume a diluting mechanism to take place. As pointed out earlier, the lifetime of positively charged 1:1 complexes of naphthenic acid and divalent cations is among other factors that depend on the

interfacial conditions. Due to lateral steric hindrance, 2:1 complexes of branched structures will be less favoured than more aliphatic ones. A similar effect is also achieved by introducing surfactants with large polar headgroups. First, these will cause an increased average intermolecular distance between the naphthenic acid monomers. Second, due to inhibitors located in between the acid monomers, the naphthenic acids also have to restructure in the interfacial layer in order to complete the reaction. Obviously, this will slow down the rate of reaction step 2 in Eq. 1.

During the last decades, interfacial behaviour of organic acids in combination with metal cations in oil–water systems has been an object of several studies [22–27]. A lot of work has also been carried out on systems involving crude oil and caustic water [17, 28–31]. However, a trend in most of the previous work has been to characterize systems after the reaction between the compounds has taken place. As a consequence, and particular for fast reactions, the detection of the initial stages of diffusion and electrostatic interaction across the interface might be lost. In this study, on the other hand, the dynamic IFT is continuously measured during in situ addition of metal cations to the aqueous phase. In this way, we can follow the entire process during one single experiment.

The study is a direct continuation of a recent work in which interfacial interactions between a model naphthenic acid (*p*-*n*-dodecyl benzoic acid) and various divalent cations were investigated by the same experimental technique [32]. Now, several more naphthenic acids, model- as well as indigenous compounds, are involved. Changes in IFT are discussed and correlated to plausible reaction mechanisms. In addition, mixtures of oil-soluble non-ionic surfactants have been introduced

in order to investigate their influence on the interfacial interaction between a synthetic naphthenic acid and calcium ions.

## Experimental

### Chemicals

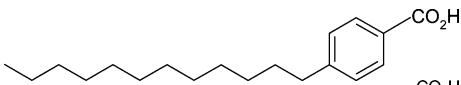
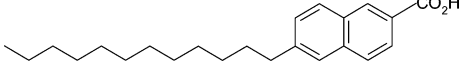
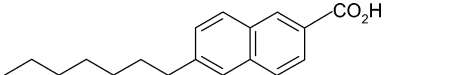
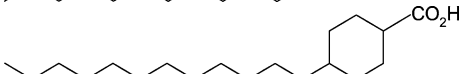
The chemicals were all of high purity delivered from various suppliers. The oil phase employed was a 1–9 volume mixture of toluene and *n*-hexadecane (99%, Acros Organics). The water phase consisted of ultra-pure water buffered to pH 8.0 or pH 9.0 by using a mixture of sodium tetraborate and hydrochloric acid (>99.5%, Acros Organics). The divalent cations were Ca<sup>2+</sup>, Mg<sup>2+</sup>, Sr<sup>2+</sup>, and Ba<sup>2+</sup>, all in form of chloride salt with hydration water (>99%, Chiron).

Totally, eight different naphthenic acids/acid fractions were involved, of those four were model compounds (>99%, Chiron), one commercial acid mixture (Fluka), and three were extracted acid fractions from different distillation cuts of a North Sea crude. The extraction procedure has been described in the literature [33].

Table 1 summarizes all the naphthenic acids used in the experiments, comprising both model compounds and indigenous acid mixtures. Concentrations are given in Table 2.

For the experiments, where surfactant mixtures were introduced to the system, pure *n*-decane (99%, Acros Organics) was used as solvent. Buffer of pH 9.0 was used as water phase. The surfactant mixtures (products 1–5) consisted of different oil-soluble non-ionic compounds.

**Table 1** An overview of the naphthenic acids utilized in the experiments

Name	M (g/mol)	Naphthenic acid structure	Source
<i>p</i> -( <i>n</i> -dodecyl) benzoic acid	290.4		Chiron AS
6-dodecyl-naphthalene- 2-carboxylic acid	340.6		Chiron AS
6-heptylnaphthalene- 2-carboxylic acid	270.4		Chiron AS
4- <i>n</i> -dodecyl-cyclohexane carboxylic acid	296.5		Chiron AS
Fluka naphthenic acid	250*	Mixture	Fluka
Naphthenic acids from North Sea crude; cut 1	200*	Mixture	Statoil ASA
Naphthenic acids from North Sea crude; cut 2	290*	Mixture	Statoil ASA
Naphthenic acids from North Sea crude; cut 3	310*	Mixture	Statoil ASA

\*Average values calculated from total acid number (TAN) by assuming only monoprotic acids



**Table 2** Naphthenic acid (NA) concentrations and divalent cation—naphthenic acid concentration ratios selected for the experiments, correlated to figure numbers

Figure	NA	Conc. NA (mM)	Conc. M <sup>2+</sup> /Conc. NA
1	<i>p</i> -( <i>n</i> -dodecyl) benzoic acid	0.1	3/1
2	4- <i>n</i> -dodecyl-cyclohexane carboxylic acid	1.0	3/1
3	6-dodecyl-naphthalene- 2-carboxylic acid	0.1	3/1
4	a) 6-heptylnaphthalene- 2-carboxylic acid	0.1	3/1
	b) 6-heptylnaphthalene- 2-carboxylic acid	1.0	10/1
5	Fluka naphthenic acid	100	3/1
6	a) Naphthenic acids from North Sea crude, cut 1	10	1/1
	b) Naphthenic acids from North Sea crude, cut 2	20	1/1
	c) Naphthenic acids from North Sea crude, cut 3	20	1/1

## Equipment

All measurements were carried out by using a CAM 200 equipment from KSV Instruments, which is based on the pendant drop technique. Reviews of the theory behind the technique have frequently been presented [34–38]. The instrument consists of a CCD video camera with telecentric optics, a frame grabber, and a LED based background light source. The resolution is 512×512 pixels and the frame interval is between 40 ms and 1,000 s. The LEDs are housed in a reflective sphere, which integrates their light and directs it towards the sample. The light is also strobed and monochromatic, and all these features help to assure sharp images and high accuracy.

## Method

To ensure a high degree of dissociation of the naphthenic acids, it is crucial to operate at an elevated pH when compared to pK<sub>a</sub>. In this work, buffer solutions of pH 9.0 were employed for all systems. At the selected concentration levels, pH 9 is also the upper limit to avoid precipitation of magnesium hydroxide. For the naphthenic acids/acid, mixtures showing high water solubility at pH 9.0, measurements were also carried out at pH 8.0.

All experiments were conducted by forming an oil droplet containing dissolved naphthenic acid upward in the aqueous solution. The concentration of acid was adjusted so that the initial IFT was in the range of 25–30 mN/m. The system was then equilibrated before dissolved metal salts were added to the water phase. The IFT was continuously captured during the entire process with a constant frame interval of one second. The measurements continued for 30 min.

In order to measure interfacial activity, dynamic IFT measurements were also carried out for oil-droplets containing 100 ppm of the oil-soluble non-ionic surfactants. The surfactants showing highest interfacial activity were further combined with one of the model naphthenic acid (*p*-(*n*-dodecyl) benzoic acid). The concentrations of acid and non-ionic surfactants were 0.25 mM and 50 ppm, respectively. Dissolved CaCl<sub>2</sub> was added to a concentration of 0.75 mM after 500 s.

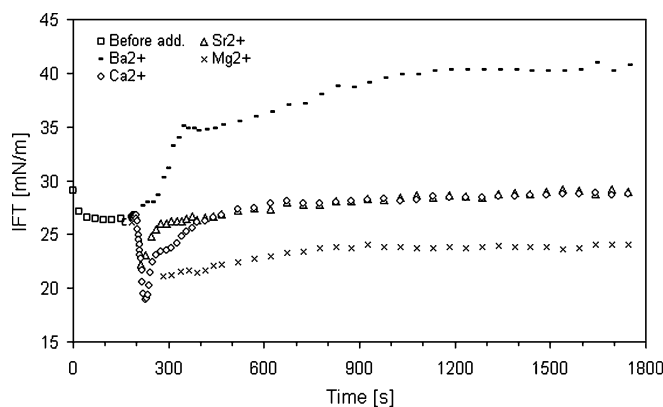


**Fig. 1** Effects of addition of divalent cations on dynamic IFT for o/w systems with *p*-(*n*-dodecyl) benzoic acid

## Results and discussion

All results are plotted as IFT versus time. The first period of time is ascribed to the initial diffusion stage, where the naphthenic acid monomers diffuse towards the o/w interface and, after reaching it, undergo dissociation when brought in contact with the alkaline aqueous phase. For most of the experiments, the initial equilibrium was reached within 3 min. Before divalent cations were added, the systems with the same pH and naphthenic acid structure were identical and showed very similar dynamic IFT. Thus, for reasons of clarity, this period is given by one single curve only, although it represents four individual experiments.

### Model compounds

#### *Naphthenic acids comprising one ring*

Result from measurements on the *p*-(*n*-dodecyl) benzoic acid, also presented in a previous work [32], is given in Fig. 1 for the sake of comparison. As the plots show, the acid monomers equilibrate quite fast at the interface and the divalent cations were thus added after 3 min. This

caused either a sudden decrease or an increase in the IFT, depending on type of added cation. In the case of  $\text{Ba}^{2+}$ , a steep increase in the IFT is observed before the curve gradually flattens out and reaches an almost constant tension value. Introducing the other cations, however, results in a sudden drop in the IFT. For  $\text{Ca}^{2+}$  and  $\text{Sr}^{2+}$ , the drop is followed by a steep increase where the curves elevate to a level slightly above the starting IFT. The curve of  $\text{Mg}^{2+}$ , on the other hand, differs from the others by showing a permanent decrease in the IFT. In this case, the curve monotonously rises only a few units above the lowest value as a function of time. The effect of adding different cations is also concentration dependent, and lower concentrations of counterions cause more similar trends in the cases of  $\text{Ca}^{2+}$ ,  $\text{Sr}^{2+}$ , and  $\text{Mg}^{2+}$  (see Fig. 1.2 in the electronic supplement).

The fact that various cations affect the stability of interfacial films in different ways is well established. During the past, a lot of work has been done in order to investigate these effects. One hypothesis is that the interfacial activity of a cation and thus its reactivity with interfacial negative charges is affected by the amount of water of hydration that surrounds the ion [39–41]. Since the degree of hydration decreases with increasing ionic size,  $\text{Ba}^{2+}$  will bind less water than the other cations in this study, and should hence show a higher affinity towards the interface. The interfacial distance between acid monomers and approaching cations (especially for  $\text{Ba}^{2+}$ ) might thus be sufficiently short for most of the acid monomers to convert to stoichiometric 2:1 structures. The suggestion that the reaction involving  $\text{Ba}^{2+}$  is fast is further supported by the observation that the IFT increases immediately after addition of divalent cations, i.e. no preliminary drop is observed under the current experimental conditions with a camera-speed of one picture a second. According to Eq. 1, this indicates that the lifetime of any monovalent complex is much shorter for  $\text{Ba}^{2+}$  than for the other cations under study.

Formation of naphthenate structures increases the hydrophobicity and decreases the interfacial activity, especially in the case of multivalent cations. The observed increase in IFT is thus a consequence of migration of the formed complexes from the interface and into the oil bulk phase. It is however noteworthy that, after 30 min of time when the curves have flattened out, the IFT is still 10–15 units below the value of the pure o/w interface. This indicates that some interfacially active material still has to be present at the interface. This was also demonstrated in a previous study where mechanical properties of interfacial Langmuir films were investigated [42]. However, since the interface is being compressed in a Langmuir film, the result is a much higher density of interfacial species than in the case of a pendant drop study. Hence, it is not fair to directly compare the results from these two techniques.

For  $\text{Mg}^{2+}$ , the situation is somewhat different than for  $\text{Ba}^{2+}$ . This cation binds six molecules of hydration water, giving it a higher affinity towards water than  $\text{Ba}^{2+}$ . Hence, a steric energy barrier against adsorption is created, which in turn may hinder the interfacially bound  $\text{Mg}^{2+}$  to react further with the second acid monomer. The observed decline in IFT most likely reflects an interfacial coverage of positively charged mono-acid complexes, where the concomitant small monotonous increase in IFT is a result of a gradual diffusion of some magnesium-diacid formed structures into bulk solution.

As indicated by the plots in Fig. 1, addition of  $\text{Ca}^{2+}$  or  $\text{Sr}^{2+}$  gave curves with slopes somewhere in between the cases discussed above. This is in accordance with the correlation between ionic size and amount of hydration water. The monovalent complexes of  $\text{Sr}^{2+}$  and  $\text{Ca}^{2+}$  will be converted into 2:1 structures at a higher rate than in the case of  $\text{Mg}^{2+}$  and, accordingly, the curves of IFT versus time will ascend steeper.

Figure 2 shows the results from the measurements carried out on 4-*n*-dodecylcyclohexane carboxylic acid. The hydrogenated ring gives a more hydrophobic and less interfacially active substance than the corresponding unsaturated structure. This is clearly demonstrated by comparing the levels of the IFT at the beginning of the experiments; the IFT has a higher value than for *p*-(*n*-dodecyl) benzoic acid, even though the concentration of acid is ten times higher. The larger decline in the IFT observed after introducing cations is thus a result of more acid monomers entering the interface. Contrary to the systems with the aromatic C12 naphthenic acid, all the plots of the saturated acid show a permanent lowering of IFT after addition of cations. The decline is even more drastic at increased concentration. Also this effect can be attributed to the hydrophobic structure of the naphthenic acid. A saturated ring will not penetrate so deeply into the interfacial layer as an aromatic one and this will cause longer interfacial distances between

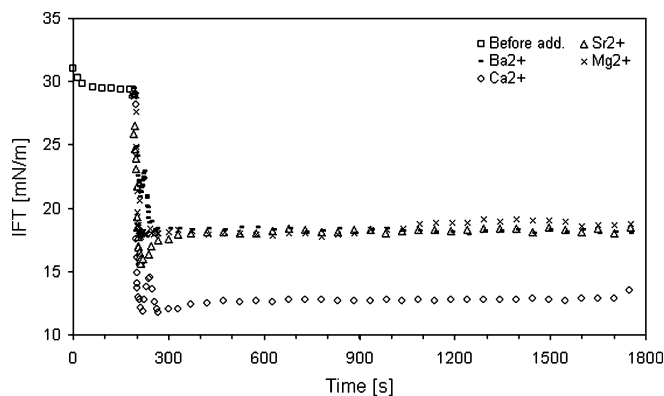


**Fig. 2** Effects of addition of divalent cations on dynamic IFT for o/w systems with 4-*n*-dodecylcyclohexane carboxylic acid

the acid monomers and the divalent cations as an average. Consequently, the interfacial conditions will not promote a completion of the reaction into a final 2:1 ratio between acid and cation. Since the effect is caused by the nature of the acid, an introduction of all cations will influence the IFT in a similar way.

Complementary to the discussion above, the steric hindrance between acid monomers would also affect the rate of reaction. Due to different conformations, the intermolecular distance between molecules containing aromatic rings will be shorter than between corresponding saturated ones. This difference in packing is enhanced by the  $\pi$ -bonds between the aromatic entities which keep the monomers at a closer distance. As a consequence, a formation of 2:1 stoichiometric complexes will be more favourable in the case of aromatic rings.

It is worthwhile noticing that in the case of the condensed structure introduction of  $\text{Ca}^{2+}$  brings about the lowest IFT. This has also been observed at lower concentrations of cations (see figure 2.2 in electronic supplement). The reason for this is, however, not clear and no further explanations are given in order to explain this effect.

#### Naphthenic acids comprising two rings

The results from the measurements performed on 6-dodecyl-naphthalene-2-carboxylic acid are given in Fig. 3. As in the case of the aromatic single-ring structure, addition of  $\text{Mg}^{2+}$  causes a permanent reduction in the IFT, which is more pronounced for 3:1 ratio than for 1:1 ratio of cation and acid (as compared with figure 3.2 in the electronic supplement). The reaction between acid and  $\text{Ba}^{2+}$ ,  $\text{Ca}^{2+}$ , and  $\text{Sr}^{2+}$  gives a rise in the IFT and the final levels in all three cases are in the range of 40–50 mN/m. The structure comprising two aromatic rings seems thus to form 2:1 stoichiometries (with the

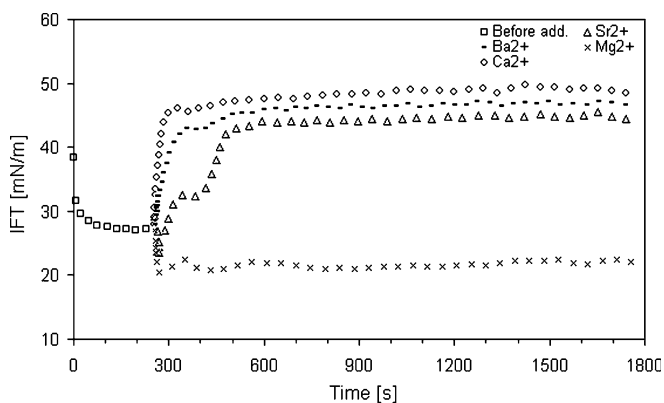


**Fig. 3** Effects of addition of divalent cations on dynamic IFT for o/w systems with 6-dodecyl-naphthalene-2-carboxylic acid

exception of  $\text{Mg}^{2+}$ ) at a higher rate than the corresponding single-ring structure. This may be attributed to the  $\pi$ -bonds; since two aromatic rings now are involved, the acid monomers will pack even denser at the interface than in the case of a single ring.

Figure 4 displays the results from the measurements carried out on 6-heptyl-naphthalene-2-carboxylic acid. Shortly, after initiating the experiments at pH 9 (Fig. 4a) and without any addition of divalent cations, the IFT gradually increases towards the tension value of the pure interface between oil and water. This indicates a migration of the ionized acid from the interface into the aqueous phase, i.e. high water-solubility. This interfacial adsorption and desorption of monomers results in a highly dynamic interface which in turn makes it difficult to identify any effect of added counterions.

At pH 8, given by the plots in Fig. 4b, the situation is very different as a more stable interface is formed. When the divalent cations are added at this pH, a steep decline in IFT is observed. This is in contrast to the curves of  $\text{Ba}^{2+}$  combined with the C12 aromatic single-ring structure, where the initial drop was lacking. In spite of this, the dynamic IFT proceeds in a quite similar way as for the aromatic single-ring acid.

The different behaviour of the curves for  $\text{Ba}^{2+}$  might be attributed to the aqueous pH; a lowering of the pH causes a lower degree of dissociation of naphthenic acid monomers and the interface will be covered by more undissociated molecules. This increases the lateral distances between the charged carboxylic groups at the interface, which in turn lower the reactivity with divalent cations. The lower degree of dissociation is also the reason why much higher concentrations of acid and counterions are required to reach the desired initial IFT.

#### Indigenous compounds

##### Fluka naphthenic acid

The Fluka naphthenic acid, obtained from crude oil distillation, consists of a number of different acid structures. Analysis by FT-IR and NMR ( $^1\text{H}$  and  $^{13}\text{C}$ ) has shown that the mixture mainly consists of saturated naphthenic acids with cyclic- as well as acyclic hydrocarbon moieties.

The results from the pendant drop study are given by Fig. 5. As for the aromatic two-ring structure with C7 aliphatic chain, the water-solubility is high at pH 9 (see figure 5.2 in electronic supplement). By decreasing the pH to 8, a fairly stable IFT is obtained, disregarding the slight monotonous decrease of about 3 units during the first 500 s of time. Due to lower degree of dissociation, however, higher concentrations of acid and cations had to be added than in the case of pH 9. The acid monomers equilibrate quite fast at the interface, as

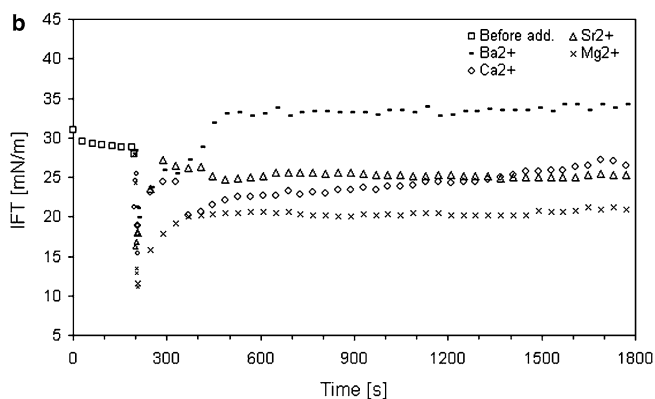
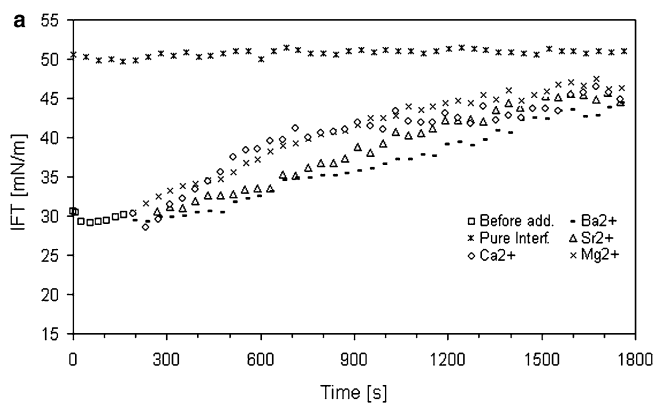


**Fig. 4** Effects of addition of divalent cations on dynamic IFT for o/w systems with 6-heptylnaphthalene-2-carboxylic acid at **a** pH 9.0, and **b** pH 8.0

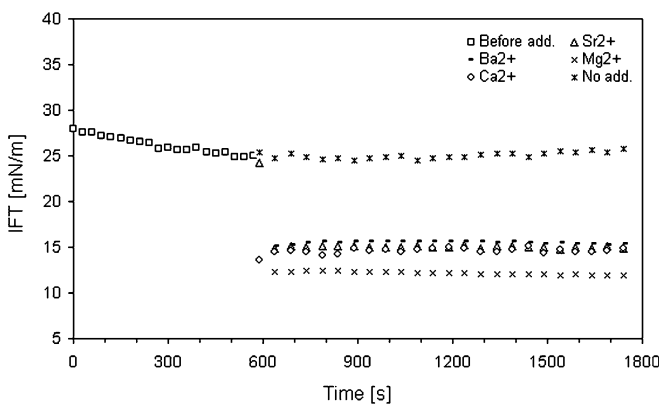


**Fig. 5** Effects of addition of divalent cations on dynamic IFT for o/w systems with Fluka naphthenic acid at pH 8.0

shown by the almost linear curve from the origin of the experiment. This indicates a presence of fast diffusing monomers with high interfacial activity, causing an almost immediate drop in IFT from 51 mN/m, representing a pure o/w interface, to 28 mN/m. The following small decrease in IFT is probably due to a slow process

where the polydisperse monomers are reorientated at the interface.

The divalent cations were added after 500 s. This caused a sudden and permanent decline in the IFT for all systems. After addition of counterions, the compounds also equilibrate quite fast at the interface since no points were captured during the drop. The permanent lowering of the IFT is similar to what observed for the saturated model acid, although addition of  $Mg^{2+}$  now brings about the lowest tension value. Hence, the behaviour is likely a result of the same mechanism as discussed before, i.e. formation of mono-acid complexes, which remain at the interface. The lower pH will also favour the formation of such complexes as more undissociated molecules are occupying the interface.

#### *Naphthenic acids from a North Sea crude*

The naphthenic acids from a North Sea crude oil were selected from three different distillation cuts at temperatures 230–250, 330–350, and 350–370°C. NMR-studies have shown that all acid fractions mainly consist of saturated structures with primary and secondary carboxylic groups, where the molecular weight increases with boiling point of the fraction.

The results from the measurements performed on the distillation cut at 230–250°C are given in Fig. 6a. After addition of cations, the IFT shows a step-wise progress until it equilibrates 10–15 units below the starting value. The step-wise curve is most likely a result of a combination of two processes. First, since the mixture is polydisperse, small molecules will be the first ones to reach the interface due to higher diffusion rates than larger ones. Gradually, however, the smallest molecules will be replaced by larger molecules. Due to their higher water solubility, the low-molecular weight species will cross the o/w interface and dissolve into the aqueous phase. A stepwise adsorption of monomers, to the interface might thus occur depending on the level of interfacial activity. Second, for polydisperse mixtures, more dynamic processes are taking place at the interface than for monodisperse surfactants and, normally, longer times are required for the system to reach equilibrium. This was also the case for the commercially available Fluka naphthenic acid before addition of cations. The sequential steps in IFT might thus refer to temporary states of equilibrium before the real equilibrium is reached as the curves flatten out. At this final state, the interface is covered by a film comprising more interfacially active molecules in combination with divalent cations.

Figure 6b gives the result from the measurements carried out on the 330–350°C fraction. With the addition of divalent cations to systems containing this acid mixture, a decline—followed by a small increase

in IFT occurs, before all curves reach a steady state. The small increase might be due to film restructuring or that a minority of the monomers react to form 2:1 complexes.

The curves of the fraction at 350–370°C, given in Fig. 6c, have very similar shapes at equilibrium as of those at 330–350°C. This indicates the presence of similar structures, which is also in accordance with the overlapping intervals in temperature.

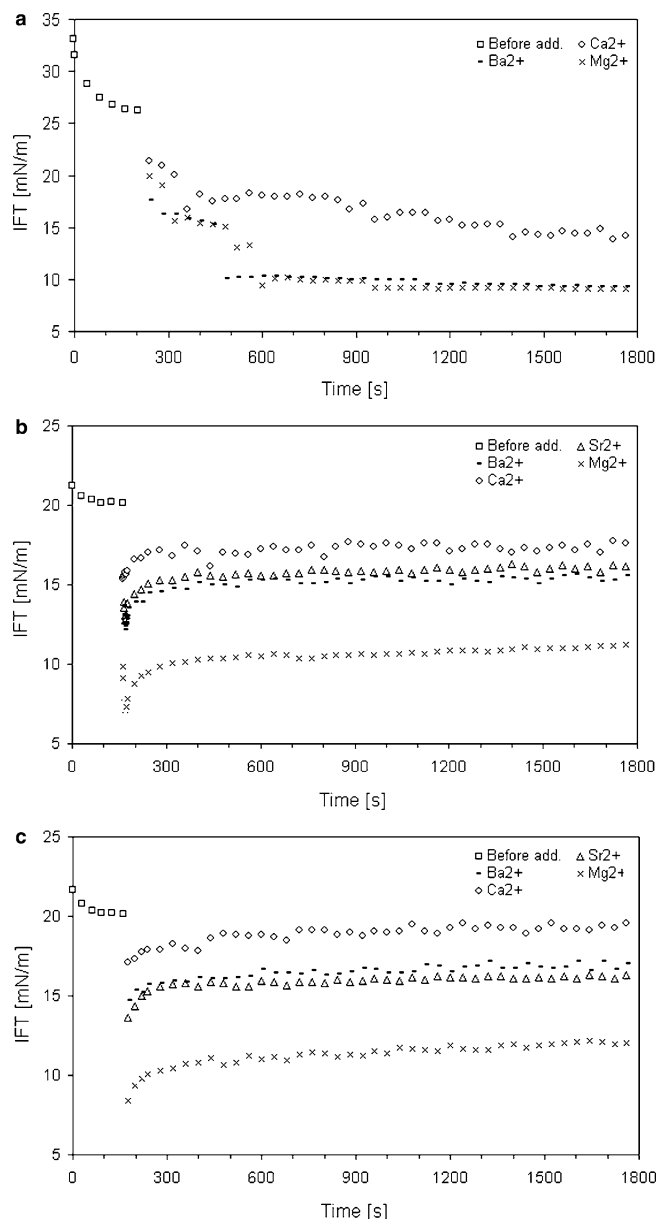


**Fig. 6** Effects of addition of divalent cations on dynamic IFT for o/w systems with North Sea naphthenic acid of **a** distillation cut 1, **b** distillation cut 2, and **c** distillation cut 3

## Introduction of oil-soluble non-ionic surfactants

Oil-soluble non-ionic surfactants have been introduced together with the ionized naphthenic acids in order to create a competitive situation at the o/w interface and to undertake a dilution of the reactive species when multivalent ions are present in the aqueous phase.

### Interfacial activity of additives

Figure 7 shows the results from the measurements of dynamic IFT of the added non-ionic surfactants. In the case of product 1, 2, and 3, the IFT decreases continuously towards a stable value, while product 4 and 5 cause a monotonous increase in the IFT, most pronounced for product 5. This increase reflects a considerable solubility in water. In the case of product 5, an almost pure oil-water interface is obtained within a period of about 20 min.

### Surfactants in combination with naphthenic acid and $\text{Ca}^{2+}$

In the upper part of Fig. 8, dynamic IFT is plotted for a system consisting of an oil droplet of *n*-decane and 0.25 mM *p*-(*n*-dodecyl) benzoic acid in aqueous borate buffer at pH 9.0. As the oil phase now is changed compared to the former studies, the reaction kinetic is a bit different as observed by comparing the result with that in Fig. 1. However, the trends are very much alike as addition of  $\text{Ca}^{2+}$  causes a sudden decrease followed by a steep increase in the IFT. The main difference is the part of the curve during the increase, which ascends steeper in the case of *n*-decane.

The lower part of Fig. 8 shows a typical result from an inhibition experiment based on the surfactants in Fig. 7. As an example, we have chosen product 2. The equilibrium IFT is now lowered several units and consequently, the decline in IFT caused by the reaction with  $\text{Ca}^{2+}$  becomes less prominent, since the interface now is mainly covered by non-ionic surfactant molecules instead of reactive acid monomers. Another conspicuous observation is that, after addition of  $\text{Ca}^{2+}$ , the curve ascends slower than in the case when no non-ionic surfactant is present. This is a consequence of the interfacial dilution and steric effects, causing a lower rate of completing the reaction to stoichiometric 2:1 compounds.

## Conclusions

The pendant drop technique has proved to be a suitable tool to investigate interfacial reactions between naphthenic acids and divalent cations across oil-water

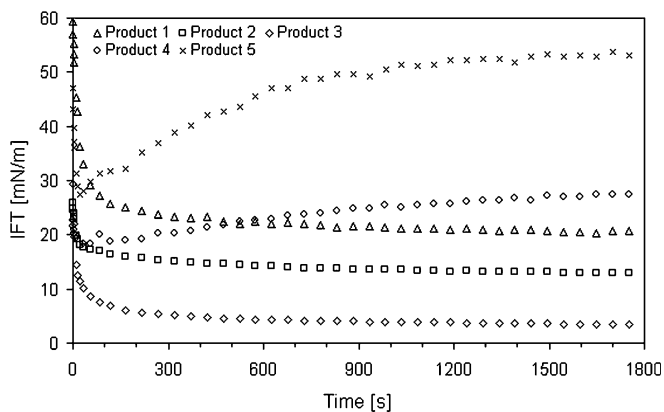


**Fig. 7** Interfacial activity of oil-soluble non-ionic surfactant mixtures (products 1–5)

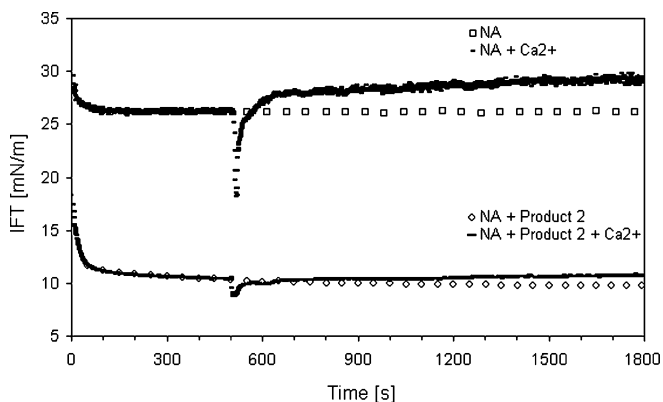


**Fig. 8** Dynamic IFT upon addition of  $\text{CaCl}_2$  in the case of only naphthenic acid and in the case of naphthenic acid combined with non-ionic surfactants of product 2

interfaces. The results show that the dynamic IFT strongly depends on the naphthenic acid structure and type and concentration of divalent cation. Before introducing divalent cations, the naphthenic acids containing aromatic rings seem to be more interfacially active than the corresponding saturated structures. This is due to a twofold effect caused by the  $\pi$ -bonds, which to start with enable the monomers to penetrate deeper

into the interfacial layer and, moreover, bring along a higher monomer density at the interface. In combination with divalent cations, the solubility behaviour is changed, either due to reaction to form 2:1 stoichiometric complexes or by forming 1:1 positively charged mono-acid complexes residing mainly at the o/w interface. The mechanism which dominates is depending on degree of cation hydration, which affects the cation affinity towards the interface and thus the distance between the interacting compounds.

Saturated naphthenic acid structures, including model as well as indigenous compounds, seem mainly to cause a permanent lowering of IFT in interaction with all the divalent cations. This condition is probably a result of the hydrophobic acid structures, which penetrate less into the interfacial layer when compared to the unsaturated model acids and hence form more well-defined o/w interfaces. Consequently, this causes longer interfacial distances between the acid and the divalent cation which hinder 2:1 stoichiometric complexes to form. In addition, steric hindrance caused by bulky monomers might also counteract a 2:1 binding of monomers as the lateral distance between the acid headgroups increases.

When oil-soluble non-ionic surfactants are introduced to systems containing the aromatic C12 acid and  $\text{Ca}^{2+}$ , two main effects are generally observed; the initial decline in IFT can be substantially reduced and the rate of the following increase in IFT is lowered. The first is a result of interfacial coverage of highly active and non-reactive surfactant molecules, which hinder the less active naphthenic acid monomers to react at the interface with the divalent cations. The second observation likely reflects interfacial dilution of the acid monomers, causing a lower converting into 2:1 complexes.

**Acknowledgements** Statoil ASA and The Norwegian Academy of Science and Letters are acknowledged for the financial support through the VISTA programme. Acknowledgements are also extended to the JIP consortium, consisting of oil industry (ChevronTexaco, Statoil, and Total) and chemical vendors (AkzoNobel, BakerPetrolite, and ChampionTechnologies), and to Heidi Mediasa (Statoil) for providing the North Sea naphthenic acid samples. The chemical vendors are thanked for supplying the non-ionic surfactant mixtures.

## References

- Brient JA, Wessner PJ, Doyle MN (1995) In: Kirk-Othmer Encyclopedia of Chemical Technology, Wiley, New York, pp 1017–1029
- Seifert WK (1975) Fortschr Chem Org Naturst 32:1–49
- Tomczyk NA, Winans RE, Shinn JH, Robinson RC (2001) Energy Fuels 15:1498–1504
- Fan T-P (1991) Energy Fuels 5:371–375
- Koike L, Reboucas LMC, Reis FdA, Marsaioli AJ, Richnow HH, Michaelis W (1992) Org Geochem 18:851–860
- Pathak AK, Kumar T (1995) In: Proceedings of PETROTECH-95, New Delhi, India
- Márquez ML (1999) In: AICHE spring national meeting, Session T6005, Houston, TX

- 
8. Acevedo S, Escobar G, Ranaudo MA, Khazen J, Borges B, Pereira JC, Méndez B (1999) *Energy Fuels* 13:333–335
  9. Goldszal A, Bourrel M, Hurtevent C, Volle J-L (2002) In: *The 3rd international conference on petroleum phase behavior and fouling*, New Orleans, USA
  10. Ese M-H, Kilpatrick PK (2004) *J Disp Sci Techn* 25:253–261
  11. Taylor SD, Czarnecki J, Masliyah J (2005) *J Colloid Interface Sci* 282:499–502
  12. Poggesi G, Hurtevent C, Buchart D (2002) In: *SPE oilfield scale symposium*, SPE74649, Aberdeen, UK
  13. Gallup DL, Smith PC, Chipponeri J, Abuyazid A, Mulyono D (2002) In: *SPE international conference on health, safety and environment in oil and gas exploration and production*, SPE73960, Kuala Lumpur, Malaysia
  14. Vindstad JE, Bye AS, Grande KV, Hustad BM, Hustvedt E, Nergård B (2003) In: *SPE 5th international symposium on oilfield scale*, SPE80375, Aberdeen, UK
  15. Albers W, Overbeek JTG (1959) *J Colloid Sci* 14:501–509
  16. McLaughlin S, Mulrine N, Gresalfi T, Vaio G, McLaughlin A (1981) *J Gen Phys* 77:445–473
  17. Jennings HY Jr (1975) *Soc Pet Eng J* 15:197–202
  18. Rousseau G, Zhou H, Hurtevent C (2001) In: *SPE oilfield scale symposium*, SPE68307, Aberdeen, UK
  19. Dyer SJ, Graham GM, Arnott C (2003) In: *SPE 5th international symposium on oilfield scale*, SPE80395, Aberdeen, UK
  20. Goldszal A, Hurtevent C, Rousseau G (2002) In: *SPE oilfield scale symposium*, SPE74661, Aberdeen, UK
  21. Gallup DL (2004) In: *SPE 6th international symposium on oilfield scale*, SPE87471, Aberdeen, UK
  22. Pilpel N (1969) *Adv Colloid Interface Sci* 2:261–296
  23. Chifu E, Sálájan M, Demeter-Vodnár I, Tomoaia-Cotisel M (1987) *Revue Roumaine de Chimie* 32:683–691
  24. Flipsen JAC, van der Hijden HTWM, Egmond MR, Verheij HM (1996) *Chem Phys Lip* 84:105–115
  25. Hoppe A, Theimer RR (1996) *Phytochem* 42:973–978
  26. Demeter-Vodnár J, Sálájan M, Lowy DA (1996) *J Colloid Interface Sci* 183:424–430
  27. Touhami Y, Hornof V, Neale GH (1998) *Colloids Surf A* 133:211–231
  28. Acevedo S, Ranaudo MA, Escobar G, Gutierrez X (1999) *Fuel* 78:309–317
  29. Trujillo EM (1983) *Soc Pet Eng J* 23:645–656
  30. McCaffery FG (1976) *J Can Pet Tech* 15:71–74
  31. Sharma MM, Jang LK, Yen TF (1989) In: *SPE reservoir engineering*, SPE12669, pp 228–236
  32. Brandal Ø, Sjöblom J, Øye G (2004) *J Disp Sci Techn* 25:367–374
  33. Mediaas H, Grande KV, Hustad BM, Rasch A, Rueslåtten HG, Vindstad JE (2003) In: *SPE 5th international symposium on oilfield scale*, SPE80404, Aberdeen, UK
  34. Andreas JM, Hauser EA, Tucker WB (1938) *J Phys Chem* 42:1001–1019
  35. Winkel D (1965) *J Phys Chem* 69:348–350
  36. Ambwani DS, Fort T Jr (1979) *Surf Colloid Sci* 11:93–119
  37. Rotenberg Y, Boruvka L, Neumann AW (1983) *J Colloid Interface Sci* 93:169–183
  38. Boucher EA, Evans MJB, Jones TGJ (1987) *Adv Colloid Interface Sci* 27:43–79
  39. Marra J, Israelachvili J (1985) *Biochem* 24:4608–4618
  40. Yazdaniyan M, Yu H, Zografi G (1990) *Langmuir* 6:1093–1098
  41. Ederth T, Claesson PM (2000) *J Colloid Interface Sci* 229:123–128
  42. Brandal Ø, Sjöblom J (2005) *J Disp Sci Techn* 26:53–58

# Paper IV



Isolation and Characterization of Naphthenic Acids  
from Metal Naphthenate Deposit. Molecular Properties  
at Oil-Water and Air-Water Interfaces.

Øystein Brandal <sup>1,\*</sup>, Ann-Mari D. Hanneseth <sup>1</sup>,  
Pål V. Hemmingsen <sup>1</sup>, Johan Sjöblom <sup>1</sup>, Sunghwan Kim <sup>2</sup>,  
Ryan P. Rodgers <sup>2</sup>, and Alan G. Marshall <sup>2,3</sup>.

<sup>1</sup> Ugelstad Laboratory, Department of Chemical Engineering, Norwegian University  
of Science and Technology, N-7491 Trondheim, Norway.

<sup>2</sup> National High Magnetic Field Laboratory, Florida State University,  
1800 East Paul Dirac Dr., Tallahassee, FL 32310-4005.

<sup>3</sup> Department of Chemistry and Biochemistry, Florida State University,  
Tallahassee, FL 32306.

\* Corresponding author (e-mail: oystein.brandal@chemeng.ntnu.no).

## ABSTRACT

Naphthenic acids from a West African metal naphthenate deposit have been isolated and characterized by means of infrared (IR), nuclear magnetic resonance (NMR), and Fourier transform ion cyclotron resonance mass spectrometry (FT-ICR MS). The sample has shown to comprise a narrow group of 4-protic naphthenic acids of molecular weight around 1230 g/mol. The determined mass of 1230.0627 amu suggests a compound with the elemental formula of  $C_{80}H_{142}O_8$ , having 6 sites of unsaturation in the hydrocarbon moiety. The NMR data show no sign of carbon-carbon multiple bonds. Hence, the sites of unsaturation are assumed to arise from condensed rings.

The naphthenic acids have proved to be highly oil-water (o/w) interfacially active. By elevating the pH from 5.6 to 9.0, the interfacial activity increases gradually due to a higher degree of dissociation of the carboxylic groups. At pH 9.0, the interfacial tension (IFT) between water and toluene-hexadecane (1-9 vol.) is lowered about 40 units at concentrations of only 0.0050-0.010 mM naphthenic acid. The decrease-rate of the IFT ( $d\gamma/dt$ ) is also concentration dependent, and a well-defined IFT is attained at long observation times.

The  $C_{80}$  naphthenic acids have shown to form relatively unstable Langmuir monolayers. The stability decreases further with increasing pH as more monomers become dissociated and dissolve into the aqueous phase. The stability is altered upon addition of calcium ions into the subphase due to formation of calcium naphthenate at the surface. In the undissociated state, the naphthenic acid has a molecular area of about  $160 \text{ \AA}^2/\text{molecule}$  in the non-interacting region. The high area reflects an extensive molecular structure comprising four carboxylic headgroups, which are likely to be separated by hydrocarbon chains.

**Key words:** *metal naphthenate, naphthenic acid characterization, interfacial activity, Langmuir monolayer properties.*

## INTRODUCTION

During the last decade, there has been an ever increasing recovery of acidic crude oils [1]. The acidity is predominantly caused by organic acids, which in the petroleum industry generally are termed as naphthenic acids. Producing and processing highly acidic crudes involve several challenges. Naphthenic acid corrosion, especially in the high temperature parts of the distillation units, is a major concern to the refining industry [2-4]. During production, the amphiphilic naphthenic acids may also accumulate at interfaces and stabilize emulsions [5-8], causing enhanced separation problems. However, the most serious production issue related to naphthenic acids is probably deposition of metal naphthenate. The release in pressure during the fluid transportation from the reservoir to the topside leads to an increase in the pH of the co-produced water, causing a higher degree of dissociation of naphthenic acids at the oil-water (o/w) interface. As a consequence, the moieties become reactive towards metal cations in the co-produced formation brine. The product from this reaction, metal naphthenate, might then accumulate and start to agglomerate in the oil phase, normally in combination with inorganic materials like clay and scale, and further adhere to process unit surfaces. Deposition of naphthenate is a problem predominantly in topside facilities like separators and de-salters, and may from an operational point of view lead to the worst case scenarios in cleaning processes and regular production shutdowns. Naphthenate deposition is becoming a common problem in a number of fields in where acidic crudes are being processed, including fields in West Africa [9, 10] and on the Norwegian continental shelf [10, 11].

Naphthenic acids are predominantly found in immature heavy crude [12, 13]. Hence, they are assumed to generate from in-reservoir biodegradation of petroleum hydrocarbons [14-16]. Several analytical techniques have been utilized to qualitatively characterize naphthenic acids extracted from crude oils. This includes various mass spectrometry (MS) methods [17-21], gas chromatography-mass spectrometry (GC-MS) methods [22-24], and these methods in combination with Fourier transform infrared (FT-IR) and/or nuclear magnetic resonance (NMR) spectrometry [25-27]. Generally, the acids have shown to comprise complex mixtures of alkyl-substituted acyclic and cycloaliphatic carboxylic acids, showing variations in structure and molecular weight.

The composition of naphthenic acids found in metal naphthenates from different sources may also differ, as pointed out by Gallup and co-workers [28, 29]. From a characterization study of a soap-sludge from an Indonesian field, they found naphthenate consisting of long-chain fatty acids and sodium. According to the authors, this is contrary

to studies from other fields, where naphthenate has shown to comprise predominantly cyclic naphthenic acid structures in combination with calcium. More recently, Baugh and co-workers [30] also demonstrated that naphthenic acids forming naphthenate do not necessarily resemble the majority of the naphthenic acids existing in the crude. By characterizing a deposit from the North Sea, they found exciting results, indicating that a narrow family of 4-protic acids in the molecular weight range 1227-1235 g/mol is the main contributor to naphthenate deposition. Allegedly, similar observations have also been found by analysing deposits from other fields, including UK sector and West Africa.

In this paper, naphthenic acids acquired from a West African naphthenate deposit are examined by means of infrared (FT-IR) spectrometry, nuclear magnetic resonance (NMR) spectrometry, and electrospray ionization (ESI) coupled to high-field (9.4 T) Fourier transform ion cyclotron resonance mass spectrometry (FT-ICR MS). The latter technique has previously shown to offer a very promising and powerful tool for detailed chemical characterization of heteroatomic species in crude oils [31], in crude oil distillates [32] as well as in humic materials [33-35].

In addition to the characterization study, this paper also presents some results from measurements of interfacial properties of the isolated naphthenic acids, including interfacial activity at o/w interfaces and compressibility of monolayers of naphthenic acids and naphthenates at air-water surfaces. The aim of this work has been to get a basic understanding of how the compounds behave and interact at interfaces, which is of major interest in order to explain the mechanisms behind naphthenate formation. The measurements have been carried out under different experimental conditions using pendant drop and Langmuir technique. The first technique is useful to measure dynamic interfacial tensions [36, 37], whereas the latter yield crucial information about molecular-molecular interactions, molecular areas, and film resistance against compression [38-42].

## EXPERIMENTAL

### I) Chemicals

All chemicals were used as supplied: toluene and n-hexadecane (p.a., Acros Organics), hydrochloric acid (p.a., Fisher), sodium tetraborate decahydrate and potassium phosphate trihydrate (>99%, Acros Organics), and calcium chloride dihydrate (>99.5%, Roth).

### II) Isolation and characterization of naphthenic acids from deposit

#### Isolation procedure

The deposit sample was collected from an oil-producing installation in West Africa. In brief, the naphthenic acids were isolated from the deposit by first washing the sample thoroughly in toluene to remove crude oil and oil-soluble fractions. This process continued till an almost clear toluene phase was obtained. The remaining solid was then exposed to a 2:1 volume mixture of toluene and 1M HCl solution to dissolve the metal naphthenate. The naphthenic acids chemically bound as naphthenate were thus converted to free acid monomers which dissolve into the toluene phase, leaving the counterions in the aqueous phase. The naphthenic acids were then selectively isolated from other potentially occurring polar compounds by ion-exchange. Finally, the solvent was removed from the naphthenic acids by evaporation on a rotary evaporator at 60 °C and further by drying in an oven at the same temperature.

#### Characterization methods

**Mass analysis:** Details of the procedures used for sample preparation and the conditions of the ESI FT-ICR MS analysis have been published previously [43, 44]. In brief, sample solutions were prepared by dissolving oil samples at a concentration of ~ 1mg/ml to 50:50 a toluene:methanol solution prior to introduction to a microelectrospray source [45] at a flow rate of 400 nl/min. One ml of sample solution was spiked with 4 µl of NH<sub>4</sub>OH to ensure efficient ionization (deprotonation) for negative-ion ESI analysis: 50 µm i.d. fused silica needle, 2 kV needle voltage, 300 V tube lens, 4 A heated capillary current. A homebuilt FT-ICR mass spectrometer equipped with a 22 cm horizontal room temperature bore 9.4 T magnet [46] was used. Ions generated in ESI source region are

first accumulated in an external linear octopole ion trap for 20-60 s and transferred through rf-only multipoles to a 10 cm diameter, 30 cm long open cylindrical Penning ion trap [47]. Multipoles [48] were typically operated at 1.7 MHz at a peak-to-peak rf amplitude of 170 V. After ions were excited in the trap by broadband frequency-sweep (chirp) dipolar excitation (70 - 641 kHz at a sweep rate of 150 Hz/ $\mu$ s and peak-to-peak amplitude of 190 V), direct mode image current detection was performed to yield 4 Mword time-domain data. Time-domain data sets were co-added (200 acquisitions) and then Hanning apodized, followed by one zero-fill before fast Fourier transformation and magnitude calculation. Frequency was converted to mass-to-charge ratio by the quadrupolar electric trapping potential approximation [49, 50]. Data acquisition and processing are conducted with the MIDAS system [51, 52]. Mass spectra were externally calibrated with respect to a G241A Agilent (Palo Alto, CA) electrospray "tuning mix." Masses obtained from the calibrated spectra were then converted to Kendrick mass and sorted according to their Kendrick mass defects [53]. Peaks were assigned by Kendrick mass defect analysis as previously reported [44]. Briefly, an elemental formula was assigned to the peak with lowest m/z value at each Kendrick mass defect. Only C, H, O, N, S,  $^{13}\text{C}$  and  $^{34}\text{S}$  atoms were considered in assigning elemental formulas. The remaining peaks were assigned by adding a series of  $\text{CH}_2$  groups to each assigned elemental formula.

**Nuclear Magnetic Resonance (NMR) Spectrometry:** All NMR experiments were performed on a Bruker DMX 400 NMR spectrometer.  $^1\text{H}$ - and  $^{13}\text{C}$ -NMR spectra were recorded at 400 MHz and 100 MHz, respectively, using deuterated methanol ( $\text{CD}_3\text{OD}$ ) as solvent, and dioxane as internal standard ( $\sim 1$  vol%).  $90^\circ$  pulses were used to suppress any nuclear Overhauser effect. In the  $^1\text{H}$ -NMR experiments a pulse delay of 20 seconds was used to cancel out any relaxation effects. The quantitative  $^{13}\text{C}$ -NMR experiments were performed upon addition of a relaxation agent, chromium trisacetylacetonate (0.1-0.2 M) in an inverse gated decoupling system with a pulse delay of 5 seconds. The NMR measurements were undertaken using 5-10 wt% solutions.

**Infrared Spectrometry:** IR spectrum was recorded in the range between 1000 and 4000  $\text{cm}^{-1}$  using a Tensor 27 FT-IR spectrometer (Bruker Optics) and a MKII Golden Gate ATR unit (Specac) in single reflection configuration. The instrument is fitted with a Michelson interferometer and a  $\text{N}_2$ -cooled MCT detector (Mercury Cadmium Telluride). One drop of the naphthenic acid sample was placed onto the diamond ATR crystal (4  $\text{mm}^2$ ) and analyzed. To improve the signal-to-noise ratio, 64 scans were recorded at a resolution of 1  $\text{cm}^{-1}$  and averaged. The resulting IR spectrum was Fourier transformed with a Blackman-Harris 3-Term apodization function and a zerofilling factor of 2.

### III) Surface and interfacial properties of naphthenic acids

#### Interfacial (o/w) activity

Naphthenic acids isolated from the naphthenate deposit were dissolved in toluene (10 vol%) and diluted by n-hexadecane at different concentrations. The concentration was calculated using the molecular weight determined in the MS study (1230 g/mol). The water phase consisted of ultra-pure water of pH 5.6, ultra-pure water buffered to pH 7.0 using potassium dihydrogen phosphate and hydrochloric acid, or ultra-pure water buffered to pH 9.0 using sodium tetraborate and hydrochloric acid.

The CAM 200 pendant drop equipment (KSV Instruments) was used to measure dynamic interfacial tensions. The theory behind the technique has frequently been presented in previous studies [54-58]. The instrument includes a CCD video camera with telecentric optics, a frame grabber, and a LED based background light source. The resolution is 512 x 512 pixels and the frame interval is between 40 ms and 1000 s. The LEDs are housed in a reflective sphere which integrates their light and directs it towards the sample. The light is also strobed and monochromatic, and all these features help to assure sharp images.

All experiments were conducted forming an oil droplet (~5  $\mu$ l) containing dissolved naphthenic acid upward in an aqueous solution (3.5 ml). The IFT was continuously determined for totally 30 minutes with a constant frame interval of one second.

#### Langmuir monolayer properties

Surface pressure-area isotherms were recorded using a KSV Langmuir minitrough double-barrier system. The trough was made of Teflon and the barriers of Derlin. Water phases of four different pH levels were selected. For the most acidic (pH 2.3) and alkaline (pH 11.6) solutions, the pH was adjusted using hydrochloric acid and sodium hydroxide, respectively. Measurements were also performed on ultra-pure water (pH 5.6) and ultra-pure water buffered to pH 9.2 using sodium tetraborate and hydrochloric acid. For the aqueous solutions of pH 5.6, 9.2, and 11.6, the effect on film compressibility upon addition of calcium chloride at different concentrations was investigated. Stability isotherms at different pH levels and  $\text{Ca}^{2+}$  concentrations were also recorded by measuring the relative area loss ( $A/A_0$ ) after compressing the monolayer to a constant surface pressure of 10 mN/m.

Toluene was used as spreading solvent for the naphthenic acid. Volumes of 50  $\mu\text{l}$  solution at a concentration of 0.2 mM showed to be adequate for the measurements. The concentration was calculated using the molecular weight determined in the MS study (1230 g/mol). The solvent was allowed to evaporate for 20 minutes before compression was initialized. Film compression was carried out with a constant barrier speed of 5 mm/min. The temperature of the aqueous subphase was kept constant at 20 °C using a Huber ministat125 temperature controller.



## RESULTS AND DISCUSSION

### I) Characterization study

Figure 1 shows a FT-IR spectrum of the naphthenic acid sample. The data exhibits a strong peak at  $1705\text{ cm}^{-1}$  which can be attributed to a C=O stretch. The broad band displayed in the region  $3300\text{-}2500\text{ cm}^{-1}$  reflects O-H stretching of existing carboxylic acid dimers (due to high concentration) whereas the moderately intense bands near  $1400$  and  $1300\text{ cm}^{-1}$  correspond to C-O-H in-plane bend and C-O stretch, respectively, and interactions between them.

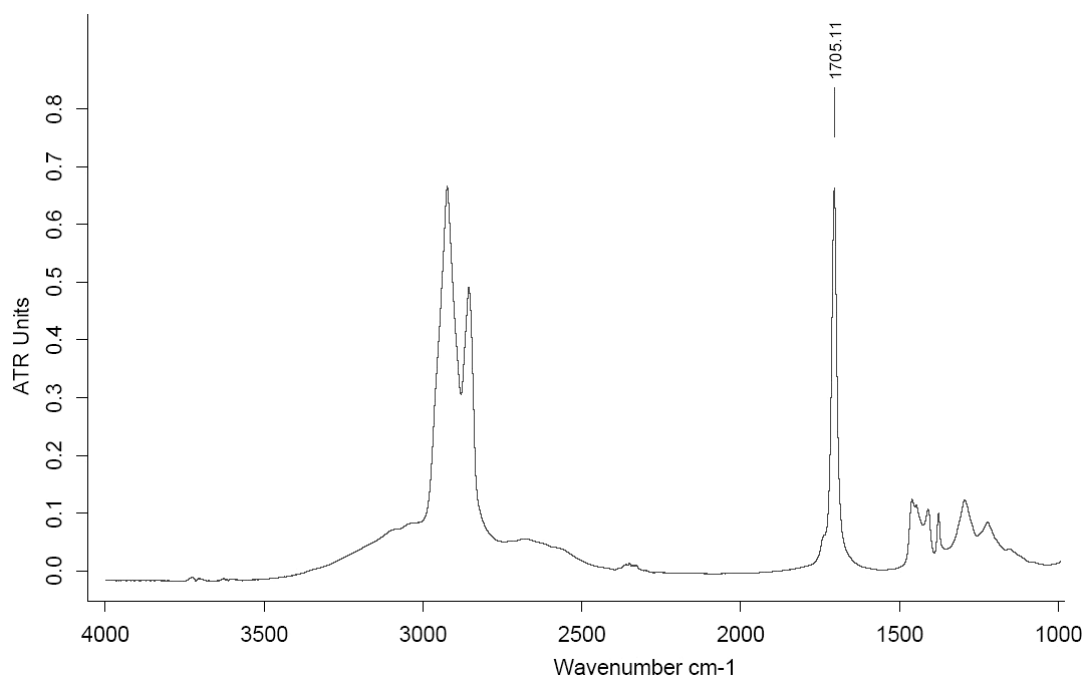


Figure 1: FT-IR spectrum of the naphthenic acid sample.

Figure 2 displays the resulting broadband mass spectrum from the ESI FT-ICR MS analysis. As observed, the spectrum is dominated by a narrow distribution of peaks located around 1230 amu. The main peak in the spectrum, exactly located at 1230.0627 amu, is consistent with the ion  $[\text{C}_{80}\text{H}_{141}\text{O}_8]^-$ , i.e. it refers to a compound with the elemental formula of  $\text{C}_{80}\text{H}_{142}\text{O}_8$  having a molecular weight of 1231.0707 g/mol.

The number of rings plus double bonds for a given elemental formula can be calculated as the so-called double bond equivalence (DBE) from the following equation:

$$DBE = 1 + \frac{1}{2} \left( \sum_i n_i (v_i - 2) \right) \quad (1)$$

in which  $n$  represents the number of atoms for element  $i$ , and  $v_i$  is the formal valence for that element. For an elemental formula of  $C_{80}H_{142}O_8$ , this gives a DBE of 10.

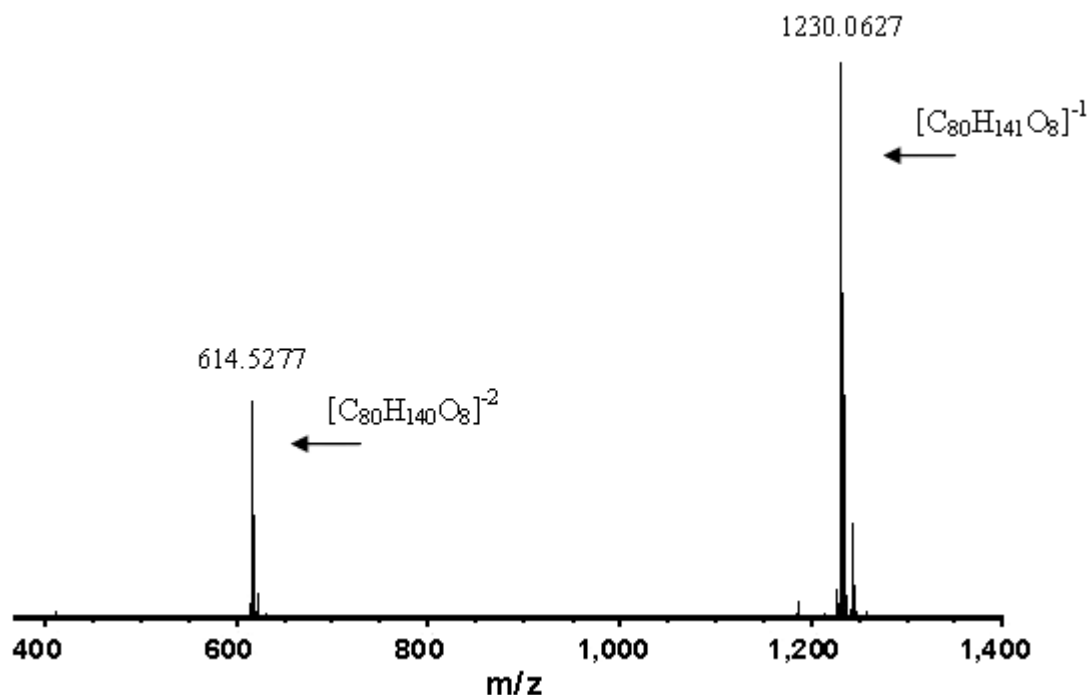


Figure 2: FT-ICR mass spectrum of the naphthenic acid sample.

Figures 3-4 show  $^{13}C$  and  $^1H$  NMR spectra of the naphthenic acid sample, respectively. Typically, NMR spectra of petroleum and petroleum fractions contain broad overlapping peaks [59-61] due to the complexity and the high number of isomers in the sample. However, for the fraction isolated from the naphthenate deposit, the  $^{13}C$ -NMR spectrum shows a single peak in the carboxylic acid region and well resolved peaks in the aliphatic region. The  $^1H$ -NMR spectrum shows four distinct regions, indicating the type of hydrogen. Neither spectra show any sign of aromatics or other carbon-carbon multiple bonds.

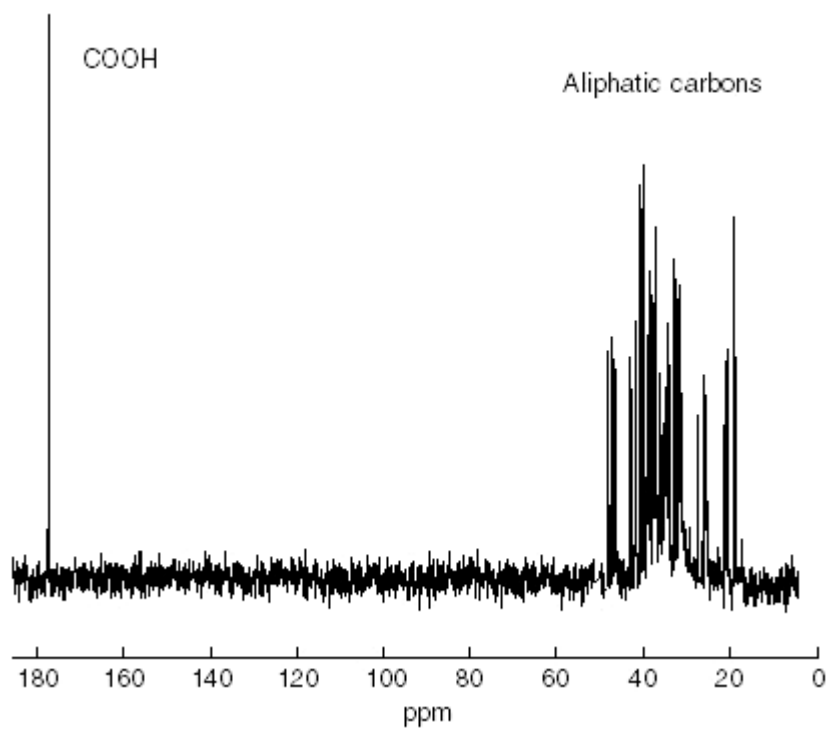


Figure 3:  $^{13}\text{C}$ -NMR spectrum of the naphthenic acid sample.

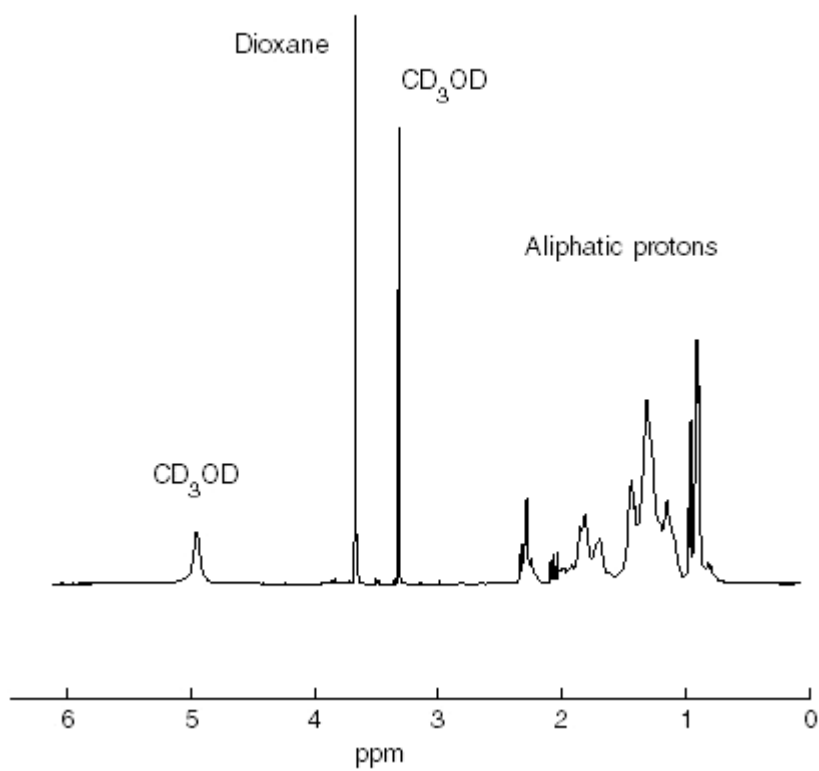


Figure 4:  $^1\text{H}$ -NMR spectrum of the naphthenic acid sample.

From the  $^{13}\text{C}$ -NMR spectrum, the C/O molar ratio can be computed from the following equation:

$$C/O = \frac{A_{C,\text{total}}}{2A_{C=O}} \quad (2)$$

where  $A_{C,\text{total}}$  is the total integrated area of the carbon signals, and  $A_{C=O}$  is the integrated area of the carboxylic acid peak. Using the same sample in both the  $^1\text{H}$ -NMR and  $^{13}\text{C}$ -NMR experiments, only adding relaxation agent in the  $^{13}\text{C}$ -NMR experiment, one can calculate the C/H ratio by:

$$C/H = \frac{A_{C,\text{total}}}{A_{H,\text{total}}} \frac{Eq_{\text{std}}^C}{Eq_{\text{std}}^H} \frac{A_{\text{std}}^H}{A_{\text{std}}^C} \quad (3)$$

where  $A_{C,\text{total}}$  and  $A_{H,\text{total}}$  are respectively the integrated areas of the sample peaks in the  $^{13}\text{C}$ -NMR and in the  $^1\text{H}$ -NMR spectrum,  $Eq_{\text{std}}^C$  and  $Eq_{\text{std}}^H$  are respectively the numbers of equivalent carbons and protons in the internal standard, and  $A_{\text{std}}^C$  and  $A_{\text{std}}^H$  are the integrated areas of the internal standard signal in the  $^{13}\text{C}$ -NMR and in the  $^1\text{H}$ -NMR spectrum. However, it might be difficult to include the carboxylic protons in  $A_{H,\text{Total}}$  from the  $^1\text{H}$ -NMR spectrum. The protons on a heteroatom differ from other protons because they are exchangeable and subject to hydrogen bonding. Carboxylic acids exist as stable hydrogen-bonded dimers in non-polar solutions, even at high dilution. In polar solvents, like methanol, the exchange rate is slow and the corresponding peak will be broad. Further, dissolved water, alcohol or acidic protons will interfere, causing a large shift and the main carboxyl peak will decrease. Since  $\text{CD}_3\text{OD}$  was used as solvent, the carboxylic protons will interchange with the alcoholic deuterium. However, the information from the  $^{13}\text{C}$ -NMR spectrum can be utilized since there is one proton per carboxylic carbon. It can be shown that this gives the following expression for the C/H ratio:

$$C/H = \frac{1}{\frac{1}{C_{\text{total}}/H_{\text{total-COOH}}} + \frac{1}{2C/O}} \quad (4)$$

where  $C_{\text{total}}/H_{\text{total-COOH}}$  is obtained from Eq. (3) not including carboxylic protons and  $C/O$  is given by Eq. (2). The analysis of the NMR spectra gives  $C/O = 10.2$  and

C/H = 0.58. Assuming one carboxylic group per molecule, this gives an average molecular weight of 313 g/mol, which is far below the determined weight in the MS study. However, assuming four carboxylic groups per molecule, the molecular weight is 1252 g/mol, which is close to the MS results. Hence, this indicates that the determined compound with the elemental formula of  $C_{80}H_{142}O_8$  and the molecular weight of 1231.0707 g/mol is a 4-protic acid. The peak appearing at 614.5277 amu in figure 2 is also consistent with doubly charged  $C_{80}H_{142}O_8$  molecules, i.e. deprotonation of two carboxylic groups ( $C_{80}H_{140}O_8^{2-}$ ). Considering a 4-protic acid, the four carboxylic groups will cover a DBE of 4. Since the total DBE of  $C_{80}H_{142}O_8$  is 10, the remaining DBE of 6 has to be due to unsaturation in the hydrocarbon moiety. As already noted, the NMR spectra show no sign of carbon-carbon multiple bonds, which indicate that the degree of unsaturation arises from six hydrogenated rings.

Overall, the obtained results are in good agreement with the findings of Baugh and co-workers [30] from analyses of metal naphthenates from other sources. Hence, their assumption that the 4-protic naphthenic acids are a general characteristic of metal naphthenate deposits is further supported.

## II) Surface and interfacial properties of naphthenic acids

### i) Interfacial (o/w) activity

In figure 5, dynamic interfacial tension (IFT) is plotted for o/w systems involving 0.010 mM  $C_{80}$  naphthenic acid at three different pH levels of the aqueous phase. As indicated, the interfacial activity increases with increasing pH as more carboxylic groups become dissociated. The interface seems to be more stable at increasing pH, as shown by the more even curves. This is due to formation of an electric double-layer of carboxylate anions and sodium ions from the borate buffer.

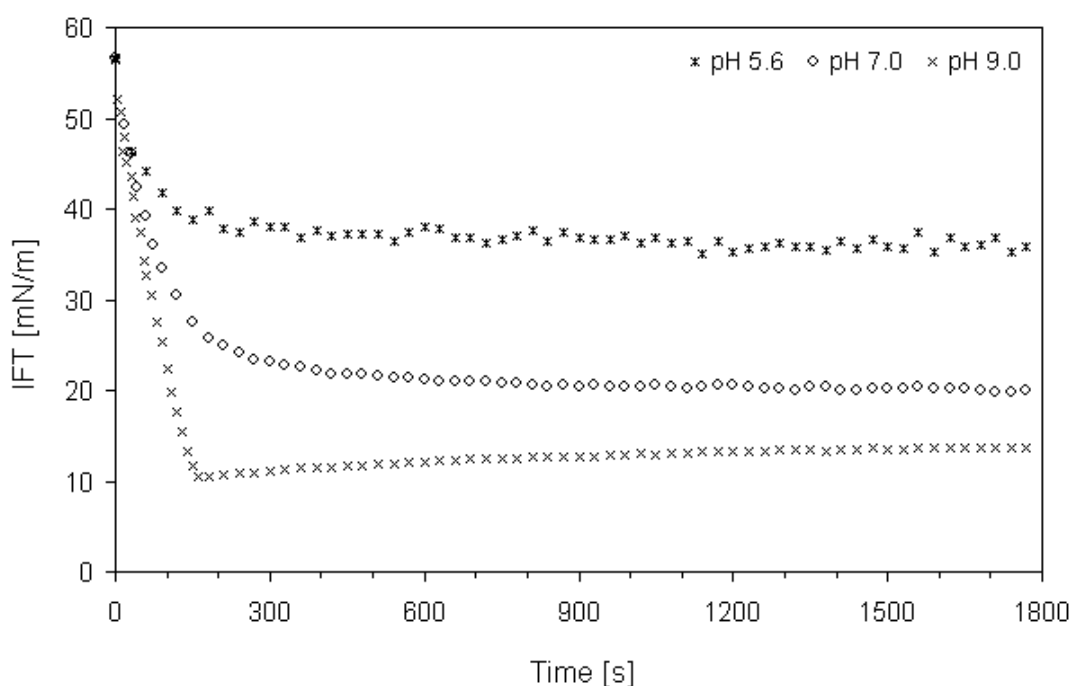


Figure 5: Dynamic IFT at different pH levels and 0.010 mM naphthenic acid.

The isotherm in the case of pH 9.0 has a quite different shape to what is normally observed for monomeric fatty acids adsorbing onto o/w interfaces. As to start with, the descending curve, reflecting diffusion and adsorption of monomers to the interface, shows an almost linear shape over a considerably long time. The adsorption process seems also to be quite slow, since it can be followed from the IFT value representing the pure o/w interface. Moreover, the decrease of the rate of IFT is clearly concentration dependent, as observed from the plots in figure 6. By lowering the concentration of naphthenic acid from 0.010 mM to 0.0075 mM and further to 0.0050 mM, the slope of the descending curve ( $-dy/dt$ ) gradually becomes smaller although the IFT in all cases is

lowered about 40 units compared to the pure o/w interface. At the lowest concentration, on the other hand, the IFT decreases only a few units during the time under consideration.

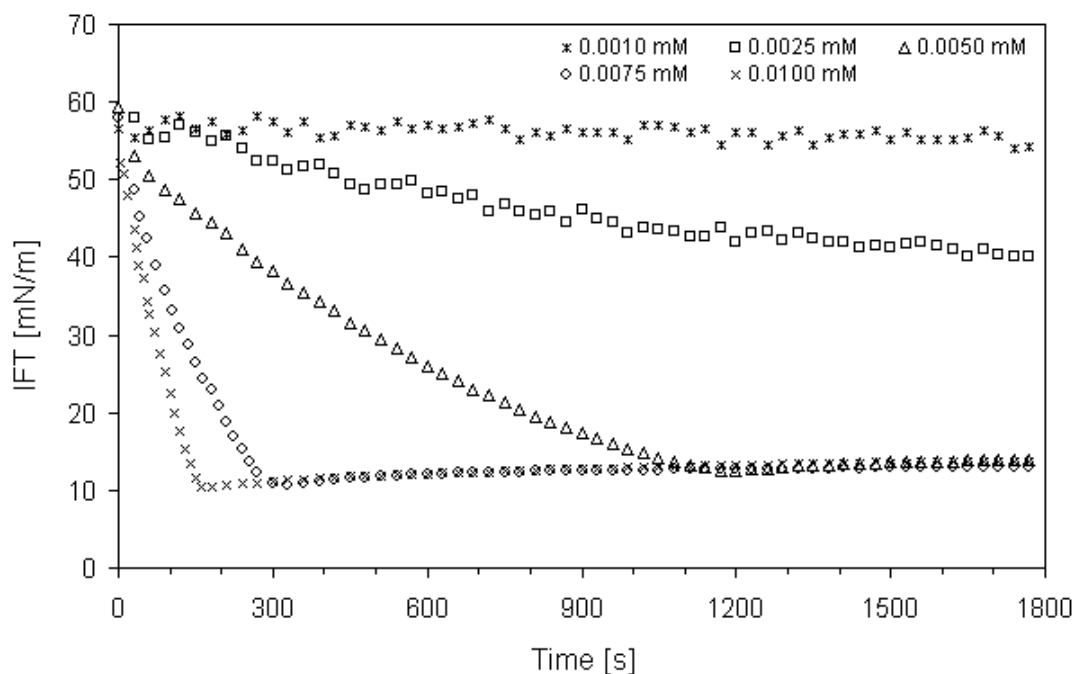


Figure 6: Dynamic IFT at different naphthenic acid concentrations and pH 9.0.

As the coverage of the interface is more complete by naphthenic acids, the curves slightly bend off. This is likely due to intermolecular interactions and reorientation of the molecules in the interfacial layer, which affect the rate of equilibration [62, 63]. For a naphthenic acid having four carboxylic groups, the groups have to orientate in the same direction to adsorb onto the o/w interface. This may be attained having a conformation where the carboxylic groups are chemically located in the same part of the structure, or otherwise, by a folding of flexible chains, directing the groups toward the interface. For both cases, and particular for the latter, the equilibration will be affected by dynamic processes taking place as the carboxylic groups are occupying the interface.

For longer observation times, the curves representing the three highest concentrations suddenly flatten out and show further an almost constant IFT. This appears at a well-defined equilibrium IFT value ( $\sim 12$  mN/m) as illustrated by the overlapping curves. Well-defined equilibrium tensions are rarely found for naphthenic acids, but have frequently been observed for larger molecules, such as peptides [64, 65]. The anomalous behaviour is likely a result of the high molecular weight (1230 g/mol) and the four carboxylic

groups, making the  $C_{80}$  acid structure much more extensive than for normal monoprotic naphthenic acids.

As demonstrated from the characterization study, the 4-protic  $C_{80}$  naphthenic acids seem to act very selectively in formation of naphthenate deposits. By taking into account all the different naphthenic acid structures existing in crude oil, it is clear that the  $C_{80}$  acids have to possess quite unique physical-chemical properties. One of these, as already disclosed, is the extremely high affinity towards the o/w interface. Considering interfacial reactions to be one of the mechanisms behind naphthenate formation [66, 67], the interfacial activity will be of major concern. The observed decline of the IFT of about 40 mN/m is quite drastic for a concentration of only 0.0050 mM naphthenic acid. As to compare with, naphthenic acids extracted from crude oil, have, under the same experimental conditions, shown to cause a lowering of the IFT of less than 30 units at 2000 times as high concentration [67].

## ii) Langmuir monolayer properties

Surface pressure-area isotherms at different pH levels are given in figure 7. At the beginning of the compression, the surface pressure remains almost constant since the area per molecule is large compared to the real molecular area (gasous-like film). As the barriers move further towards smaller area, the rise in pressure sets in as the naphthenic acid monomers start to interact. Early in this stage, the position of the hydrophobic tails of the molecules will change from horizontal to vertical to the surface. The film goes then through a liquid kind of state as the slope of the isotherms increases. At a specific point, however, the resistance of the film is reaching its maximum and film collapse occurs. The initial monolayer is then broken into multilayers and/or forced into the aqueous solution, and a further compression has just a small influence on the surface pressure.



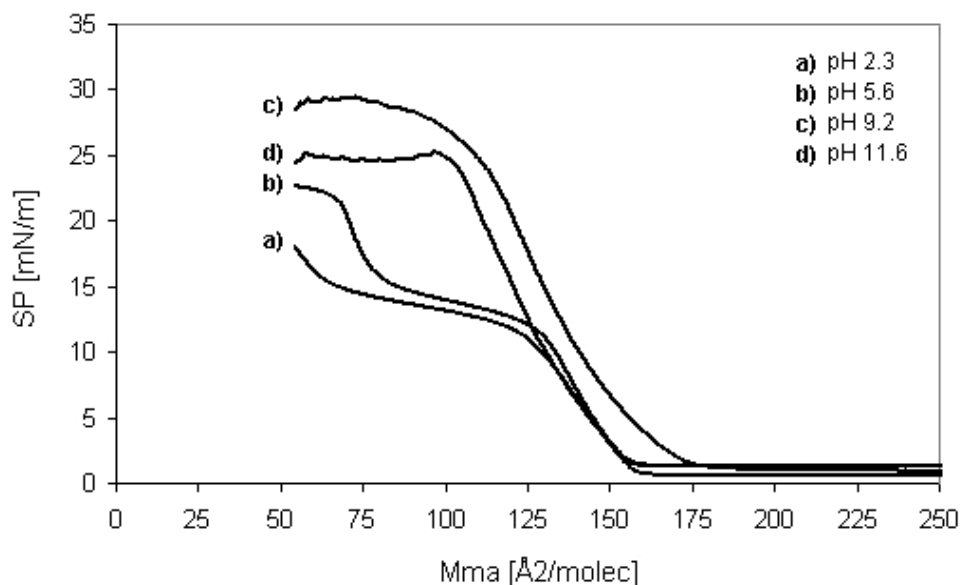


Figure 7: Surface pressure (SP) vs. molecular area ( $\text{\AA}^2/\text{molec}$ ) at different pH levels.

As observed from figure 7, the surface pressure is reaching a higher value at elevated pH. This is a result of electrostatic repulsion between dissociated carboxylic groups. At pH 2.3, 5.6, and 11.6, the plots show further that the pH effect is rather small with regard to changes in area/molecule when the pressure starts to increase. In the case of pH 9.2, on the other hand, the rise in pressure sets in at an earlier stage. This is due to the ionized carboxylic groups, which, due to electrostatic repulsion, require larger area than the corresponding molecules in an undissociated state. The reason why this effect is missing at pH 11.6 is most likely because of dissolution into water; at such high pH, the naphthenic acid monomers become completely dissociated, resulting in an enhanced water solubility and hence loss of initial film material. The surface concentration will thus be lower than at the beginning of the experiment, and, accordingly, the obtained molecular area will be lower. The considerable solubility in water due to dissociation is also well illustrated in figure 8, where relative area loss ( $A/A_0$ ) versus time at a constant surface pressure of 10 mN/m is plotted. As observed, the film stability increases by lowering the subphase pH. The film at pH 2.3 is much more stable than that at pH 5.6, which demonstrates that the film resistance decreases dramatically when the acids become slightly dissociated. Under alkaline conditions, the films become very unstable, and 60% of the initial area is lost within 10 minutes.

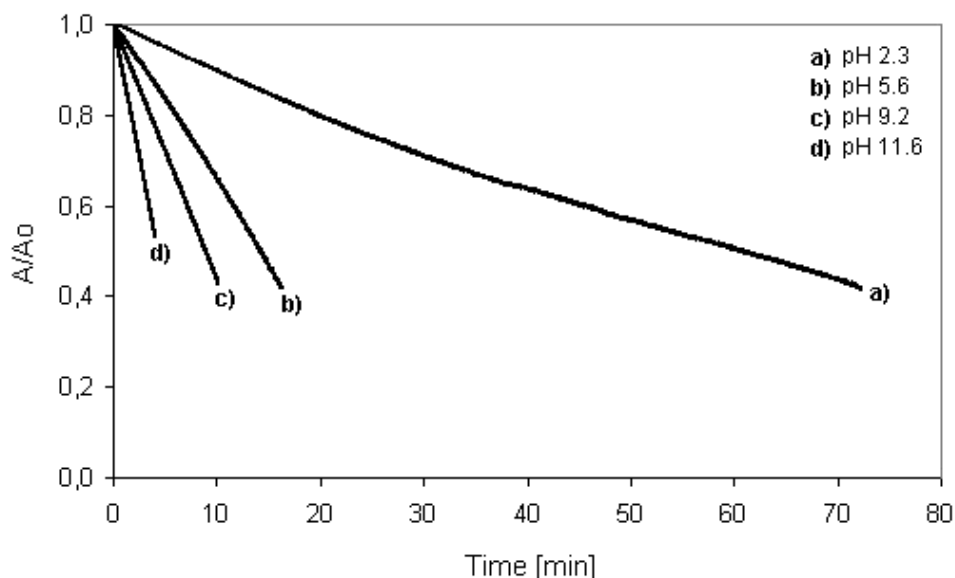


Figure 8: Stability isotherms (surface pressure of 10 mN/m) at different pH levels.

As figure 7 shows, the pressure-area isotherms at pH 2.3 and 5.6 have quite similar shapes. This indicates that the degree of dissociation is low, probably also at pH 5.6. At these pH levels, however, no distinct break in the curve reflecting film collapse is observed. The isotherms gradually flatten out, forming a plateau, before the pressure again increases. This effect is likely a result of phase transitions and structural rearrangement in the film where the molecules are pushed even closer due to the lack of repulsive charges pulling the molecules apart. The process may also involve intramolecular compression of the monomers, which is more favourable at low pH because of lower degree of repulsion between negatively charged acidic groups. In addition, aggregates may form as a result of hydrogen bond interactions, which in turn make the film more compressible.

Considering the undissociated state of the naphthenic acids, the surface pressure starts to increase at a molecular area of about  $160 \text{ \AA}^2/\text{molecule}$ . The high area reflects the extensive molecular structure of the  $C_{80}$  acids, comprising four surface active headgroups. The carboxylic groups alone do however not cover the entire area. As to compare with, saturated monomeric long-chain fatty acids have a molecular area around  $20 \text{ \AA}^2/\text{molecule}$  [68], and four tight-packed groups will thus give an area about the half of what observed for the  $C_{80}$  compound. The functional groups are thus likely to be separated from each other by hydrocarbon chains.

The effect on the surface pressure-area isotherms upon addition of calcium ions to the subphase at different pH levels is shown in figures 9-11. At pH 5.6 (fig. 9), the effect is rather small since the carboxylic headgroups are less ionized. Slight interactions seem however to occur, as the monolayer tend to tolerate some higher pressure upon addition of  $\text{Ca}^{2+}$ . On the other hand, as indicated by the plots of relative area loss versus time in figure 12, a concentration of 0.010 M  $\text{Ca}^{2+}$  has only a negligible effect on the film stability at a surface pressure of 10 mN/m.

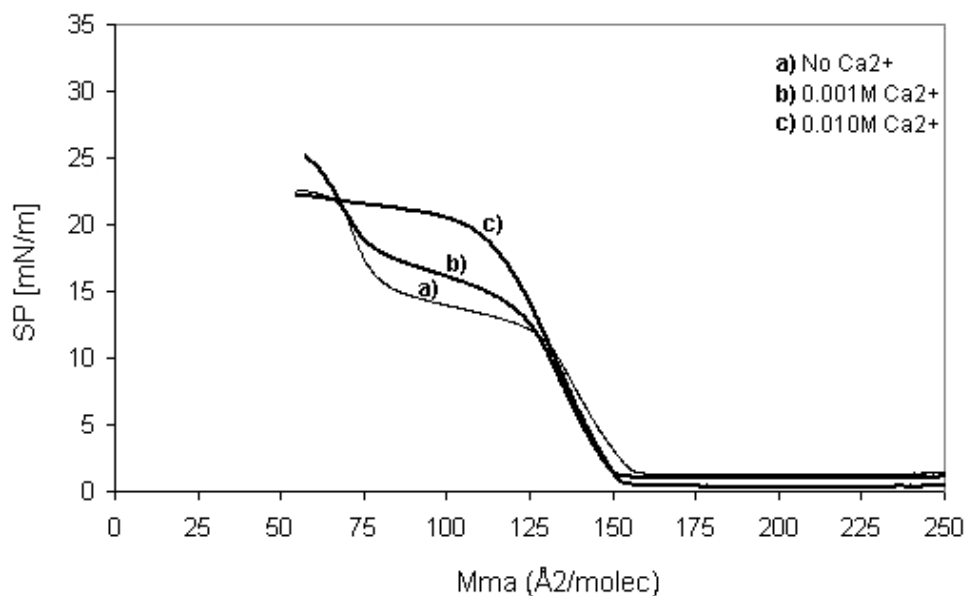


Figure 9: Surface pressure (SP) vs. molecular area ( $\text{\AA}^2/\text{molec}$ ) at pH 5.6 and different concentrations of  $\text{Ca}^{2+}$ .

At higher pH;s, the effect on onset area upon addition of  $\text{Ca}^{2+}$  is more striking, as observed by the isotherms in figures 10-11. In the case of pH 9.2 (fig. 10), the onset area decreases in presence of calcium ions. This is due to the electrostatic attraction forces acting between the dissociated carboxylic groups and the  $\text{Ca}^{2+}$  ions, eliminating repulsive forces between negatively charged moieties. The curves also ascend steeper in presence of  $\text{Ca}^{2+}$ , and the point reflecting monolayer collapse is more marked. Furthermore, as observed by the plots in figure 12, a presence of 0.010 M calcium ions in the subphase increases the film stability significantly at 10 mN/m. All these effects may be attributed to the formation of calcium naphthenate at the surface, which reduces the film compressibility and causes a more distinctive monolayer break-up. As a result of having four carboxylic groups, the monomers may be cross-linked by the calcium ions to form some kind of polymeric structure. This potential behaviour is in deep contrast to that of normal monoprotic acids, which are only able to form distinct particles.

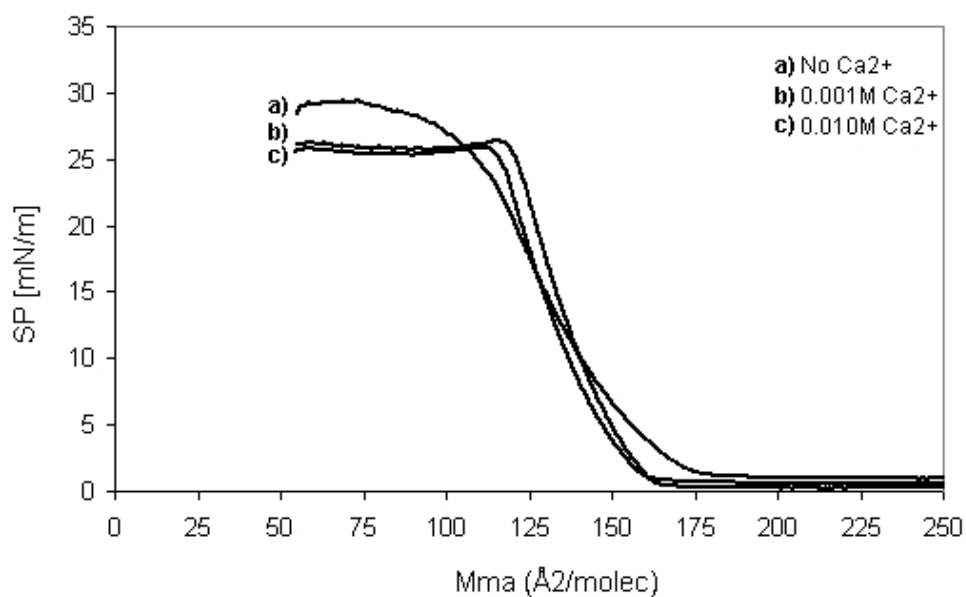


Figure 10: Surface pressure (SP) vs. molecular area ( $\text{\AA}^2/\text{molec}$ ) at pH 9.2 and different concentrations of  $\text{Ca}^{2+}$ .

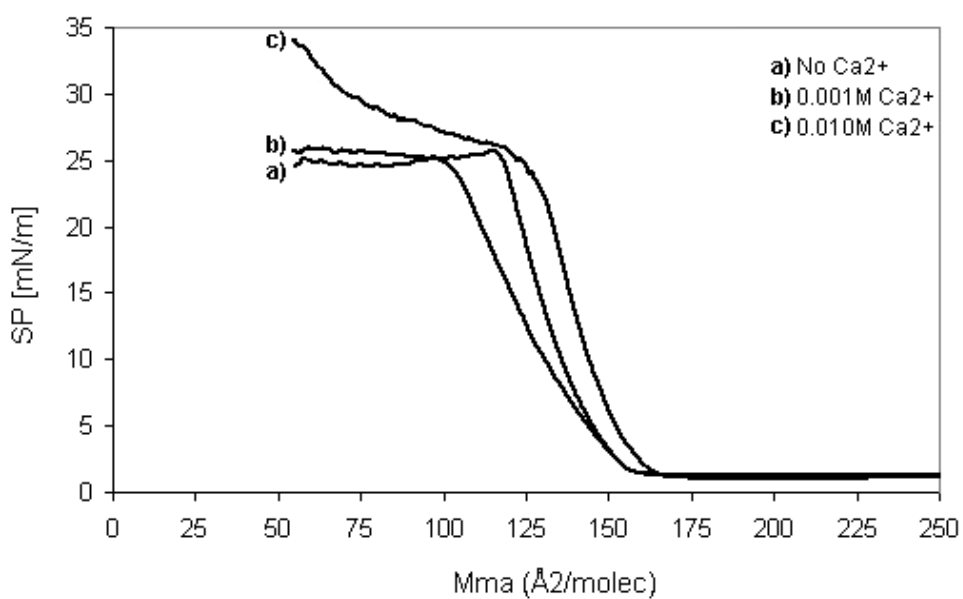


Figure 11: Surface pressure (SP) vs. molecular area ( $\text{\AA}^2/\text{molec}$ ) at pH 11.6 and different concentrations of  $\text{Ca}^{2+}$ .

At pH 11.6 (fig. 11), the isotherms are a bit different from those obtained at pH 9.2 and the rise in pressure occurs at an earlier stage in the case of the highest concentration of calcium ions. As already mentioned, this is likely because of a considerable solubility of

the dissociated molecules in water in absence of calcium ions. By adding  $\text{Ca}^{2+}$  to the subphase, less film material is lost due to the electrostatic forces exerted by the counterions upon the de-protolysed monolayer, leading to formation of calcium naphthenate at the surface. The increase of the film stability by increasing the concentration of  $\text{Ca}^{2+}$  in the subphase at pH 11.6 is clearly demonstrated in figure 13.

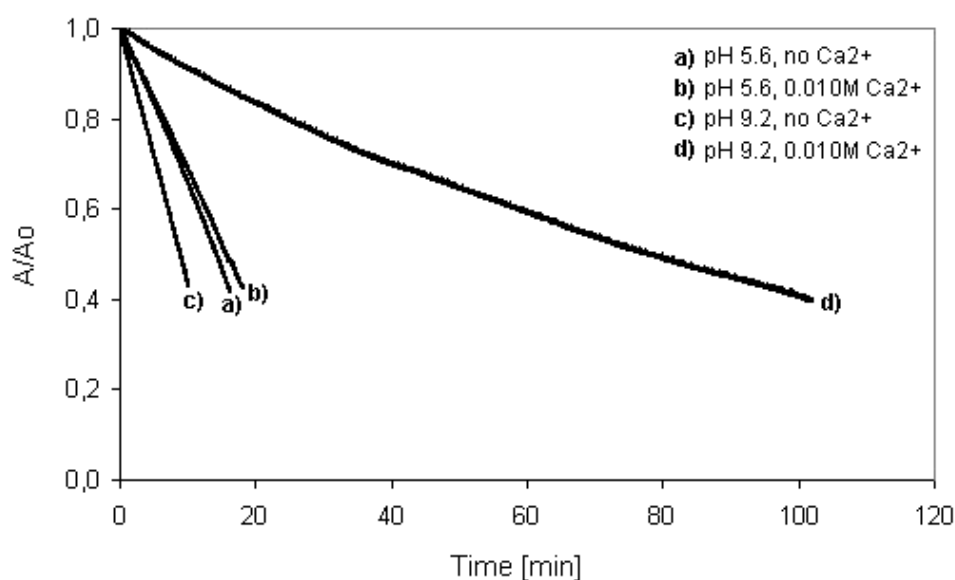


Figure 12: The effect on monolayer stability (surface pressure of 10 mN/m) upon addition of  $\text{Ca}^{2+}$  at different concentrations at pH 5.6 and 9.2.

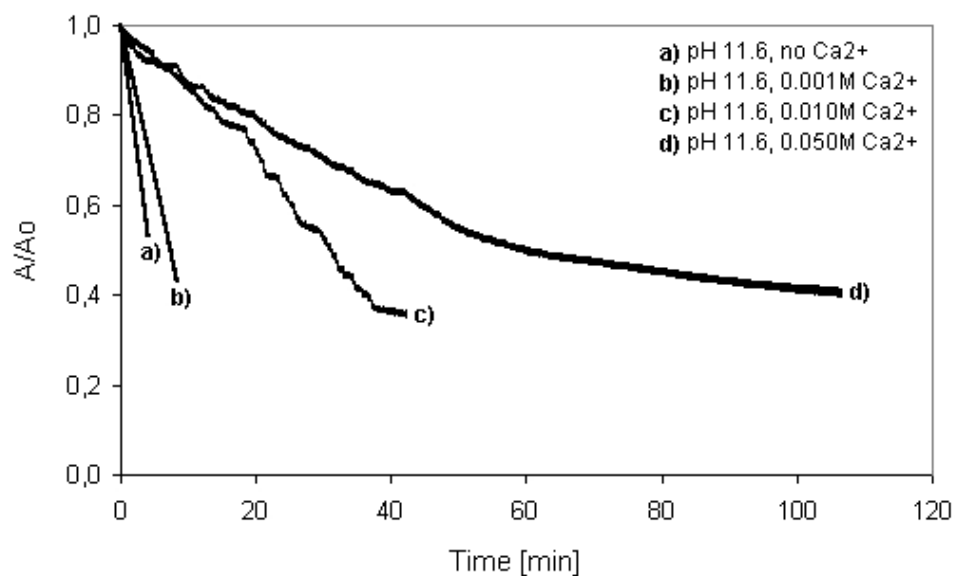


Figure 13: The effect on monolayer stability (surface pressure of 10 mN/m) upon addition of  $\text{Ca}^{2+}$  at different concentrations at pH 11.6.

In contrast to the curves of area loss versus time at lower pH levels, which tend to descend evenly, the curves at pH 11.6, and particular in presence of 0.010 M  $\text{Ca}^{2+}$ , have quite uneven shapes. As mentioned earlier, due to the four reactive carboxylic groups, the monomers may be cross-linked by  $\text{Ca}^{2+}$  to form a network of calcium naphthenate at the surface. A possible reason for the uneven curve-shapes is thus a subsequent fragmentation of the network layer. However, as the molecular structure is unknown, this approach is only speculative.

Although the relative film stability has shown to be altered by adjusting the pH and by adding calcium ions into the subphase, the overall stability is rather low compared to what normally is referred to as stable films. In all cases, a monotonous decrease in the relative area is observed. In general, the  $\text{C}_{80}$  acids seem thus to form quite unstable Langmuir monolayers, due to dissolution of film forming material into the aqueous phase, which is significant considering the huge volume difference between the surface active material and the subphase.

## CONCLUSIONS

A narrow group of 4-protic naphthenic acids with molecular weight around 1230 g/mol has shown to be dominating in a naphthenate deposit collected from an offshore installation in West Africa. The determined mass of 1230.0627 amu suggests a compound with the elemental formula of  $C_{80}H_{142}O_8$ . The compound has six sites of unsaturation in the hydrocarbon moiety, arising from condensed rings. The result is consistent with recent findings from other fields [30].

The  $C_{80}$  naphthenic acids become highly o/w interfacially active by increasing the pH of the aqueous phase from 5.6 to 9.0. The increasing interfacial activity is due to a higher degree of dissociation at the interface. At pH 9.0 and at concentrations of only 0.0050-0.010 mM of acid, the interfacial tension (IFT) is found to be about 40 mN/m lower than the value of the pure toluene/hexadecane (1:9 vol.) – water interface. The rate of IFT decrease is also concentration dependent within this concentration range, and a well-defined IFT value is attained at long observation times. The naphthenic acids acquired from the deposit sample are much more interfacially active than naphthenic acids extracted from crude oil. This property is likely one of the reasons why the  $C_{80}$  acids are found to dominate in naphthenate deposits.

In general, the  $C_{80}$  naphthenic acids form relatively unstable Langmuir monolayers. The stability decreases further with increasing pH as more monomers become dissociated and dissolve into the aqueous phase. By adding calcium ions into the subphase at high pH, the films become less soluble due to formation of calcium naphthenate at the surface. In the non-interacting region, the undissociated naphthenic acids have a molecular area of about  $160 \text{ \AA}^2/\text{molecule}$ . The high area reflects an extensive molecular structure comprising four carboxylic headgroups, which are likely to be separated by hydrocarbon chains.

## ACKNOWLEDGEMENTS

Statoil ASA and The Norwegian Academy of Science and Letters are acknowledged for the financial support through the VISTA programme. Acknowledgements are also extended to the JIP consortium, consisting of oil industry (ChevronTexaco, Statoil, and Total) and chemical vendors (AkzoNobel, BakerPetrolite, and ChampionTechnologies), and to Norman MacLeod (ChevronTexaco) for providing the deposit sample. Finally, Dr. Marit-Helen Ese is thanked for discussions and comments regarding the Langmuir film experiments.

## REFERENCES

1. Goldszal, A., Hurtevent, C., and Rousseau, G., *Scale and naphthenate inhibition in deep-offshore fields*. In *SPE Oilfield Scale Symposium*, SPE74661, (2002), Aberdeen, UK.
2. Slavcheva, E., Shone, B., and Turnbull, A., *Review of naphthenic acid corrosion in oil refining*, British Corrosion Journal, **34** (1999) 125-131.
3. Babaian-Kibala, E., Craig, H. L., Rusk, G. L., Blanchard, K. V., Rose, T. J., Uehlein, B. L., Quinter, R. C., and Summers, M. A., *Naphthenic acid corrosion in refinery settings*, Mater Performance, **32** (1993) 50-55.
4. Piehl, R. L., *Naphthenic acid corrosion in crude distillation units*, Mater Performance, **27** (1988) 37-43.
5. Pathak, A. K., and Kumar, T., *Study of indigenous crude oil emulsions and their stability*. In *Proceedings of PETROTECH-95, Technology trends in oil industry*, (1995), New Dehli.
6. Acevedo, S., Escobar, G., Ranaudo, M. A., Khazen, J., Borges, B., Pereira, J. C., and Méndez, B., *Isolation and characterization of low and high molecular weight acidic compounds from Cerro Negro extraheavy crude oil. Role of these acids in the interfacial properties of the crude oil emulsions*, Energy & Fuels, **13** (1999) 333-335.
7. Goldszal, A., Bourrel, M., Hurtevent, C., and Volle, J.-L., *Stability of water in acidic crude oil emulsions*. In *The 3rd International Conference on Petroleum Phase Behavior and Fouling*, (2002), New Orleans, USA.
8. Ese, M.-H., and Kilpatrick, P. K., *Stabilization of water-in-oil emulsions by naphthenic acids and their salts: model compounds, role of pH, and soap:acid ratio*, Journal of Dispersion Science and Technology, **25** (2004) 253-261.
9. Poggesi, G., Hurtevent, C., and Buchar, D., *Multifunctional chemicals for West African deep offshore fields*. In *SPE Oilfield Scale Symposium*, SPE74649, (2002), Aberdeen, UK.
10. Rousseau, G., Zhou, H., and Hurtevent, C., *Calcium carbonate and naphthenate mixed scale in deep-offshore fields*. In *SPE Oilfield Scale Symposium*, SPE68307, (2001), Aberdeen, UK.
11. Dyer, S. J., Graham, G. M., and Arnott, C., *Naphthenate scale formation - examination of molecular controls in idealised systems*. In *SPE 5th International Symposium on Oilfield Scale*, SPE 80395, (2003), Aberdeen, UK.
12. Seifert, W. K., *Carboxylic acids in petroleum and sediments*, Fortschritte der Chemie Organischer Naturstoffe, **32** (1975) 1-49.



13. Brient, J. A., Wessner, P. J., and Doyle, M. N., *Naphthenic acids* In *Encyclopedia of Chemical Technology* (Kirk-Othmer, Ed.), (1995), John Wiley & Sons, New York.
14. Meredith, W., Kelland, S.-J., and Jones, D. M., *Influence of biodegradation on crude oil acidity and carboxylic acid composition*, *Organic Geochemistry*, **31** (2000) 1059-1073.
15. Jaffe, R., and Gallardo, M. T., *Application of carboxylic acid biomarkers as indicators of biodegradation and migration of crude oils from the Maracaibo Basin, Western Venezuela*, *Organic Geochemistry*, **20** (1993) 973-984.
16. Behar, F. H., and Albrecht, P., *Correlations between carboxylic acids and hydrocarbons in several crude oils. Alteration by biodegradation*, *Organic Geochemistry*, **6** (1984) 597-604.
17. Dzidic, I., Somerville, A. C., Raia, J. C., and Hart, H. V., *Determination of naphthenic acids in California crudes and refinery wastewaters by fluoride ion chemical ionization mass spectrometry*, *Analytical Chemistry*, **60** (1988) 1318-1323.
18. Fan, T.-P., *Characterization of naphthenic acids in petroleum by fast-atom-bombardment mass-spectrometry*, *Energy & Fuels*, **5** (1991) 371-375.
19. Wong, D. C. L., van Compernelle, R., Nowlin, J. G., O'Neal, D. L., and Johnson, G., *Use of supercritical fluid extraction and fast ion bombardment mass spectrometry to identify toxic chemicals from a refinery effluent adsorbed onto granular activated carbon*, *Chemosphere*, **32** (1996) 1669-1697.
20. Hsu, C. S., Dechert, G. J., Robbins, W. K., and Fukuda, E. K., *Naphthenic acids in crude oil characterized by mass spectrometry*, *Energy & Fuels*, **14** (2000) 217-223.
21. Gabryelski, W., and Froese, K. L., *Characterization of naphthenic acids by electrospray ionization high-field asymmetric waveform ion mobility mass spectrometry*, *Analytical Chemistry*, **75** (2003) 4612-4623.
22. St.John, W. P. R., Jagdish; Green, Sarah.A; McGinnis, Gary.D., *Analysis and characterization of naphthenic acids by gas chromatography-electron impact mass spectroscopy of tert.- butyldimethylsilyl derivatives*, *Journal of Chromotography A*, **807** (1998) 241-251.
23. Holowenko, F. M., MacKinnon, M. D., and Fedorak, P. M., *Characterization of naphthenic acids in oil sands wastewaters by gas chromatography-mass spectroscopy*, *Water Research*, **36** (2002) 2843-2855.
24. Koike, L., Reboucas, L. M. C., Reis, F. d. A., Marsaioli, A. J., Richnow, H. H., and Michaelis, W., *Naphthenic acids from crude oils of Campos Basin*, *Organic Geochemistry*, **18** (1992) 851-860.

25. Seifert, W. K., and Teeter, R. M., *Identification of polycyclic naphthenic, mono-, and diaromatic crude oil carboxylic acids*, *Analytical Chemistry*, **42** (1970) 180-189.
26. Tomczyk, N. A., Winans, R. E., Shinn, J. H., and Robinson, R. C., *On the nature and origin of acidic species in petroleum. 1. Detailed acid type distribution in a California crude oil*, *Energy & Fuels*, **15** (2001) 1498-1504.
27. Rudzinski, W. E., Oehlers, L., Zhang, Y., and Najera, B., *Tandem mass spectrometric characterization of commercial naphthenic acids and a Maya crude oil*, *Energy & Fuels*, **16** (2002) 1178-1185.
28. Gallup, D. L., Smith, P. C., Chipponeri, J., Abuyazid, A., and Mulyono, D., *Formation & mitigation of "metallic soap" sludge, Attaka, Indonesia field*. In *SPE International Conference on Health, Safety and Environment in Oil and Gas Exploration and Production*, SPE73960, (2002), Kuala Lumpur, Malaysia.
29. Gallup, D. L., *Soap sludges: aggravating factors and mitigation measures*. In *6th SPE Oilfield Scale Symposium*, SPE87471, (2004), Aberdeen, UK.
30. Baugh, T. D., Wolf, N. O., Mediaas, H., Vindstad, J. E., and Grande, K. V., *Characterization of a calcium naphthenate deposit - The ARN acid discovery*, *Preprints - American Chemical Society, Division of Petroleum Chemistry*, **49** (2004) 274-276.
31. Marshall, A. G., and Rodgers, R. P., *Petroleomics: The next grand challenge for chemical analysis*, *Accounts of Chemical Research*, **37** (2004) 53-59.
32. Zhan, D., and Fenn, J. B., *Electrospray mass spectrometry of fossil fuels*, *International Journal of Mass Spectrometry*, **194** (2000) 197-208.
33. Kim, S., Simpson, A. J., Kujawinski, E. B., Freitas, M. A., and Hatcher, P. G., *High resolution electrospray ionization mass spectrometry and 2D solution NMR for the analysis of DOM extracted by C18 solid phase disk*, *Organic Geochemistry*, **34** (2003) 1325-1335.
34. Kujawinski, E. B., *Electrospray ionization Fourier transform ion cyclotron resonance mass spectrometry (ESI FT-ICR MS), characterization of complex environmental mixtures*, *Environmental Forensics*, **3** (2002) 207-216.
35. Stenson, A. C., Landing, W. M., Marshall, A. G., and Cooper, W. T., *Ionization and fragmentation of humic substances in electrospray ionization Fourier transform ion cyclotron resonance mass spectrometry*, *Analytical Chemistry*, **74** (2002) 4397-4409.
36. Márquez, M. L., *Interfacial activity of native acids in heavy crude oil*. In *AICHE Spring National Meeting, Session T6005*, 99sp 56d, (1999), Houston, Texas.

37. Chiwetelu, C. I., Hornof, V., and Neale, G. H., *The measurement of dynamic interfacial tension by photo-micropendography.*, Journal of Colloid and Interface Science, **125** (1988) 586-601.
38. Wolstenholme, G. A., and Schulman, J. H., *Metal-monolayer interactions in aqueous systems: I. Interaction of monolayers of long-chain polar compounds with metal ions in the underlying solution*, Transactions of the Faraday Society, **46** (1950) 475-487.
39. Durham, K., *Molecular interaction in mixed monolayers of fatty acids*, Journal of Applied Chemistry, **8** (1958) 724-728.
40. Goddard, E. D., and Ackilli, J. A., *Monolayer properties of fatty acids*, Journal of Colloid Science, **18** (1963) 585-595.
41. Havre, T. E., Ese, M.-H., Sjöblom, J., and Blokhus, A. M., *Langmuir Films of Naphthenic acids at different pH and electrolyte concentrations*, Colloid and Polymer Science, **280** (2002) 647-652.
42. Brandal, Ø., and Sjöblom, J., *Interfacial behaviour of naphthenic acids and multivalent cations in systems with oil and water. Part II: Formation and stability of metal naphthenate films at oil-water interfaces*, Journal of Dispersion Science and Technology, **26** (2005) 53-58.
43. Hughey, C. A., Hendrickson, C. L., Rodgers, R. P., and Marshall, A. G., *Elemental composition analysis of processed and unprocessed diesel fuel by electrospray ionization Fourier transform ion cyclotron resonance mass spectrometry*, Energy & Fuels, **15** (2001) 1186-1193.
44. Hughey, C. A., Hendrickson, C. L., Rodgers, R. P., Marshall, A. G., and Qian, K., *Kendrick mass defect spectrum: a compact visual analysis for ultrahigh-resolution broadband mass spectra*, Analytical Chemistry, **73** (2001) 4676-4681.
45. Emmett, M. R., White, F. M., Hendrickson, C. L., Shi, S. D.-H., and Marshall, A. G., *Application of micro-electrospray liquid chromatography techniques to FT-ICR MS to enable high-sensitivity biological analysis*, Journal of the American Society for Mass Spectrometry, **9** (1998) 333-340.
46. Senko, M. W., Hendrickson, C. L., Pasa-Tolic, L., Marto, J. A., and White, F. M., *Electrospray ionization Fourier transform ion cyclotron resonance at 9.4 T.*, Rapid Communications in Mass Spectrometry, **10** (1996) 1824-1828.
47. Senko, M. W., Hendrickson, C. L., Emmett, M. R., Shi, S. D.-H., and Marshall, A. G., *External accumulation of ions for enhanced electrospray ionization Fourier transform ion cyclotron resonance mass spectrometry*, Journal of the American Society for Mass Spectrometry, **8** (1997) 970-976.

48. Hendrickson, C. L., Quinn, J. P., Emmett, M. R., and Marshall, A. G., *Quadrupole mass filtered external accumulation for Fourier transform ion cyclotron resonance mass spectrometry*. In *48th ASMS Conference on Mass Spectrometry and Allied Topics*, pp. MP083, (2000), Long Beach, CA.
49. Ledford, E. B., Jr., Rempel, D. L., and Gross, M. L., *Space charge effects in Fourier transform mass spectrometry. II. Mass calibration.*, *Analytical Chemistry*, **56** (1984) 2744-2748.
50. Shi, S. D.-H., Drader, J. J., Freitas, M. A., Hendrickson, C. L., and Marshall, A. G., *Comparison and interconversion of the two most common frequency-to-mass calibration functions for fourier transform ion cyclotron resonance mass spectrometry*, *International Journal of Mass Spectrometry*, **195-196** (2000) 591-598.
51. Senko, M. W., Canterbury, J. D., Guan, S., and Marshall, A. G., *A high-performance modular data system for Fourier transform ion cyclotron resonance mass spectrometry*, *Rapid Communications in Mass Spectrometry*, **10** (1996) 1839-1844.
52. Blakney, G. T., van der Rest, G., Johnson, J. R., Freitas, M. A., Drader, J. J., Shi, S. D.-H., Hendrickson, C. L., Kelleher, N. L., and Marshall, A. G., *Further improvements to the MIDAS data station for FT-ICR mass spectrometry*. In *49th ASMS Conference on Mass Spectrometry and Allied Topics*, pp. WPM265, (2001), Chicago, IL.
53. Kendrick, E., *A mass scale based on CH<sub>2</sub> =14.0000 for high resolution mass spectrometry of organic compounds*, *Analytical Chemistry*, **35** (1963) 2146-2154.
54. Andreas, J. M., Hauser, E. A., and Tucker, W. B., *Boundary tension by pendant drops*, *Journal of Physical Chemistry*, **42** (1938) 1001-1019.
55. Winkel, D., *Theoretical refinement of the pendant drop method for measuring surface tensions*, *Journal of Physical Chemistry*, **69** (1965) 348-350.
56. Ambwani, D. S., and Fort, T., Jr., *Pendant drop technique for measuring liquid boundary tensions*, *Surface and Colloid Science*, **11** (1979) 93-119.
57. Rotenberg, Y., Boruvka, L., and Neumann, A. W., *Determination of surface-tension and contact-angle from the shapes of axisymmetric fluid interfaces*, *Journal of Colloid and Interface Science*, **93** (1983) 169-183.
58. Boucher, E. A., Evans, M. J. B., and Jones, T. G. J., *The computation of interface shapes for capillary systems in a gravitational field*, *Advances in Colloid and Interface Science*, **27** (1987) 43-79.
59. Williams, R. B., *Nuclear magnetic resonance in petroleum analytical research*, *Spectrochimica Acta*, **14** (1959) 24-44.

60. Clutter, D. R., Petrakis, L., Stenger, R. L., Jr., and Jensen, R. K., *Nuclear magnetic resonance spectrometry of petroleum fractions. Carbon-13 and proton nuclear magnetic resonance characterizations in terms of average molecule parameters*, Analytical Chemistry, **44** (1972) 1395-1405.
61. Urdahl, O., Brekke, T., and Sjöblom, J., *Carbon-13 N.M.R. and multivariate statistical analysis of adsorbed surface-active crude oil fractions and the corresponding crude oils.*, Fuel, **71** (1992) 739-746.
62. Van Hunsel, J., Bleys, G., and Joos, P., *Adsorption kinetics at the oil/water interface*, Journal of Colloid and Interface Science, **114** (1986) 432-441.
63. Demeter-Vodnár, J., Sálájan, M., and Lowy, D. A., *Kinetic study of the diffusion and adsorption of fatty acids at the benzene-water interface*, Journal of Colloid and Interface Science, **183** (1996) 424-430.
64. Middelberg, A. P. J., Radke, C. J., and Blanch, H. W., *Peptide interfacial adsorption is kinetically limited by the thermodynamic stability of self association*, Proceedings of the National Academy of Sciences of the United States of America, **97** (2000) 5054-5059.
65. Wang, L., Atkinson, D., and Small, D. M., *Interfacial properties of an amphipathic  $\alpha$ -helix consensus peptide of exchangeable apolipoproteins at air/water and oil/water interfaces*, Journal of Biological Chemistry, **278** (2003) 37480-37491.
66. Brandal, Ø., Sjöblom, J., and Øye, G., *Interfacial behaviour of naphthenic acids and multivalent cations in systems with oil and water, Part I: A pendant drop study of interactions between n-dodecyl benzoic acid and divalent cations*, Journal of Dispersion Science and Technology, **25** (2004) 367-374.
67. Brandal, Ø., Hanneseth, A. M., and Sjöblom, J., *Interactions between synthetic and indigenous naphthenic acids and divalent cations across water-oil interfaces. Effects of adding oil-soluble non-ionic surfactants*, Colloid and Polymer Science, Accepted, 2005.
68. Gaines, G. L., *Insoluble monolayers at liquid-gas interfaces*, (1966), Interscience, New York.

# Paper V

Formation, Growth, and Inhibition of Calcium Naphthenate  
Particles in Oil/Water Systems as Monitored by means of  
Near Infrared Spectroscopy.

Ann-Mari D. Hanneseth, Øystein Brandal <sup>\*</sup>, and Johan Sjöblom

Ugelstad Laboratory, Department of Chemical Engineering, Norwegian University of  
Science and Technology, N-7491 Trondheim, Norway.

\* Corresponding author (e-mail: [oystein.brandal@chemeng.ntnu.no](mailto:oystein.brandal@chemeng.ntnu.no)).

## **Abstract**

A new experimental setup based on near infrared (NIR) spectroscopy has been utilized to monitor the formation, growth and inhibition of calcium naphthenate particles in oil-water (o/w) systems under different experimental conditions. The naphthenic acids were dissolved in toluene and brought in contact with an aqueous solution. The reaction between the dissociated acid monomers and  $\text{Ca}^{2+}$  at the o/w interface was initiated by adding dissolved  $\text{CaCl}_2$  to the water phase. By using stirrers in both bulk phases, the formed particles were dispersed into the oil phase and the changes in optical density (OD) of the naphthenate solution were continuously monitored using a fiber optic NIR probe. Due to the particles present in the solution, the baseline of the NIR spectra was shifted upwards compared to the pure toluene phase, depending on the size and the number of particles detected by the probe. The formation and growth of naphthenate particles have shown to depend on the naphthenic acid structure, concentrations, and pH of the aqueous phase. In addition, the presence of oil-soluble surfactants has shown to cause a lowering of the particle volume. Possible mechanisms behind this effect are briefly discussed.

**Keywords:** near infrared (NIR) spectroscopy, naphthenic acid, naphthenate particle formation, particle growth.



## Introduction

Deposition of metal naphthenates in process facilities is from an operational point of view one of the most challenging separation issues. The problem arises from drop in pressure and release of CO<sub>2</sub> from the co-produced formation water during fluid transport from the reservoir to the topside, which in turn causes an increase in pH and a higher degree of dissociation of the naphthenic acids at the oil-water (o/w) interface. As a consequence, the dissociated moieties react with the counterions in the brine and precipitation of metal naphthenates may occur [1-3]. The product may then start to agglomerate in the oil phase, normally in combination with inorganic materials, and further adhere and accumulate to process unit surfaces. Naphthenate deposition is becoming a serious problem in a number of fields where acidic crudes are being processed, including fields in West Africa [4, 5], on the Norwegian continental shelf [5, 6], and in Southeast Asia [7, 8].

In order to reduce naphthenate deposition, chemical mixtures of various compositions are injected into the well stream. This includes surfactant mixtures consisting of ethoxylates and alcohol, which have shown to reduce deposition significantly [8]. Although the mechanism behind naphthenate inhibition using surfactants is not clarified in detail, it is likely due to a competitive process which takes place at the interface. Some alkyloxylates are highly interfacially active and may have a much higher affinity towards the o/w interface than the naphthenic acids. Consequently, they may dilute the interface and bring about longer lateral distances between the dissociated acid monomers [9]. Hence, the naphthenic acids have to restructure in the interfacial layer in order to complete the reaction, which in turn will slow down the reaction rate.

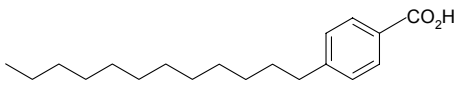
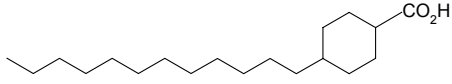
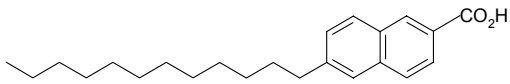
In this paper, we report a new experimental setup based on near infrared (NIR) spectroscopy to monitor the formation and growth of calcium naphthenate particles in o/w systems under different experimental conditions. The particles were formed at the o/w interface and dispersed into the oil phase upon stirring. Changes in optical density (OD) due to light scattering by particles were then correlated to the rate of particle formation and growth by plotting the square root of OD versus time.

## Experimental

### Chemicals

All chemicals were used as supplied; toluene (p.a., Acros Organics), calcium chloride dihydrate (>99.5%, Roth), pH 8.0 and 9.0 borate buffer solutions (Merck), three synthetic naphthenic acids (>99%, Chiron), and three different oil-soluble surfactants. Information about the synthetic naphthenic acids is given in table 1.

Table 1: The synthetic naphthenic acids used in the study.

Name	MW [g/mol]	Chemical structure
[1A-C12] p-(n-dodecyl) benzoic acid	290.4	
[1C-C12] 4-n-dodecyl-cyclohexane carboxylic acid	296.5	
[2A-C12] 6-dodecyl-naphthalene-2- carboxylic acid	340.6	

### Methods

The naphthenic acids and the oil-soluble surfactants were dissolved in toluene at different concentrations. The water phase consisted of either ultrapure water (purified with a Millipore Simplicity system) or borate buffer solutions of pH 8.0 and 9.0. A 1:1 volume ratio of water and toluene containing naphthenic acid was then poured into a glass bottle to a total volume of 80 ml. The oil and the water phase were continuously stirred according to the experimental setup illustrated in figure 1. The position of all the setup units and the level of the stirrers were fixed to get the experimental conditions as constant as possible for the different systems. The experiments were initiated by injecting a solution of dissolved  $\text{CaCl}_2$  at a given concentration into the aqueous phase to start the reaction between dissociated naphthenic acids and  $\text{Ca}^{2+}$ . The concentration of  $\text{Ca}^{2+}$  was always twice the concentration of naphthenic acid. The naphthenate particles formed at the o/w interface were then dispersed into the oil bulk solution and the

changes in optical density (OD) caused by light-scattering by particles were monitored using a fiber optic NIR sampling probe.

All near infrared measurements were performed with a Multi-Purpose Analyzer (Bruker Optics), equipped with a fibre optic sampling probe for transmittance measurements. The total path length of the probe was 2 mm. NIR spectra were recorded with a time interval of five minutes. The wavenumber region was set to  $10000\text{-}6000\text{ cm}^{-1}$  and the total scans per spectrum to 32. In order to follow the formation and growth of particles as a function of time, the results from a single wavenumber ( $9500\text{ cm}^{-1}$ ) were utilized.

Dynamic interfacial tensions (IFT) for o/w systems containing naphthenic acids (2mM) and the different surfactants (50ppm) were measured using the CAM 200 pendant drop technique (KSV Instruments). In some cases, this technique was also utilized to determine surface tensions (ST) of bulk water.

Particle sizes for some solutions were measured by using a Malvern Zetasizer 3000HS (Malvern Instruments). Totally 20 single measurements were undertaken for each series after which a mean particle size was calculated. The measurements of each series took about 10 minutes.

All the different experiments were performed at room temperature ( $22\text{ }^{\circ}\text{C}$ ).

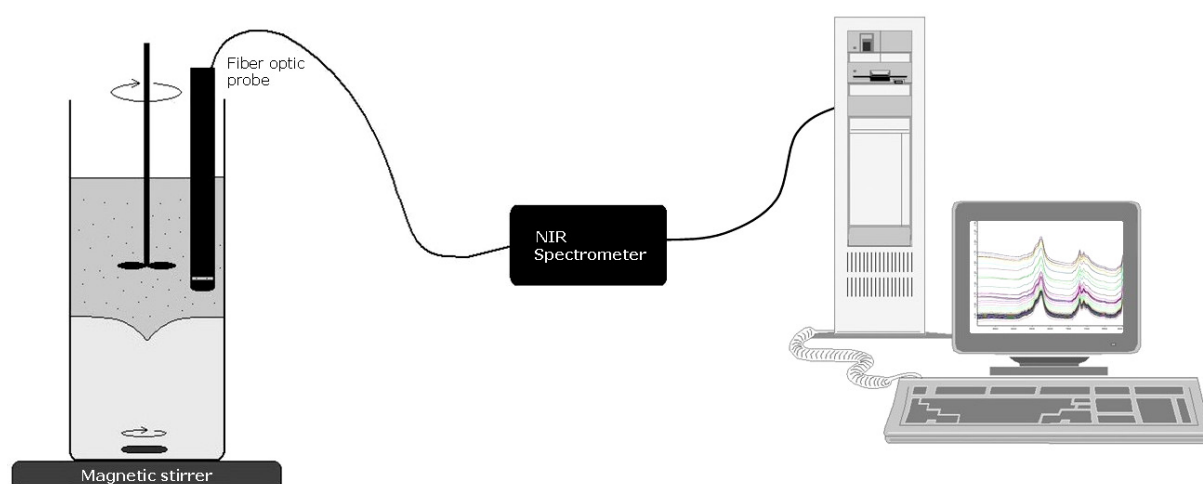


Figure 1: A sketch of the experimental setup used in the NIR spectroscopic study.

## Theory

### Light scattering by particles in the near infrared (NIR) region

One of the main advantages of using NIR spectroscopy in colloidal systems is the ability to gain information about the physical state of particles in the solution. Due to scattering, the NIR spectra will display a baseline elevation depending on the size and the number of particles. This phenomenon has frequently been benefited from to qualitatively study aggregation or disintegration of crude oil fractions [10, 11], or to estimate the sizes of different kinds of particles [12-15]. Light scattering in the NIR region is described in detail by Mullins [16] and Kerker [17]. A brief description is given below.

For slightly lossy dielectric particles in the Rayleigh limit  $r/\lambda \leq 0.05$ , where  $r$  is the particle radius and  $\lambda$  is the wavelength of the incident light, the light extinction can be considered as a sum of the scattering and the absorbance:

$$\sigma_{tot} = \sigma_{sc} + \sigma_{abs} \quad (1)$$

where  $\sigma_{tot}$ ,  $\sigma_{sc}$ , and  $\sigma_{abs}$  are the total, scattering, and absorption cross-sections, respectively. The absorption cross-section scales with the third power of the radius ( $r^3$ ). The scattering cross-section, on the other hand, scales with  $r^6$ , according to equation 2:

$$\sigma_{sc} = \frac{2^7 \pi^5 r^6}{3 \lambda^4} \left( \frac{n^2 - 1}{n^2 + 2} \right)^2 \quad (2)$$

where  $n$  is the ratio of the discrete phase to the continuous phase index of refraction, and  $\pi = 3.14...$  Hence, the particle size is very important for determining the magnitude of the particle scattering. The light intensities and the number of particles  $N$  in a given total cross-section may be related to optical density  $OD$  by the following equation:

$$OD = \log \left( \frac{I_0}{I} \right) = 0.434 N \sigma_{tot} \quad (3)$$

where  $I$  and  $I_0$  are the intensities of the transmitted and the incident light, respectively. The effect of multiple scattering is not accounted for in this equation. In the case of multiple scattering, the scattering and the absorption cannot be treated separately.

## Results and Discussion

Figure 2 shows NIR spectra of toluene and dispersed calcium naphthenate particles of *p*-(*n*-dodecyl) benzoic acid. The lowest spectrum is that of pure toluene. By adding  $\text{Ca}^{2+}$ , the baseline is shifted upwards due to scattering by the formed aggregates. Since the OD is a function of both particle number and size, the longer the observation time, the more and the larger particles are formed, and the higher is the baseline elevation. Since only the scattering contribution is of interest, the reference spectrum of pure toluene was subtracted from all the naphthenate solution spectra. The time between each recorded spectrum is five minutes.

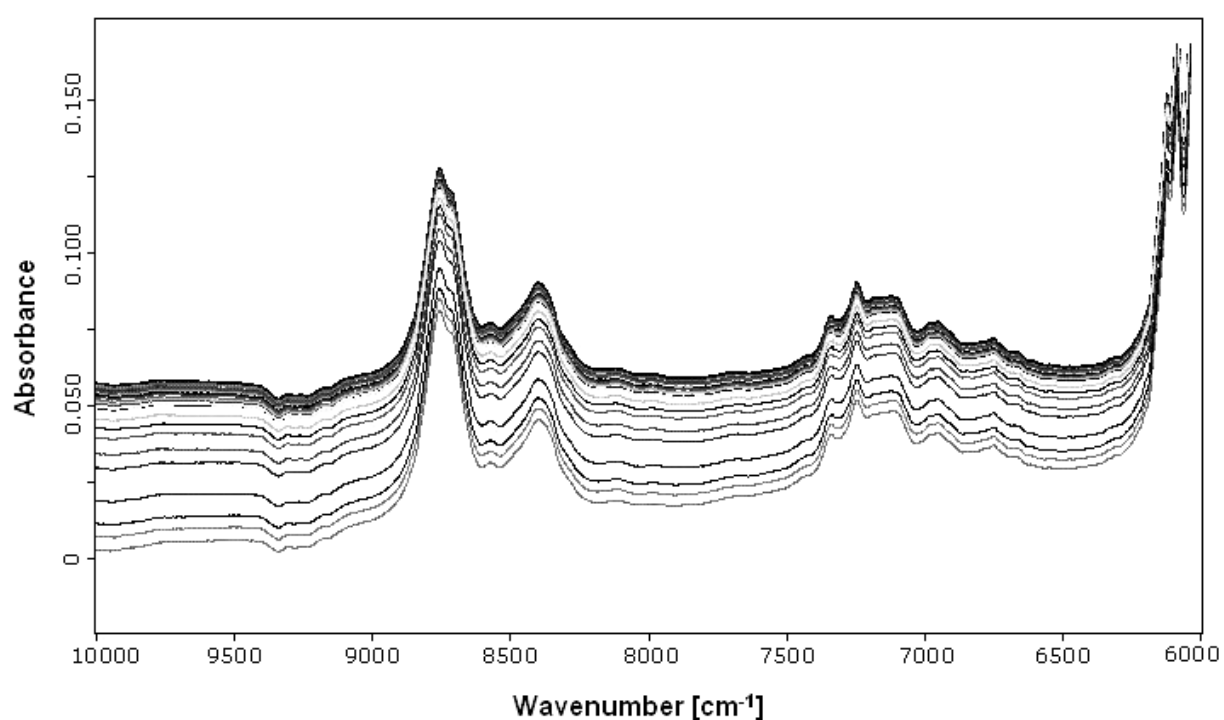


Figure 2: Spectra of toluene and calcium naphthenate-toluene solutions illustrating the baseline elevation due to formation and growth of particles. The time interval between each recorded spectrum is 5 minutes.

In order to follow the formation and growth of particles as a function of time, the OD at the wavenumber  $9500\text{ cm}^{-1}$  was considered where the hydrocarbon absorption is low. The square root of OD was then plotted versus time. The reason for calculating the square root of OD is that OD is proportional to the sixth power of the radii and thus to the square of the volume within the Rayleigh regime. Hence, any change in the square root of OD will reflect change in the volume of particles.

- **Effect of naphthenic acid structure**

The square root of OD versus time for toluene-naphthenate solutions of the different naphthenic acids is plotted in figure 3. As indicated, the naphthenic acids with aromatic rings are forming particles at a higher rate and with a larger volume than the acid with condensed ring. The reason for this is the higher interfacial affinity, as shown by the dynamic IFT plots in figure 4, which causes a higher density of acid monomers at the o/w interface. Due to the aromatic rings and the  $\pi$ -bonds between them, the acid monomers will pack more densely at the interface than the acid with condensed ring, favouring interfacial formation of 2:1 complexes of acid and  $\text{Ca}^{2+}$ . Monomers with two aromatic rings will pack even denser than monomers with only one ring, causing a higher reaction rate as demonstrated by comparing the slopes of the ascending curves at the beginning of the experiments. These findings are in good agreement to earlier studies in which dynamic IFT between an oil droplet containing naphthenic acid and alkaline aqueous solution were measured upon addition of different divalent cations [1, 9].

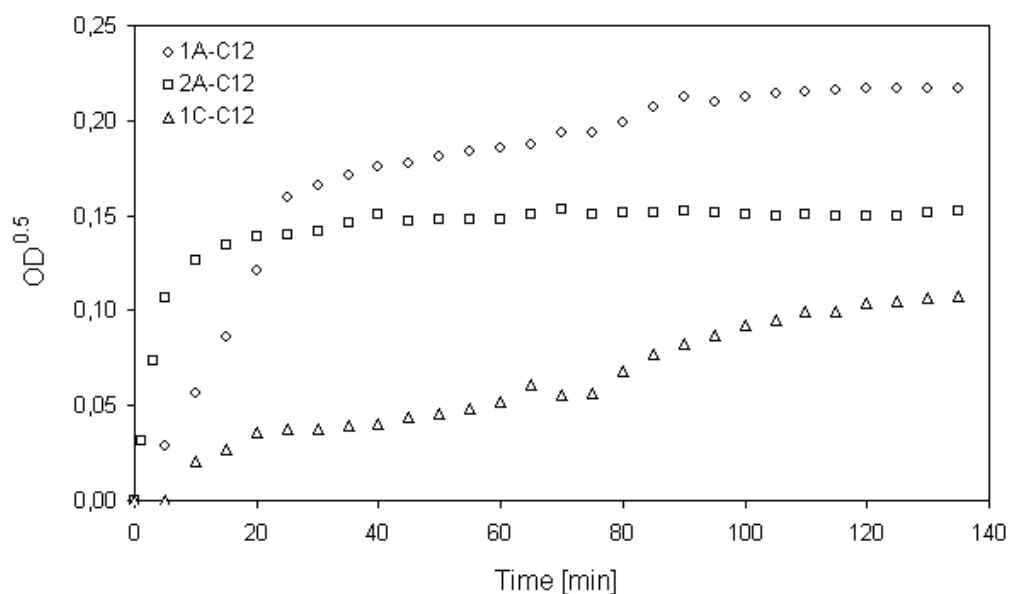


Figure 3: Square root of OD vs. time for naphthenate solutions of different naphthenic acid structures. The naphthenic acids are termed by short-names according to table 1. The concentrations of acid and  $\text{Ca}^{2+}$  are 2mM and 4mM, respectively.

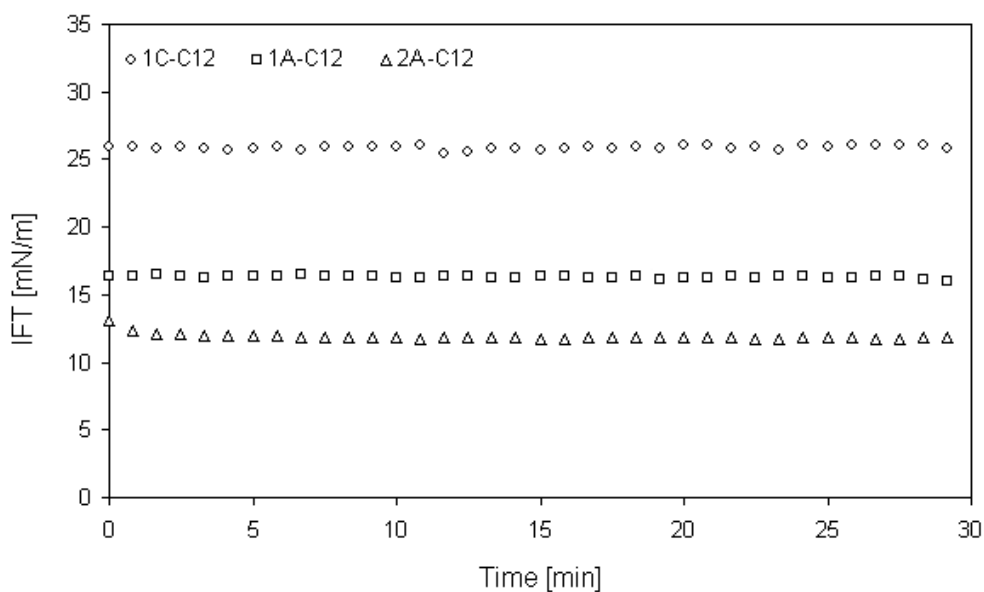


Figure 4: Dynamic interfacial tension of the toluene-water pH9 interface in presence of 2mM of the naphthenic acids in the toluene phase, clearly showing their different affinities towards the o/w interface. The naphthenic acids are termed by short-names according to table 1.

After some time, most pronounced in the case of the aromatic two-ring structure, a steady state is reached as the curves flatten out and show an almost constant OD value. The explanation for this behaviour is likely twofold. First, the maximum number of single particles formed will depend on the concentration of the naphthenic acid as  $\text{Ca}^{2+}$  is in excess. The steady state may thus reflect that all the naphthenic acid monomers have reacted to form particles. Second, the almost constant OD also indicates that the contribution from particle growth is minimal in this region. This could indicate that particles with a similar size gradually are formed. However, the ability of the particles to scatter light will increase with their size only up to a certain size. Within the Rayleigh regime, as noted in the theory part, the intensity of the scattered light increases in proportion to the sixth power of the radius. Far beyond the Rayleigh criteria, on the other hand, the OD will relate to the particle radius with a power less than six. Consequently, the particles will not contribute so much to an increase in OD when the particles become sufficiently large and a further particle growth may not be detected by monitoring the OD.

- **Effect of concentration and pH**

Figure 5 shows plots of  $OD^{0.5}$  versus time of naphthenate solutions for systems consisting of different concentrations of p-(n-dodecyl) benzoic acid and  $Ca^{2+}$ . As clearly indicated, the OD increases more rapidly the higher the concentration of reactants as more particles are formed at the interface. The rate of particle formation and growth is also highly dependent on the pH of the aqueous phase, as illustrated by the plots in figure 6. At pH 5.6 and pH 8.0, the OD increases only slightly compared to the pure toluene phase. This is due to low degree of dissociation of the naphthenic acid monomers, causing formation of less particles than at pH 9.0. In that respect, it is interesting to observe the large shift in OD by shifting the pH only one unit from 8.0 to 9.0, which indicates that the pH has to be elevated up to 9.0 to get the naphthenic acid sufficiently dissociated to form particles, i.e. the dissociation of the p-(n-dodecyl) benzoic acid seems to be low, even at pH 8.0.

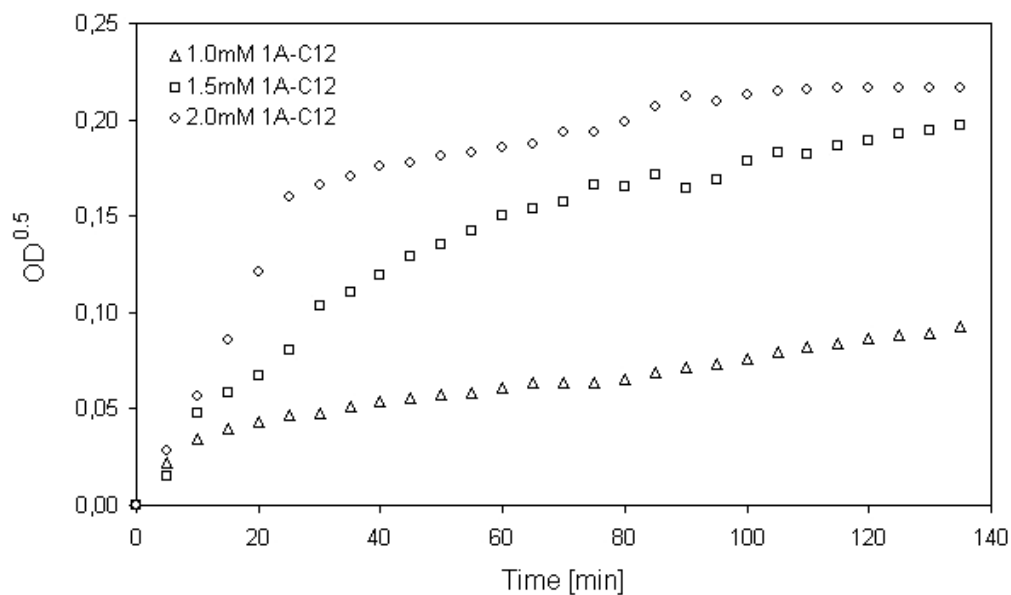


Figure 5: Plots of the square root of OD vs. time for naphthenate solutions of different concentrations of the p-(n-dodecyl) benzoic acid (1A-C12). The concentration of  $Ca^{2+}$  is in all cases twice the concentration of acid.



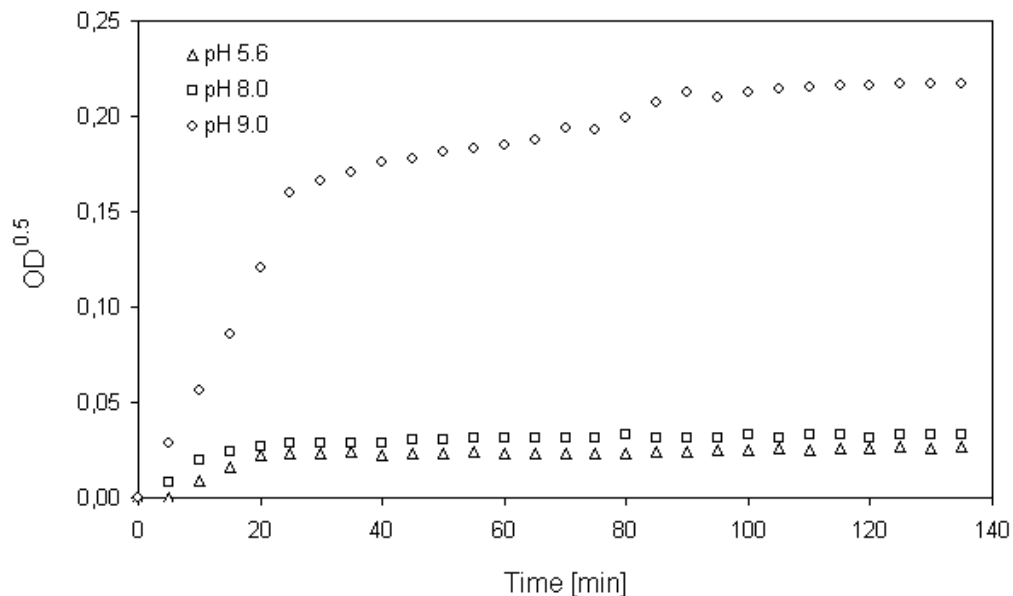


Figure 6: Plots of the square root of OD vs. time for naphthenate solutions of the p-(n-dodecyl) benzoic acid (1A-C12) at different pH levels of the aqueous phase. The concentrations of acid  $\text{Ca}^{2+}$  are 2mM and 4mM, respectively.

- **Effect of addition of surfactants**

Different oil-soluble surfactants were added in order to study their effect on the naphthenate particle formation. Surfactants are used to reduce the amount of naphthenate deposition during crude oil production. Dynamic interfacial tension (IFT) between water of pH 9.0 and toluene containing 50ppm of three different surfactants, named A, B, and C, is plotted in figure 7. As observed, the surfactant A is the most interfacially active, whereas C lowers the toluene-water IFT only slightly. The surfactant B, on the other hand, seems to be quite water soluble as indicated by the monotonous increase in the IFT towards the tension value of the pure interface ( $\sim 36 \text{ mN/m}$ ).

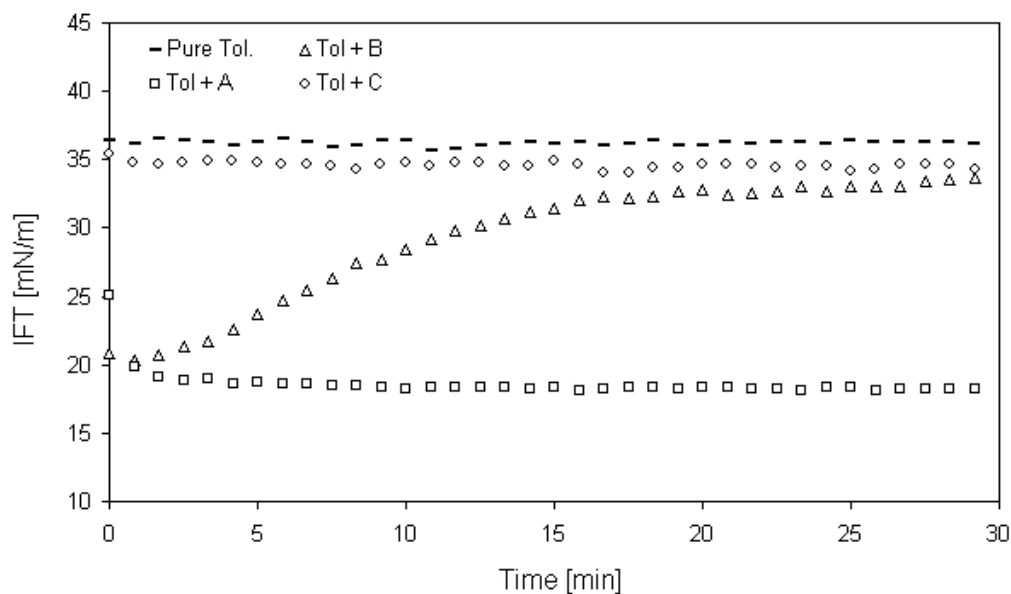


Figure 7: Plots of dynamic IFT of water pH 9.0 and toluene containing 50 ppm of the different surfactants (A, B, and C). The shortname “Tol” stands for toluene.

The p-(n-dodecyl) benzoic acid was chosen for the inhibition measurements. Figure 8 shows plots of the square root of OD versus time for naphthenate solutions both in absence and in presence of surfactants. As observed, all the additives cause a lowering of the OD. The surfactant C, which is the less interfacially active, seems to be less efficient than those of A and B. An interesting observation from figure 8 is that addition of surfactant B, which is water-soluble, results in a lower particle volume than addition of surfactant A. Due to the low o/w interfacial affinity it is unlikely that the mechanism is interfacial dilution of acid monomers. The partitioning of B into water was further investigated for two different systems by measuring the surface tension (ST) of bulk water (pH 9.0) in contact with; 1) toluene (1:1 vol) containing B (50ppm), and 2) toluene containing naphthenic acid (2mM) and B (50ppm) upon addition of  $\text{Ca}^{2+}$  to the water. The results (table 2) show that the surfactant B does not partition into the water when naphthenate particles are formed in the system. Possible reasons for this are interactions between the surfactant and the reactants, i.e.  $\text{Ca}^{2+}$  and/or the naphthenic acid, or interactions between the surfactant and the particles, causing disintegration into smaller aggregates. To check the assumption about smaller particles, the particle size was measured at different times for naphthenate solutions both in presence and in absence of B by using the Malvern instrumentation. The results are given in table 3. As indicated, for the solution without surfactant, the average particle diameter increases slightly with time from about  $0.9\mu\text{m}$  up to  $1.4\mu\text{m}$ . For the system upon addition of B, on the other hand, particles could not be detected up to 110 minutes. This is because of

limitations in the Malvern instrument, which only makes it possible to measure on particle solutions above a lower dilution level. At 110 minutes, however, this limit was exceeded and, as suggested, the particles were found to be smaller as an average than the particles in the solution without additives.

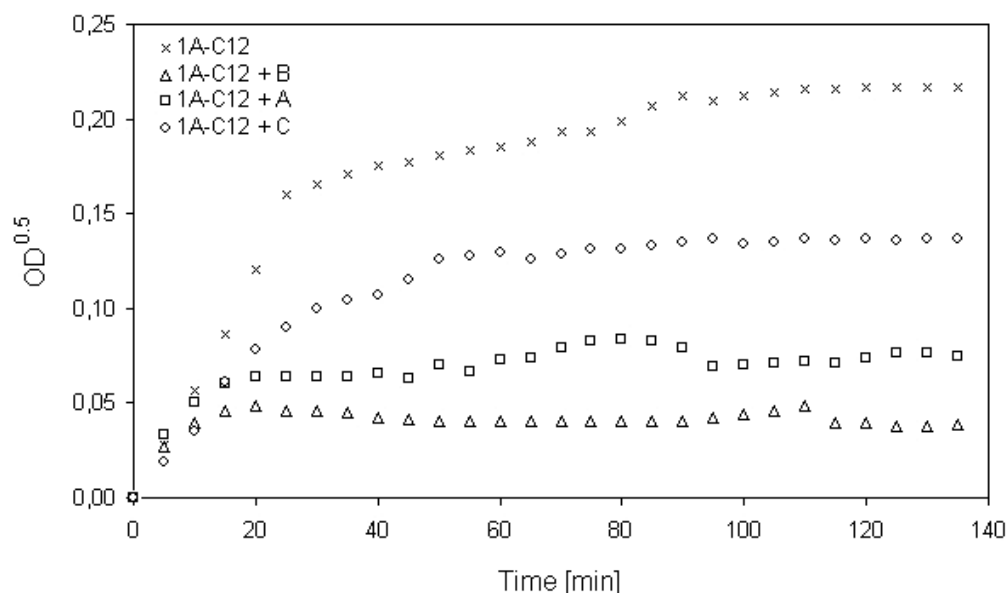


Figure 8: Square root of OD vs. time for naphthenate solutions in addition of the different surfactants compared to the system without additives.

For the selected wavenumber of  $9500\text{ cm}^{-1}$ , the Rayleigh condition is only valid for particles with radii up to about 55 nm. However, investigations by Heller [18] have shown the uncertainty to be low at considerable larger particles and less than 5% for  $r/\lambda \leq 0.25$ . At  $9500\text{ cm}^{-1}$ , this corresponds to a particle radius of 265 nm, which is still lower than the mean sizes determined using the Malvern equipment. Strictly spoken, the square root of OD is also directly proportional to the particle volume in systems consisting of a constant number of monodisperse particles. Nevertheless, the curves have shown to give a good qualitative description of the calcium naphthenate formation under different experimental conditions.

Table 2: Surface tensions (ST) of different water phases (bulk water) in contact with: toluene containing 50 ppm of B (water 1), and toluene containing 50 ppm of B and 2mM 1A-C12 upon addition of 4mM Ca<sup>2+</sup> (water 2).

Time [min]	ST [mN/m] of water 1	ST [mN/m] of water 2
0	72.5	72.4
5	60.6	72.5
10	57.2	72.4
15	53.0	72.5
20	51.7	72.6
90	50.5	72.5

Table 3: Particle sizes measured by using the Malvern. Solution 1: naphthenate particles of 1A-C12, Solution 2: naphthenate particles of 1A-C12 in presence of 50ppm of B.

Time [min]	Average particle diameter [ $\mu\text{m}$ ] in solution 1	Average particle diameter [ $\mu\text{m}$ ] in solution 2
20	0.9	-
40	1.3	-
60	1.3	-
80	1.4	-
110		0.7

## **Conclusions**

A new experimental setup based on near infrared spectroscopy has been used to study the formation and growth of metal naphthenate particles in oil-water systems. The particle formation and growth have shown to depend on the naphthenic acid structure, concentration of reactants, and the pH of the aqueous phase. Moreover, addition of various oil-soluble surfactants has shown to cause a reduction of the particle volume. Likely mechanisms behind this effect are interfacial dilution of naphthenic acid monomers, interactions between the surfactants and the reactants, i.e. that the surfactants bind  $\text{Ca}^{2+}$  or the naphthenic acid, or interactions between the surfactants and the particles, causing smaller aggregates. Although the method involves some limitations and uncertainties, it has shown to be a promising tool to qualitatively follow the particle formation and growth under different experimental conditions.

## **Acknowledgements**

Øystein Brandal would like to acknowledge Statoil ASA and The Norwegian Academy of Science and Letters for the financial support through the VISTA programme. Acknowledgements are also extended to the JIP consortium, consisting of petroleum companies (ChevronTexaco, Statoil, and Total) and chemical vendors (AkzoNobel, BakerPetrolite, and ChampionTechnologies).

## References

1. Brandal, Ø., Sjöblom, J., and Øye, G., *Interfacial behaviour of naphthenic acids and multivalent cations in systems with oil and water. I. A pendant drop study of interactions between n-dodecyl benzoic acid and divalent cations*, Journal of Dispersion Science and Technology, **25** (2004) 367-374.
2. Brandal, Ø., and Sjöblom, J., *Interfacial behaviour of naphthenic acids and multivalent cations in systems with oil and water. II. Formation and stability of metal naphthenate films at oil-water interfaces*, Journal of Dispersion Science and Technology, **26** (2005) 53-58.
3. Brandal, Ø., Hanneseth, A. M., Hemmingsen, P. V., Sjöblom, J., Kim, S., Rodgers, R. P., and Marshall, A. G., *Isolation and characterization of naphthenic acids from metal naphthenate deposit. Molecular properties at oil-water and air-water interfaces*, Journal of Dispersion Science and Technology, Accepted, 2005.
4. Poggesi, G., Hurtevent, C., and Buchart, D., *Multifunctional chemicals for West African deep offshore fields*. In *SPE Oilfield Scale Symposium*, SPE74649, (2002), Aberdeen, UK.
5. Rousseau, G., Zhou, H., and Hurtevent, C., *Calcium carbonate and naphthenate mixed scale in deep-offshore fields*. In *SPE Oilfield Scale Symposium*, SPE68307, (2001), Aberdeen, UK.
6. Dyer, S. J., Graham, G. M., and Arnott, C., *Naphthenate scale formation - examination of molecular controls in idealised systems*. In *SPE 5th International Symposium on Oilfield Scale*, SPE 80395, (2003), Aberdeen, UK.
7. Gallup, D. L., Smith, P. C., Chipponeri, J., Abuyazid, A., and Mulyono, D., *Formation & mitigation of "metallic soap" sludge, Attaka, Indonesia field*. In *SPE International Conference on Health, Safety and Environment in Oil and Gas Exploration and Production*, SPE73960, (2002), Kuala Lumpur, Malaysia.
8. Gallup, D. L., *Soap sludges: aggravating factors and mitigation measures*. In *6th SPE Oilfield Scale Symposium*, SPE87471, (2004), Aberdeen, UK.
9. Brandal, Ø., Hanneseth, A. M., and Sjöblom, J., *Interactions between synthetic and indigenous naphthenic acids and divalent cations across water-oil interfaces. Effects of addition of oil-soluble non-ionic surfactants*, Colloid and Polymer Science, Accepted, 2005.
10. Aske, N., Kallevik, H., Johnsen, E. E., and Sjöblom, J., *Asphaltene aggregation from crude oils and model systems studied by high-pressure NIR spectroscopy*, Energy & Fuels, **16** (2002) 1287-1295.

11. Aufler, I. H., Havre, T. E., and Sjöblom, J., *Near infrared study on the dispersive effects of amphiphiles and naphthenic acids on asphaltenes in model heptane-toluene mixtures*, *Colloid and Polymer Science*, **280** (2002) 695-700.
12. Gossen, P. D., MacGregor, J. F., and Pelton, R. H., *Composition and particle diameter for styrene/methyl methacrylate copolymer latex using UV and NIR spectroscopy*, *Applied Spectroscopy*, **47** (1993) 1852-1870.
13. Frake, P., Gill, I., Luscombe, C. N., Rudd, D. R., Waterhouse, J., and Jayasorriya, U. A., *Near-infrared mass median particle size determination of lactose monohydrate, evaluating several chemometric approaches*, *Analyst*, **123** (1998) 2043-2046.
14. Santos, A. F., Lima, E. L., and Pinto, J. C., *In-line evaluation of average particle size in styrene suspension polymerizations using near-infrared spectroscopy*, *Journal of Applied Polymer Science*, **70** (1998) 1737-1745.
15. Pasikatan, M. C., Steele, J. L., Spillman, C. K., and Haque, E., *Near infrared reflectance spectroscopy for online particle size analysis of powders and ground materials*, *Journal of Near Infrared Spectroscopy*, **9** (2001) 153-164.
16. Mullins, O. C., *Asphaltenes in crude oil: Absorbers and/or scatters in the near-infrared region?*, *Analytical Chemistry*, **62** (1990) 508-514.
17. Kerker, M., *The scattering of light and other electromagnetic radiation* In *Physical Chemistry. A Series of Monographs* (E. M. Loebel, Ed.), (1969), Academic Press, New York.
18. Heller, W., *Theoretical Investigations on the Light Scattering of Spheres. XVI. Range of Practical Validity of the Rayleigh Theory*, *Journal of Chemical Physics*, **42** (1965) 1609-1615.